PB83-156281

REPORT NO.
UCB/EERC-82/09
AUGUST 1982

EARTHQUAKE ENGINEERING RESEARCH CENTER

FLUID-STRUCTURE INTERACTIONS: ADDED MASS COMPUTATIONS FOR INCOMPRESSIBLE FLUID

by

JAMES SHAW-HAN KUO

Report to the National Science Foundation

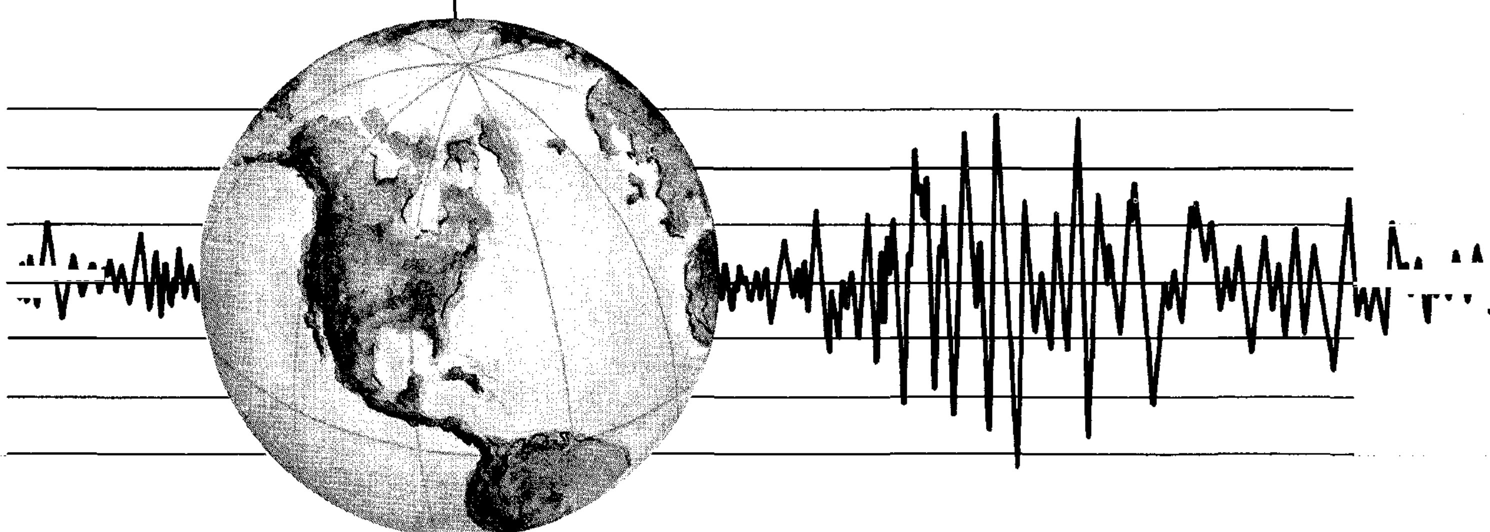

COLLEGE OF ENGINEERING

UNIVERSITY OF CALIFORNIA · Berkeley, California

For sale by the National Technical Information Service, U.S. Department of Commerce, Springfield, Virginia 22161.

See back of report for up to date listing of EERC reports.

DISCLAIMER

FLUID-STRUCTURE INTERACTIONS:
ADDED MASS COMPUTATIONS FOR INCOMPRESSIBLE FLUID

by

James Shaw-Han Kuo

Report to the National Science Foundation

Report No. UCB/EERC-82/09
Earthquake Engineering Research Center
College of Engineering
University of California
Berkeley, California

August 1982

50272-101

REPORT DOCUMENTATION PAGE	1. REPORT NO. NSF/CEE-82014	2.	3. Recipient's Accession No. PB83 156281

4. Title and Subtitle	5. Report Date
Fluid-Structure Interactions: Added Mass Computations for Incompressible Fluid	August 1982
	6.
7. Author(s) James Shaw-Han Kuo	8. Performing Organization Rept. No. UCB/EERC-82/09
9. Performing Organization Name and Address Earthquake Engineering Research Center University of California, Berkeley 47th Street and Hoffman Blvd. Richmond, Calif. 94804	10. Project/Task/Work Unit No. 11. Contract(C) or Grant(G) No. (C) (G) PFR-78-19333
12. Sponsoring Organization Name and Address National Science Foundation 1800 G. Street, N.W. Washington, D.C. 20550	13. Type of Report & Period Covered 14.

15. Supplementary Notes

16. Abstract (Limit: 200 words)

In this report, dam-reservoir interaction effects considering incompressible fluid are presented. The hydrodynamic effect represented by an added-mass matrix is evaluated by two basically different procedures -- a Generalized Westergaard Formula and the Galerkin Finite Element Method. Pressure solutions acting on gravity dams, cylindrical arch dams and general arch dams are compared for different procedures. Rigorous mode shape and frequency correlations are carried out, and based on the results of the correlation studies a most efficient procedure is suggested, which is shown to be adequate for engineering purposes.

17. Document Analysis a. Descriptors

b. Identifiers/Open-Ended Terms

c. COSATI Field/Group

18. Availability Statement:	19. Security Class (This Report)	21. No. of Pages
Release Unlimited	UNCLASSIFIED	126
	20. Security Class (This Page) UNCLASSIFIED	22. Price

(See ANSI-Z39.18) See Instructions on Reverse OPTIONAL FORM 272 (4-77) (Formerly NTIS-35) Department of Commerce

ABSTRACT

This report consists of Part I of the dissertation submitted by the author to the Graduate Division of the University of California, Berkeley, in partial satisfaction of the requirements for the degree of Doctor of Philosophy in Engineering.

In this report, the dam-reservoir interaction effects considering incompressible fluid are presented. The hydrodynamic effect represented by an added-mass matrix is evaluated by two basically different procedures--a Generalized Westergaard Formula and the Galerkin Finite Element Method. Pressure solutions acting on gravity dams, cylindrical arch dams and general arch dams are compared for the different procedures. Rigorous mode shape and frequency correlations are carried out, and based on the results of the correlation studies a most efficient procedure is suggested, which is shown to be adequate for engineering purposes.

ACKNOWLEDGEMENTS

Many people have assisted me during the course of my graduate studies. I am most thankful to Professor Ray W. Clough, my thesis advisor and the Chairman of my dissertation committee.His inspiration, patience and guidance are deeply appreciated, and I will always remember his fine example.

I am also grateful to Professors E. L. Wilson and C. D. Mote, members of my dissertation committee, for their valuable suggestions, encouragement and friendly guidance.

I wish to express my gratitude to Dr. John F. Hall for many valuable discussions during the first part of my research, and to Professor R. L. Taylor for making his computer program FEAP available.

This research has been part of the U.S.-R.O.C. Cooperative Research Program. Financial support from the National Science Foundation is gratefully acknowledged. Computer facilities were provided by the Lawrence Berkeley Laboratory, University of California, Berkeley. I also want to thank Toni Avery for her excellent typing.

I am greatly indebted to Drs. Bill & Lydia Yap and Don & Nancy Mangold, two Christian couples, who provided care concern and encouragement throughout my graduate studies.

Above all, I wish to express my gratitude to my family for their unfailing support, understanding,encouragement and love.

TABLE OF CONTENTS

Page

LIST OF FIGURES

1. INTRODUCTION

1.1 Objectives

Hydrodynamic effects induced by the impounded water may have significant influence on the response of a dam subjected to earthquake excitation. Current technique is well capable of analyzing a linear dam-reservoir interaction system, taking into account the hydrodynamic effects. (4-7, 9-13,16,18,19). But the responses of dam-reservoir systems to most Design Base Earthquake (DBE)* are likely to be nonlinear, so that we can no longer employ the frequency domain solution technique to deal with hydrodynamic effects as in many of the works being done up to date. (4-7,16,18,19). Time domain solution is left as the only alternative. While to economically include the water compressibility of infinite reservoir+ in time domain solution is still under research, the hydrodynamic effects due to an incompressible water reservoir can be readily taken into account in the time domain solution of a dam-reservoir interaction system. The easiest way to deal with the hydrodynamic effects of an imcompressible water reservoir is by employing the "added-mass" concept (1). It is the objective of this work to investigate and select a most reasonable and economical method that can count for the hydrodynamic effects of incompressible water reservoir in the form of added-mass. For the general geometry of concrete dams, the Generalized Westergaard Formula and the Galerkin Finite Element Method are among the candidates. Rigorous analyses of mode shapes and frequencies are compared with the field experimental work, and the results serve as the major indication of the validity of the method.

---

* DBE is an earthquake intensity corresponding to a return period of 100 years (also see Section 5.3).

\+ Infinite reservoir has been used in general for easier analytical solution simulating out-bound energy radiation condition for a very large reservoir.

1.2 State of the Art

The Finite Element Method with the aid of high speed digital computer has enabled us to analyze all types of complex civil engineering structures. But one of the difficulties remained in today's structural analysis techniques is to evaluate the effects of various kinds of loadings arise from the environment where the structures are located. The hydrodynamic loading effects upon the dams are few among them. Since the early part of the twenties, the influence of hydrodynamic effects on the responses of the dams have long been an interested topic, especially in the event of earthquake.

In 1933, professor H. M. Westergaard (1) firstly established a rational standard procedure to take into account the hydrodynamic loadings on gravity dams during earthquakes. Although the case he studied was limited to rigid dams with vertical upstream face, and infinitely long reservoirs, ignoring surface waves and considering only small displacements of fluid particles, this work was regarded as a milestone. Especially the concept of added-mass, which he introduced for the incompressible water reservoir, greatly simplified the analysis procedure of the response of a dam considering hydrodynamic effects during earthquakes. Brahtz and Heilbron (2) followed up with a discussion on the effects of a finite reservoir, compressibility of the water and flexibility of the dams. In 1952, Zangar (3) furthered Westergaard's work; by using an electric analog he investigated the effects of a sloping upstream face and provided results on added-mass representations of hydrodynamic effects for a broader class of dams that can be idealized as 2-dimensional monoliths. Zienkiewicz and Nath (13) later used the same technique to apply Zangar's work to 3-dimensional arch dams.

Lately, Chopra has carried out a series of investigations (4-7) on various aspects of hydrodynamic effects in the earthquake response of gravity dams; in the more recent work he included also effects of the foundation modelled as an elastic half-space (24). Following pretty much the same path, Porter (18) extended the work of Perumalswami (25) to formulate explicit mathematical solutions for the fluid domain retained by an arch dam considering the responses to all components of ground motion. The reservoir considered was defined by a cylindrical dam face of constant radius, a horizontal floor, and vertical radial banks enclosing a central angle of 90^{o}. Recently, Hall (19) has developed a numerical scheme to deal with arbitrary geometries of reservoir of arch dams. Effects of water compressibility, flexibility of the dam, energy radiation in infinite reservoir and vertical ground motion contributions (14) are thoroughly treated by his procedure. At the same time, in modelling an infinite reservoir, Saini et al.(16) used an infinite element and obtained similar results as Chopra; Nath (17) employed a conformal mapping technique and obtained economical and reasonably good accuracy. However, all these works are restricted to solutions in frequency domain.

Priscu et al. (8) used a finite difference method to solve for arch dam-reservoir system responses in the time domain, considering compressible water reservoir. Contrary to Chopra, he concluded that the water compressibility could change significantly the seismic response of a slender dam (e.g., arch dam). In the particular case he studied, the dam displacements could reduce up to 50% if water compressibility is not neglected. This discrepancy in findings concerning the effects of water compressibility implies the need for further research.

More recently, Muller (26) attempted an approximation method in the time domain, taking into account the water compressibility of the reservoir by a "second added mass" concept; the idea is good, but it still falls short in its ability to handle a large reservoir.

1.3 Scope

In Chapter 2, the simpliest representation of hydrodynamic effect, that is, the added-mass derived from Westergaard's classical solution, is reviewed and generalized, considering arbitrary geometry and orientation of the upstream face of arch dams. Also an appropriate lumping process is described.

The Galerkin Finite Element Discretization of the wave equation that governs the pressure behavior in an imcompressible fluid domain is presented in Chapter 3. A consistent lumping process for this procedure that maintains symmetry of the resulting added-mass is also presented.

Chapter 4 describes computer implementations of the preceding concepts, and also presents numerical solutions for pressures given by the various schemes and compares their results. The range of applicability of each method is indicated.

In Chapter 5, numerical solutions of the mode shapes and frequencies obtained by each method are correlated with results of field measurements on Techi Arch Dam; variable water level is considered. From these correlation studies, a most reasonable and economical method is suggested. Finally, stress responses of Techi Arch Dam due to static loadings, the Design Base Earthquake and hydrodynamic effects calculated by the suggested method are presented.

Final conclusions and remarks concerning the needs in further research on the time domain solutions of infinite compressible water reservoir are discussed in Chapter 6.

2. GENERALIZED WESTERGAARD FORMULA

2.1 Review of the Classical Westergaard Formula

In Westergaard's classical work (1), dealing with water pressures on dams during earthquakes, he did not try to consider every possible effect; rather, as a good engineer will do, he made reasonable assumptions for the case he studied, and was able to obtain reasonable solutions for engineering use.

The assumptions he made are the following:

(1) dam was idealized as a 2-dimensional rigid monolith with vertical upstream face;

(2) the reservoir extends to infinity in the upstream direction;

(3) displacements of fluid particles are small;

(4) surface waves are ignored;

(5) only horizontal ground motion in the upstream-downstream direction is considered.

According to these assumptions, he posed an initial boundary value problem, and obtained pressure solutions on the upstream face of the dam. For the purpose of practical engineering use, he approximated the pressure solution (for an incompressible reservoir) with a parabola, which he felt to be better than a quadrant of an ellipse. Later, he observed that "the pressures are the same as if a certain body of water were forced to move back and forth with the dam while the remainder of the reservoir is left inactive". The amount of the water included was determined by equating the inertia forces of this body of water to the pressures that actually were exerted upon the face of the dam under the same motion of the dam.

Thus, Westergaard suggested (Fig. I-1(a)), that the dynamic pressure could be expressed as:

$$p_Z = \frac{7}{8} aw\sqrt{H(H-Z)} = \frac{7}{8} \rho\ddot{r}_g\sqrt{H(H-Z)} \qquad (2.1)$$

where

a = horizontal ground acceleration, in units of g (gravitational acceleration)

w = unit weight of water

$\ddot{r}_g$ = horizontal ground acceleration

ρ = unit mass of water

H = depth of reservoir above the base of the dam

Z = distance from the base of the dam

p_Z = hydrodynamic pressure at height Z from the base of the dam, applied normally to the dam face.

Equation (2.1) indicates that the hydrodynamic pressure exerted normally on the upstream face of the dam, at height Z above the base of the dam, due to ground acceleration $\ddot{r}_g$ (that is, the total acceleration of dam face at height Z, because the dam is rigid), is equivalent to the inertia force of a prismatic body of water of unit cross-section and length $\frac{7}{8}\sqrt{H(H-Z)}$, attached firmly to the face of the dam, and moving with the dam back and forth in the direction normal to the face of the dam (that is, horizontally) without friction.

This body of water attached to the dam face and moving with the dam, is the "added-mass" applied by the reservoir to the dam, a concept first introudced by Westergaard, that has greatly simplified the dynamic response analysis of dams with hydrodynamic effects.

2.2 Generalized Westergaard Formula (9,10,27)

Employing the concept of "added-mass" as mentioned in Section 2.1 above, we now generalize it by applying the following assumption:

The hydrodynamic pressure exerted on any point of the upstream face of a dam, due to the total acceleration $\ddot{r}_n^t$ normal to the dam face at that point, is equal to the inertia force produced by a prismatic body of water of unit cross-section with length $\frac{7}{8}\sqrt{H(H-Z)}$, where Z is the height of that point above the base of the dam, that attached firmly normal to the dam face at that point, and moving back and forth with the dam in the normal direction without friction. (Fig. I-1(b)).

According to this definition, the "added-mass" is generalized to be applicable to the general geometry of the upstream face of flexible arch dams, because it depends only on the total normal acceleration at local points.

Now in the finite element analysis of the response of the dam, if we have discretized the dam body into finite elements, then, at a certain node "i" on the upstream face of the dam, the hydrodynamic pressure is:

$$p_i = \alpha_i \ddot{r}_{ni}^t \tag{2.2}$$

where

p_i = hydrodynamic pressure at node "i", compression as positive

$\ddot{r}_{ni}^t$ = total normal acceleration at node "i"

α_i = Westergaard pressure coefficient $\frac{7}{8}\rho\sqrt{H_i(H_i-Z_i)}$

ρ = mass density of the water

H_i = depth of water at the vertical section that includes node "i"

Z_i = height of node "i" above the base of the dam

But the total normal acceleration $\ddot{r}_{ni}^t$ can be represented in terms of cartesian coordinate compoents of the ground acceleration $\ddot{r}_{gx}$, $\ddot{r}_{gy}$, $\ddot{r}_{gz}$, and of acceleration components at node i relative to the base of the dam $\ddot{r}_{xi}$, $\ddot{r}_{yi}$ and $\ddot{r}_{zi}$. Making use of direction cosines with respect to the normal direction at node i, we have:

$$\ddot{r}^t_{ni} = \lambda_i \ddot{r}^t_i = \lambda_i \left(\begin{Bmatrix} \ddot{r}_x \\ \ddot{r}_y \\ \ddot{r}_z \end{Bmatrix} + \underline{\beta}_i \begin{Bmatrix} \ddot{r}_{gx} \\ \ddot{r}_{gy} \\ \ddot{r}_{gz} \end{Bmatrix} \right) \tag{2.3}$$

where

$\ddot{r}^t_i = \langle \ddot{r}^t_x \; \ddot{r}^t_y \; \ddot{r}^t_z \rangle^T_i$ total acceleration of degrees of freedom at node i

$\lambda_i = \langle \lambda_x \; \lambda_y \; \lambda_z \rangle_i$, normal direction cosines at node "i"

$\underline{\beta}_i$ = a (3 x 3) displacement transformation matrix of which the entry β_{jk} stands for the acceleration of node "i" in j-direction (j,k = 1,2,3 representing x,y,z-direction, respectively) due to a unit ground acceleration in k-direction while the dam is undergoing rigid body motion.

Substituting Eq. (2.3) into Eq. (2.2) leads to the hydrodynamic pressure at node i expressed in terms of ground accelerations and relative accelerations at node i:

$$p_i = \alpha_i \lambda_i \ddot{r}^t_i = \alpha_i \lambda_i (\ddot{r}_i + \underline{\beta}_i \ddot{r}_g) \tag{2.4}$$

Hydrodynamic pressures at any point on the face of the dam can be found in a similar way. But in the finite element solution procedure, these external pressures must be integrated over the appropriate surface of the dam to obtain the nodal loads. In this lumping process, the hydrodynamic nodal forces are expressed in terms of nodal accelerations, by Eqs. (2.2) and (2.3), thus, the coefficient in this expression will be the equivalent added-mass.

2.3 Tributary Area Lumping Process

The easiest way to lump hydrodynamic pressures into equivalent hydrodynamic nodal forces, is to multiply by the tributary area associated with a node i; thus:

$$F_{ni} = -p_i \, A_i \tag{2.5}$$

where

F_{ni} = equivalent normal hydrodynamic nodal force, outward normal from the dam face as positive

p_i = hydrodynamic pressure at node i, compression as positive

A_i = tributary area associated with node i.

Note here, that the hydrodynamic pressure was assumed to be constant over the tributary area, and to have the magnitude as at node i. Also, since the hydrodynamic pressures act normal to the dam face, so is the equivalent hydrodynamic nodal force, in the average sense, also normal to the dam face. Hence, the 3 components of the equivalent hydrodynamic forces at node i in Rectangular Cartesian Coordinate (RCC) frame can be found as before. Premultiplying F_{ni} by normal direction cosines at node i, thus leads to the cartesian coordinate values

$$\underset{\sim}{F}_i = F_{ni} \, \underset{\sim}{\lambda}_i^T \tag{2.6}$$

where

$\underset{\sim}{F}_i = \langle F_x \; F_y \; F_z \rangle_i^T$

$\underset{\sim}{\lambda}_i = \langle \lambda_x \; \lambda_y \; \lambda_z \rangle_i$

Substituting Eqs. (2.4)and (2.5) into Eq. (2.6), leads to;

$$\underset{\sim}{F}_i = -\underline{M}_{as_i}(\underset{\sim}{\ddot{r}}_i + \underline{\beta}_i \underset{\sim}{\ddot{r}}_g) \tag{2.7}$$

where

$\underset{\sim}{\ddot{r}}_i = \langle \ddot{r}_x \; \ddot{r}_y \; \ddot{r}_z \rangle_i^T$

$\underset{\sim}{\ddot{r}}_g = \langle \ddot{r}_{gx} \; \ddot{r}_{gy} \; \ddot{r}_{gz} \rangle_i^T$

$$\underline{M}_{as_i} = \alpha_i \, A_i \, \underset{\sim}{\lambda}_i^T \, \underset{\sim}{\lambda}_i = \alpha_i \, A_i \begin{bmatrix} \lambda_x^2 & & \underline{\text{sym.}} \\ \lambda_y \lambda_x & \lambda_y^2 & \\ \lambda_z \lambda_x & \lambda_z \lambda_y & \lambda_z^2 \end{bmatrix}_i \tag{2.8}$$

$\underline{M}_{as_i}$ is the added-mass matrix associated with node i and following the direct stiffness assembly procedure, the equivalent hydrodynamic nodal force equations for the dam became:

$$\begin{Bmatrix} \underset{\sim}{F}_1 \\ \underset{\sim}{F}_2 \\ \vdots \\ \underset{\sim}{F}_m \end{Bmatrix} = - \begin{bmatrix} \underline{M}_{as1} & & & \\ & \underline{M}_{as2} & & \\ & & \ddots & \\ & & & \underline{M}_{asm} \end{bmatrix} \begin{Bmatrix} \ddot{\underset{\sim}{r}}_i \\ \ddot{\underset{\sim}{r}}_z \\ \vdots \\ \ddot{\underset{\sim}{r}}_m \end{Bmatrix} - \begin{bmatrix} \underline{M}_{as1} & & & \\ & M_{as2} & & \\ & & \ddots & \\ & & & \underline{M}_{asm} \end{bmatrix} \begin{Bmatrix} \underline{\beta}_1 \\ \underline{\beta}_2 \\ \vdots \\ \underline{\beta}_m \end{Bmatrix} \begin{Bmatrix} \ddot{r}_{gx} \\ \ddot{r}_{gy} \\ \ddot{r}_{gz} \end{Bmatrix}$$

or,

$$\underset{\sim}{F}_{(3m\times1)} = -\underline{M}_{as_{(3m\times3m)}} \ddot{\underset{\sim}{r}}_{(3m\times1)} - \underline{M}_{as_{(3m\times3m)}} \underline{B}_{(3m\times3)} \ddot{\underset{\sim}{r}}_{g(3\times1)} \qquad (2.9)$$

where m = total number of nodes of the dam on its upstream face.

$\underline{M}_{as}$ in Eq. (2.9) is the added-mass coefficient matrix for the dam resulting from the hydrodynamic pressures upon the upstream face of the dam. It is uncoupled between nodal points. Also, notice that the same Westergaard pressure coefficient is used, regardless whether the total nodal accelerations came from the vertical or horizontal component of ground accelerations.

The equivalent hydrodynamic nodal force $\underset{\sim}{F}$ from Eq. (2.9) is an additional loading vector to be incorporated into the right hand side of the equation of motion of the dam:

$$\underline{M}_{(n\times n)} \ddot{\underset{\sim}{v}}^t_{(n\times1)} + \underline{C}_{(n\times n)} \dot{\underset{\sim}{v}}_{(n\times1)} + \underline{K}_{(n\times n)} \underset{\sim}{v}_{(n\times1)} = \underset{\sim}{P}_{(n\times1)} \qquad (2.10)$$

where

$\underline{M}$, $\underline{C}$, $\underline{K}$ = mass, damping and stiffness matrices respectively of the dam structure;

$\dot{\underset{\sim}{v}}$, $\underset{\sim}{v}$ = velocity and displacement vectors respectively of the entire dam, including internal degrees of freedom of the dam structure;

$\ddot{\underset{\sim}{v}}^t$ = total acceleration vector of the dam structure;

$$\underset{\sim}{P} = \left\{ \begin{array}{c} \underset{\sim}{0} \\ \hline \underset{\sim}{F}_{(3m\times1)} \end{array} \right\}$$, where $\underset{\sim}{F}$ is obtained from Eq. (2.9);

n = total number of degrees of freedom of the entire dam structure.

Alternatively, if we write Eq. (2.9) as follows:

$$\left\{ \begin{array}{c} \underset{\sim}{0} \\ \underset{\sim}{F} \end{array} \right\}_{(n\times1)} = - \begin{bmatrix} 0 & 0 \\ 0 & \underline{M}_{as} \end{bmatrix}_{n\times n} \left\{ \begin{array}{c} \ddot{\underset{\sim}{r}}{}^t_d \\ \ddot{\underset{\sim}{r}}{}^t_s \end{array} \right\} = -\underline{M}_a \, \ddot{\underset{\sim}{v}}{}^t \tag{2.11}$$

where

$\ddot{\underset{\sim}{r}}{}^t_d$ = total acceleration of internal degrees of freedom of the dam;

$\ddot{\underset{\sim}{r}}{}^t_s = \ddot{\underset{\sim}{r}}_{(3m\times1)} + \underline{B}\,\ddot{\underset{\sim}{r}}_g$, from Eq. (2.9).

Then, Eq. (2.10) can be rewritten as:

$$(\underline{M} + \underline{M}_a)\, \ddot{\underset{\sim}{v}}{}^t + \underline{C}\, \dot{\underset{\sim}{v}} + \underline{K}\, \underset{\sim}{v} = 0 \tag{2.12}$$

3. GALERKIN FINITE ELEMENT METHOD

3.1 Galerkin Method for Wave Equation (11,12,27)

In this formulation of reservoir interaction, the hydrodynamic pressures in the reservoir are assumed to be governed by the pressure wave equation (Fig. I-2(a)):

$$\nabla^2 p(x,y,z,t) = \frac{1}{C^2}\ \ddot{p}(x,y,z,t) \tag{3.1}$$

where

$p(x,y,z,t)$ = pressure distributions in the reservoir;

$C = \sqrt{K/\rho}$ is the sonic wave velocity;

K = bulk modulus of the fluid;

ρ = mass density of the fluid.

In order to find the hydrodynamic pressures acting on the face of a dam, Eq. (3.1) must be solved with appropriate boundary conditions. Since our interest is in finding added-mass representations of the hydrodynamic effects, after we have found the hydrodynamic pressures due to accelerations at face of the dam, they must be lumped into equivalent hydrodynamic nodal forces. Thus, the hydrodynamic forces are related to accelerations at the nodal degrees of freedom on the face of the dam leading to the added-mass coefficient matrix. For this purpose, the boundary conditions to be imposed on the reservoir boundaries (Fig. I-2(b)) are as follows:

(1) at dam-reservoir interface: $\frac{\partial p}{\partial n_s} = -\rho \ddot{v}^t_{n_s}$;

(2) at floor or reservoir: $\frac{\partial p}{\partial n_s} = 0$, or $\ddot{v}^t_{n_s} = 0$;

(3) at upstream end of reservoir: $\frac{\partial p}{\partial n_s} = 0$, or $\ddot{v}^t_{n_s} = 0$;

(4) at free surface of reservoir: $p = 0$, or surface waves are neglected ;

(5) at canyon walls: $\frac{\partial p}{\partial n_s} = 0$, or, $\ddot{v}^t_{n_s} = 0$. (3.2)

where n_s is the outward normal direction from the reservoir surface, and

$\ddot{v}^t_{n_s}$ is the total normal acceleration of the fluid at the boundaries of the reservoir. The acceleration is positive when fluid moves outward from the reservoir. It is also of interest to note that, if we want to include surface waves, then, condition (4) becomes $\frac{\partial p}{\partial n_s} = - \ddot{P}$; if we want to consider the flexibility of the floor and canyon walls, conditions (2) and (5) become $\frac{\partial p}{\partial n_s} = - \rho \ddot{v}^t_{n_s}$, where the acceleration $\ddot{v}^t_{n_s}$ is defined as was mentioned above; if we want to investigate the effects due to relative motion at upstream end of the reservoir, condition (3) becomes $\frac{\partial p}{\partial n_s} = - \rho \ddot{v}^t_{n_s}$, etc.

Now we proceed to seek the hydrodynamic pressure solution of Eq. (3.1) with the boundary conditions of Eq. (3.2). But because the geometry of the reservoir generally is irregular, it will be extremely difficult to find a closed form solution; therefore, we seek a numerical solution based on the Galerkin Finite Element Method.

The Galerkin Method is a weighted residual method; its residual is weighted in such a way that the approximate numerical solution will be orthogonal to the error of the numerical solution; and thus, in the energy norm, the numerical solution minimizes the residual caused by the error.

Letting $\overline{p}$ be the approximate numerical solution of Eq. (3.1) with boundary conditions Eq. (3.2), then the residual of Eq. (3.1) due to the error in approximate solution $\overline{p}$ is,

$$\nabla^2 \overline{p} - \frac{1}{C^2} \ddot{\overline{p}} = R \tag{3.3}$$

where R is a residual of very small magnitude.

The Galerkin Method is expressed as,

$$\iiint_V \underset{\sim}{N}^T \left(\nabla^2 \overline{p} - \frac{1}{C^2} \ddot{\overline{p}}\right) dV = \underset{\sim}{0} \tag{3.4}$$

where $\underset{\sim}{N}$ is a row vector of weighting functions. Applying Green's Theorem (or integration by parts) to Eq. (3.4), we have,

$$\iint_S \underset{\sim}{N}_s^T \frac{\partial \bar{p}}{\partial n_s}\, dA - \frac{1}{C^2} \iiint_V \underset{\sim}{N}^T \ddot{\bar{p}}\, dV - \iiint_V \nabla \underset{\sim}{N}^T \cdot \nabla \underset{\sim}{\bar{p}}\, dV = 0 \qquad (3.5)$$

The first term of Eq. (3.5) only exists along the boundaries; applying the boundary condition Eq. (3.2) to it, we have,

$$\iint_S \underset{\sim}{N}_s^T \frac{\partial \bar{p}}{\partial n_s}\, dA = -\rho \iint_S \underset{\sim}{N}_s^T \ddot{v}^t_{n_s}\, dA \qquad (3.6)$$

which now only exists along dam-reservoir interface, because $\ddot{v}^t_{n_s}$ vanishes along all other boundaries according to Eq. (3.2). To relate this to the motion of dam face, we observe that at the same point on the dam-reservoir interface, the fluid acceleration $\ddot{v}^t_{n_s}$ can be expressed in terms of the acceleration of the dam face $\ddot{r}^t_{n_s}$. However, it must be noticed that $\ddot{r}^t_{n_s}$ is positive when outward normal from the dam face (Fig. I-2(a)), while $\ddot{v}^t_{n_s}$ is positive when outward normal from the reservoir (Fig. I-2(b)), thus,

$$\ddot{v}^t_{n_s} = - \ddot{r}^t_{n_s} \qquad (3.7)$$

Moreover, the normal acceleration of the dam face $\ddot{r}^t_{n_s}$ can be expressed in terms of the normal direction cosines and three RCC components; that is,

$$\ddot{r}^t_{n_s} = \underset{\sim}{\lambda}\, \underset{\sim}{\ddot{U}}^t \qquad (3.8)$$

where

$\underset{\sim}{\lambda} = \langle \lambda_x\ \lambda_y\ \lambda_z \rangle$ the direction cosines at the point where $\ddot{r}^t_{n_s}$ locates

$\underset{\sim}{\ddot{U}}^t = \langle \ddot{U}^t_x\ \ddot{U}^t_y\ \ddot{U}^t_z \rangle^T$ total acceleration of the dam face in RCC components.

Substituting Eqs. (3.6), (3.7) and (3.8) into (3.5), we have,

$$\rho \iint_S \underset{\sim}{N}_s^T \underset{\sim}{\lambda}\, \underset{\sim}{\ddot{U}}^t\, dA = \frac{1}{C^2} \iiint_V \underset{\sim}{N}^T \ddot{\bar{p}}\, dV + \iiint_V \nabla \underset{\sim}{N}^T \cdot \nabla \underset{\sim}{\bar{p}}\, dV \qquad (3.9)$$

For compressible water, C = 4720 ft/sec, but for incompressible water, $C \to \infty$, thus Eq. (3.9) becomes,

$$\iiint_V \nabla \underset{\sim}{N}^T \cdot \nabla \underset{\sim}{\bar{p}} \, dV = \rho \iint_S \underset{\sim}{N}_S^T \, \underset{\sim}{\lambda} \, \underset{\sim}{\ddot{U}}^t \, dA \tag{3.10}$$

This is the Galerkin weak form of pressure wave equation; for an incompressible reservoir, it relates liquid pressures to the accelerations of the face of the dam.

3.2 Finite Element Formulations

According to Galerkin Finite Element Method, after the Galerkin form of the field differential equation has been obtained, we discretize the domain by Finite Element Method, using as weighting functions the basic interpolation functions of the elements.

Examine again Eq. (3.10),

$$\iiint_V \nabla \underset{\sim}{N}^T \cdot \nabla \underset{\sim}{\bar{p}} \, dV = \rho \iint_S \underset{\sim}{N}_S^t \, \underset{\sim}{\lambda} \, \underset{\sim}{\ddot{U}}^t \, dA \tag{3.10}$$

where V is the fluid domain, S is the dam-reservoir interface. We now discretize the fluid domain into 3-D finite elements, and the interface correspondingly into 2-D finite elements(the interface is 2-D in natural coordinates, but 3-D in RCC space). For a point within the element e in the fluid domain, its appropriate hydrodynamic pressures $\bar{p}^{(e)}$can be expressed as follows, according to the Finite Element Method:

$$\bar{p}^{(e)} = \underset{\sim}{N}^{(e)} \, \underset{\sim}{p}^{(e)} \tag{3.11}$$

where

$\underset{\sim}{N}^{(e)}$ = row vector of interpolation functions associated with nodes of the element e,

$\underset{\sim}{p}^{(e)}$ = column vector of nodal pressures of the element e.

Then, substituting Eq. (3.11) into the left hand side of Eq. (3.10), we have for element e:

$$\iiint_{V^{(e)}} \nabla \underset{\sim}{N}^{(e)^T} \cdot \nabla \underset{\sim}{\bar{p}}^{(e)} dV^{(e)} = \iiint_{V^{(e)}} \nabla \underset{\sim}{N}^{(e)^T} \cdot \nabla \underset{\sim}{N}^{(e)} dV^{(e)} \underset{\sim}{p}^{(e)}$$

or,

$$\iiint_{V^{(e)}} \nabla \underset{\sim}{N}^{(e)^T} \cdot \nabla \underset{\sim}{\bar{p}}^{(e)} dV^{(e)} = \underline{g}^{(e)} \underset{\sim}{p}^{(e)} \tag{3.12}$$

where

$$\underline{g}^{(e)}_{(KDxKD)} = \iiint_{V^{(e)}} \left(\frac{\partial \underset{\sim}{N}^{(e)^T}}{\partial x} \frac{\partial \underset{\sim}{N}^{(e)}}{\partial x} + \frac{\partial \underset{\sim}{N}^{(e)^T}}{\partial y} \frac{\partial \underset{\sim}{N}^{(e)}}{\partial y} + \frac{\partial \underset{\sim}{N}^{(e)^T}}{\partial z} \frac{\partial \underset{\sim}{N}^{(e)}}{\partial z} \right) dV^{(e)} \tag{3.13}$$

KD = number of nodes of 3-D fluid element e.

For 2-D interface elements, the accelerations $\ddot{\underset{\sim}{U}}^t$ can be approximated in a similar way. For 2-D interface element i, we have,

$$\ddot{\underset{\sim}{U}}^{(i)^t} = \underline{\phi}_s^{(i)} \ddot{\underset{\sim}{r}}^{(i)^t} \tag{3.14}$$

where

$\underline{\phi}_s^{(i)}{}_{(3x3ND)}$ = matrix of interpolation functions associated with nodal degrees of freedom of interface element i ,

$\ddot{\underset{\sim}{r}}^{(i)^t}{}_{(3NDx1)}$ = columns vector of total nodal accelerations of 2-D interface element i in RCC components ,

ND = number of nodes of 2-D interface element i.

Substituting Eq. (3.14) into the right hand side of Eq. (3.10), we have for element i:

$$\rho \iint_{S^{(i)}} \underset{\sim}{N}_s^{(i)^T} \underset{\sim}{\lambda}^{(i)} \ddot{\underset{\sim}{U}}^{(i)^t} dA^{(i)} = \rho \iint_{S^{(i)}} \underset{\sim}{N}_s^{(i)^T} \underset{\sim}{\lambda}^{(i)} \underline{\phi}_s^{(i)} dA^{(i)} \ddot{\underset{\sim}{r}}^{(i)^t}$$

or,

$$\rho \iint_{S^{(i)}} \underset{\sim}{N}_s^{(i)^T} \underset{\sim}{\lambda}^{(i)} \ddot{\underset{\sim}{U}}^{(i)^t} dA^{(i)} = \rho\, \underline{h}_s^{(i)} \ddot{\underset{\sim}{r}}^{(i)^t} \tag{3.15}$$

where

$$\underset{\sim}{h}_{s\,(ND\times 3ND)}^{(i)} = \iint_{S^{(i)}} \underset{\sim}{N}_s^{(i)^T} \underset{\sim}{\lambda}^{(i)} \underset{\sim}{\phi}_s^{(i)} dA^{(i)} \tag{3.16}$$

$\underset{\sim}{N}_{s\,(1\times ND)}^{(i)}$ = the part of the 3-D fluid element interpolation function that reduce to its 2-D interface boundary only, which is corresponding to the 2-D interface element i.

Now assembling Eq. (3.12) for all 3-D fluid elements in the reservoir, and assembling Eq. (3.15) for all 2-D interface elements on the dam-reservoir interface, we have the discretized form of Eq. (3.10):

$$\sum_e \underset{\sim}{g}^{(e)} \underset{\sim}{p}^{(e)} = \rho \sum_i \underset{\sim}{h}_s^{(i)} \underset{\sim}{\ddot{r}}^{(i)^t} \tag{3.17}$$

or,

$$\begin{bmatrix} \underset{\sim}{g}_{rr} & \underset{\sim}{g}_{rs} \\ (NER\times NER) & (NER\times NES) \\ \underset{\sim}{g}_{sr} & \underset{\sim}{g}_{ss} \\ (NES\times NER) & (NES\times NES) \end{bmatrix} \begin{Bmatrix} \underset{\sim}{p}_r \\ (NER\times 1) \\ \underset{\sim}{p}_s \\ (NES\times 1) \end{Bmatrix} = \rho \begin{bmatrix} 0 & 0 \\ & (NER\times NLL) \\ 0 & \underset{\sim}{h}_s \\ & (NES\times NLL) \end{bmatrix} \begin{Bmatrix} \underset{\sim}{0} \\ \\ \underset{\sim}{\ddot{r}}_s^t \\ (NLL\times 1) \end{Bmatrix} \tag{3.18}$$

where

$\underset{\sim}{p}_r$ = nodal pressures of fluid elements that are not on an interface nor on a free surface;

$\underset{\sim}{p}_s$ = nodal pressures of fluid elements that are on the dam-reservoir interface, but not at a free surface;

$\underset{\sim}{g}_{rr}$, $\underset{\sim}{g}_{rs}$, $\underset{\sim}{g}_{sr}$, $\underset{\sim}{g}_{ss}$ = submatrices of $\underset{\sim}{g}$ partitioned according to $\underset{\sim}{p}_r$ and $\underset{\sim}{p}_s$;

$\underset{\sim}{g}$ = assembled matrix of Eq. (3.13) over the entire fluid domain;

$\underset{\sim}{h}_s$ = assembled matrix of Eq. (3.16) over the dam-reservoir interface;

$\underset{\sim}{\ddot{r}}_s^t$ = nodal total accelerations of dam face, including those nodes at free surface;

NER = number of nodes of fluid elements that are not on an interface nor on a free surface;

NES = number of nodes of fluid elements that are on an interface, but not on free surface;

NER+NES = NEQ, total number of nodes in the reservoir, excluding all free surface nodes;

NLL = total number of nodal acceleration RCC components on the interface including those at the free surface.

The pressures on the free surface vanish according to boundary condition (4) of Eq. (3.2), therefore, they do not enter into the assembling process of matrix $\underline{g}$.

Since we are only interested in finding the hydrodynamic pressures acting upon the interface, that is the vector $\underset{\sim}{p}_s$, we don't have to solve the entire system of equations of Eq. (3.18); rather it is convenient and more economical to do a static condensation on Eq. (3.18) first, to condense out NER equations that are associated with $\underset{\sim}{p}_r$. Since there is nothing on the right hand side associated with $\underset{\sim}{p}_r$, we need only to do static condensation operations on the left hand side of Eq. (3.18), that is, on matrix $\underline{g}$. Thus we have,

$$\underline{g}_s \, \underset{\sim}{p}_s = \rho \, \underline{h}_s \, \ddot{\underset{\sim}{r}}_s^t \tag{3.19}$$

where

$$\underline{g}_{s\,(NES \times NES)} = \underline{g}_{ss} - \underline{g}_{sr} \, \underline{g}_{rr}^{-1} \, \underline{g}_{rs} \tag{3.20}$$

is a symmetric matrix, and,

$$\underset{\sim}{p}_s = \rho \, \underline{g}_s^{-1} \, \underline{h}_s \, \ddot{\underset{\sim}{r}}_s^t \tag{3.21}$$

After $\underset{\sim}{p}_s$, that is the hydrodynamic pressures acting upon the dam-reservoir interface, have been found from Eq. (3.21), the next step is to lump the hydrodynamic pressures into equivalent nodal hydrodynamic forces, and thus to obtain the added-mass coefficient matrix. This operation is equivalent to that described in Chapter 2.

3.3 Consistent Lumping Process

The consistent lumping process making use of the virtual displacement method is the most appropriate procedure for converting the hydrodynamic pressures of Eq.(3.21) into equivalent nodal forces (Fig. I-3(c)); that is, by introducing a virtual displacement field into the domain and equating to zero the virtual work. Let's now consider a 2-D interface element i, which corresponds to a 3-D fluid element e; in other words, element i overlaps the upstream surface of concrete element e of the dam at dam-reservoir interface. From Eq. (3.21) we can obtain pressure values at discrete nodal points; that is, for element i, we can obtain its nodal pressures. Then, the pressure distributions over the domain of element i can be expressed as,

$$\bar{p}_s^{(i)} = \underset{\sim}{N}_s^{(i)} \; \underset{\sim}{p}_s^{(i)} \tag{3.22}$$

where

$\bar{p}_s^{(i)}$ = pressure at any point on interface element i ;

$\underset{\sim}{N}_{s\,(1xND)}^{(i)}$ = part of fluid element e interpolation functions that are reduced to its 2-D interface boundary only, that is, nonvanishing only on the surface corresponding to interface element i ;

$\underset{\sim}{p}_{s\,(NDx1)}^{(i)}$ = nodal pressures of interface element i.

Now we introduce a virtual displacement field, $\delta\underset{\sim}{U}^{(i)}$ at any point, into the domain of interface element i by introducing nodal displacements at nodal points of element i, $\delta\underset{\sim}{r}^{(i)}$, and, as in Eq. (3.14), with the interpolation functions $\underset{\sim}{\phi}_s^{(i)}$, we have,

$$\delta\underset{\sim}{U}^{(i)} = \underset{\sim}{\phi}_s^{(i)} \; \delta\underset{\sim}{r}^{(i)} \tag{3.23}$$

Then, equating the virtual work done by the hydrodynamic pressures to the virtual work done by their equivalent hydrodynamic nodal forces, we have,

$$\delta \underset{\sim}{r}^{(i)^T} \underset{\sim}{F}^{(i)} = - \iint_{S^{(i)}} \delta r_{n_s}^{(i)} \, \bar{p}_s^{(i)} \, dA^{(i)} \tag{3.24}$$

where

$\underset{\sim}{F}^{(i)}_{(3NDx1)}$ = equivalent hydrodynamic nodal forces of 2-D interface element i ,

$\delta r_{n_s}^{(i)}$ = normal virtual displacement at the point where $\bar{p}_s^{(i)}$ applies.

Notice here that the negative sign is due to the fact that $\bar{p}_s^{(i)}$ is positive for compression and $\delta r_{n_s}^{(i)}$ is positive when the interface moving outward normal from the dam face,therefore,resulting in negative virtual work. Furthermore, as in Eq. (3.8), we can express $\delta r_{n_s}^{(i)}$ in terms of $\delta \underset{\sim}{U}^{(i)}$, that is,

$$\delta r_{n_s}^{(i)} = \underset{\sim}{\lambda} \, \delta \underset{\sim}{U}^{(i)} = \delta \underset{\sim}{U}^{(i)^T} \underset{\sim}{\lambda}^T \tag{3.25}$$

where $\underset{\sim}{\lambda}$ is the normal direction cosines at the point where $\delta \underset{\sim}{U}^{(i)}$ locates. Substituting Eqs. (3.22), (3.23) and (3.25) into Eq. (3.24), we have

$$\delta \underset{\sim}{r}^{(i)^T} \underset{\sim}{F}^{(i)} = - \delta \underset{\sim}{r}^{(i)^T} \iint_{S^{(i)}} \underline{\Phi}_s^{(i)^T} \underset{\sim}{\lambda}^T \underset{\sim}{N}_s^{(i)} \, dA^{(i)} \, \underset{\sim}{p}_s^{(i)}$$

or,

$$\underset{\sim}{F}^{(i)} = - \underline{h}_s^{(i)^T} \underset{\sim}{p}_s^{(i)} \tag{3.26}$$

where $\underline{h}_s^{(i)}$ is defined in Eq. (3.16).

Assembling Eq. (3.26) over the entire dam-reservoir interface, we have,

$$\underset{\sim}{F}_{(NLLx1)} = - \underline{h}^T_{s\,(NLLxNES)} \, \underset{\sim}{p}_{s\,(NESx1)} \tag{3.27}$$

Then, introducing Eq. (3.21) into Eq. (3.27), we find,

$$\underset{\sim}{F} = - \rho \, \underline{h}_s^T \, \underline{g}_s^{-1} \, \underline{h}_s \, \ddot{\underset{\sim}{r}}_s^t$$

or,

$$\underset{\sim}{F} = - \underline{M}_{a_s} \ddot{\underset{\sim}{r}}_s^t \tag{3.28}$$

where

$$\underline{M}_{a_s} = \rho \, \underline{h}_s^t \, \underline{g}_s^{-1} \, \underline{h}_s \tag{3.29}$$

is the symmetric added-mass coefficient matrix for the dam, resulting from the hydrodynamic pressures acting upon the upstream face of the dam. Notice that the added-mass coefficient matrix of Eq. (3.29) which came from the Galerkin Finite Element discretization of the wave equation in the reservoir using a consistent lumping process, is in general a full matrix, coupled not only between nodal points but also among nodal degrees of freedom that are perpendicular to each other.

Expressing total accelerations $\ddot{\underset{\sim}{r}}_s^t$ in terms of relative and ground accelerations, we can rewrite Eq. (3.28) in the form similar to Eq. (2.9), thus,

$$\underset{\sim}{F}_{(NLLx1)} = - \underline{M}_{a_{s(NLLxNLL)}} \ddot{\underset{\sim}{r}}_{(NLLx1)} - \underline{M}_{a_{s(NLLxNLL)}} \underline{B}_{(NLLx3)} \ddot{\underset{\sim}{r}}_{g(3x1)} \tag{3.30}$$

As before, the equivalent hydrodynamic nodal force vector $\underset{\sim}{F}$ of Eq. (3.30) is ready to be incorporated into the right hand side of the equation of motion of the dam as an additional effective loading vector.

4. COMPUTER IMPLEMENTATIONS AND NUMERICAL SOLUTIONS

4.1 Computer Implementations

In order to illustrate the efficiency and validity of the scheme for added-mass coefficient matrix computation presented in Chapter 2 and 3, a Fortran program RSVOIR (28) was developed. It serves as a general purpose incompressible fluid added-mass preprocessor for arch dams of general geometry. The added-mass coefficient matrix can be computed from this preprocessor and then assembled with the concrete mass matrix of the dam at appropriate locations, so that the response of the dam including incompressible hydrodynamic effects can be obtained. The computational procedures (20,21,22) for obtaining the added-mass matrix with each scheme are detailed in the following sections.

4.1.1 Generalized Westergaard Formula Procedure

From Eq. (2.8) we have the added-mass coefficient matrix according to the Generalized Westergaard Formula. For the computation of added-mass coefficients associated with node i, three pieces of information are necessary:

(a) Westergaard Pressure Coefficient $\alpha_i = \frac{7}{8} \rho\sqrt{H_i(H_i-Z_i)}$

(b) tributary area A_i

(c) normal direction cosines $\underset{\sim}{\lambda}_i = \langle\lambda_x \; \lambda_y \; \lambda_z\rangle_i$

The first item, α_i, may be calculated readily when the location of node i is known. The second, A_i, is a collection of the area contributions from every interface element associated with node i, that is (Fig. I-3(b)),

$$A_i = \sum_k A_i^{(k)} \tag{4.1}$$

in which the $A_i^{(k)}$'s are evaluated most easily as,

$$A_i^{(k)} = A^{(k)} / ND(k) \tag{4.2}$$

where $A^{(k)}$ = area of interface element k

$ND(k)$ = number of nodes of interface k

The normal direction cosines, $\underset{\sim}{\lambda}_i$ (Fig. I-4), can be found from the properties of the interface finite elements associated with node i (Appendix A). Due to the finite element discretization, the normal direction cosines of the same node may differ from element to element. Therefore, the nodal mass is obtained through element by element assembly:

$$\underline{M}_{as_i} = \sum_k \alpha_i \, A_i^{(k)} \, \underset{\sim}{\lambda}_i^{(k)^T} \, \underset{\sim}{\lambda}_i^{(k)} \tag{4.3}$$

where $\underset{\sim}{\lambda}_i^{(k)}$ = normal direction cosines of interface element k, at node i. But in the standard direct stiffness method assembly procedure, the assembly is not carried out node by node, locally; rather, it is carried out element by element, globally. Therefore, the local assembly of Eq. (4.3) is accomplished only after the program has looped through the computations and assembly of all the interface elements associated with node i. The global added-mass matrix is obtained while the computations and assembly are carried out for every interface element on the dam-reservoir interface.

4.1.2 Galerkin Finite Element Procedure

The added-mass matrix of Eq. (3.29) is not obtained from the assembly process; rather, it comes from the solution at the global level. But its ingredient matrices, $\underline{g}_s$ and $\underline{h}_s$, are the result of assembling elemental contributions. In order to find added-mass matrix of Eq. (3.29), it is necessary to form the matrices $\underline{g}_s$ and $\underline{h}_s$ first.

4.1.2.1 Formation of matrix $\underline{g}_s$

As shown by Eq. (3.20), matrix $\underline{g}_s$ is a product of static condensation operating on matrix $\underline{g}$, which in turn is the global assembled form of the element coefficient matrices $\underline{g}^{(e)}$ of Eq. (3.13).

For 3-D fluid element e, the integral of Eq. (3.13) is computed numerically, thus, recall

$$\underline{g}^{(e)} = \iiint_{V^{(e)}} \left(\frac{\partial \tilde{N}^{(e)}}{\partial x}^T \frac{\partial \tilde{N}^{(e)}}{\partial x} + \frac{\partial \tilde{N}^{(e)}}{\partial y}^T \frac{\partial \tilde{N}^{(e)}}{\partial y} + \frac{\partial \tilde{N}^{(e)}}{\partial z}^T \frac{\partial \tilde{N}^{(e)}}{\partial z}\right) dV^{(e)} \tag{3.13}$$

or,

$$g_{ij}^{(e)} = \iiint_{V^{(e)}} \left(\frac{\partial N_i^{(e)}}{\partial x} \frac{\partial N_j^{(e)}}{\partial x} + \frac{\partial N_i^{(e)}}{\partial y} \frac{\partial N_j^{(e)}}{\partial y} + \frac{\partial N_i^{(e)}}{\partial z} \frac{\partial N_j^{(e)}}{\partial z}\right) dV^{(e)} \tag{4.4}$$

Employing Gaussian Quadrature to numerically integrate Eq. (4.4), we have,

$$g_{ij}^{(e)} = \sum_k \sum_m \sum_n w_k\, w_m\, w_n\, f_{ij}^{(e)}(r_k, s_m, t_n) |J_{kmn}^{(e)}| \tag{4.5}$$

where

(r_k, s_m, t_n) = Gaussian Quadrature integration points in natural coordinates (r,s,t)

w_k, w_m, w_n = Gaussian Quadrature weighting functions

$f_{ij}^{(e)}(r_k, s_m, t_n) = \left(\frac{\partial N_i^{(e)}}{\partial x} \frac{\partial N_j^{(e)}}{\partial x} + \frac{\partial N_i^{(e)}}{\partial y} \frac{\partial N_j^{(e)}}{\partial y} + \frac{\partial N_i^{(e)}}{\partial z} \frac{\partial N_j^{(e)}}{\partial z}\right)$ of element e, evaluated at (r_k, s_m, t_n).

$|J_{kmn}^{(e)}|$ = determinant of Jacobian matrix of element e, $\underline{J}^{(e)}$, evaluated at (r_k, s_m, t_n), where

$$\underline{J}^{(e)} = \begin{bmatrix} \tilde{N}_{,r}^{(e)} \tilde{X}^{(e)} & \tilde{N}_{,r}^{(e)} \tilde{Y}^{(e)} & \tilde{N}_{,r}^{(e)} \tilde{Z}^{(e)} \\ \tilde{N}_{,s}^{(e)} \tilde{X}^{(e)} & \tilde{N}_{,s}^{(e)} \tilde{Y}^{(e)} & \tilde{N}_{,s} \tilde{Z}^{(e)} \\ \tilde{N}_{,t}^{(e)} \tilde{X}^{(e)} & \tilde{N}_{,t}^{(e)} \tilde{Y}^{(e)} & \tilde{N}_{,t}^{(e)} \tilde{Z}^{(e)} \end{bmatrix}$$

in which

$$\underset{\sim}{N}^{(e)}_{,r},\ \underset{\sim}{N}^{(e)}_{,s},\ \underset{\sim}{N}^{(e)}_{,t} = \frac{\partial \underset{\sim}{N}^{(e)}}{\partial r},\ \frac{\partial \underset{\sim}{N}^{(e)}}{\partial s},\ \frac{\partial \underset{\sim}{N}^{(e)}}{\partial t} \quad \text{respectively, and}$$

$X^{(e)}, Y^{(e)}, Z^{(e)}$ = x, y, z components, respectively, of coordinates of all the nodes pertaining to element e.

Finally,

$$\begin{Bmatrix} \dfrac{\partial N_i^{(e)}}{\partial x} \\ \dfrac{\partial N_i^{(e)}}{\partial y} \\ \dfrac{\partial N_i^{(e)}}{\partial z} \end{Bmatrix} = \underline{J}^{(e)^{-1}} \cdot \begin{Bmatrix} \dfrac{\partial N_i^{(e)}}{\partial r} \\ \dfrac{\partial N_i^{(e)}}{\partial s} \\ \dfrac{\partial N_i^{(e)}}{\partial t} \end{Bmatrix}$$

Now, the numerical calculations (Eq. (4.5))are carried out for all fluid elements in the reservoir, and the results are assembled according to the direct stiffness method to form the global matrix $\underline{g}$. But so far, we have not mentioned what kind of 3-D fluid element should be used and how big should be the domain of reservoir included in the discretization.

In general, 13 to 20 node 3-D elements (Fig. I-5(b) and Appendix B) allowing quadratic variation in upstream-downstream direction are appropriate to be used as fluid elements, because they provide possible exponential decay of pressure solutions in the upstream direction. As for the size of reservoir domain to be included, it is clear that it's impossible to model an infinite reservoir; therefore, the reservoir extent in the upstream direction should be found by studies on the convergence of hydrodynamic pressures while gradually increasing reservoir domain. It has been found that for an incompressible reservoir, the hydrodynamic pressures converge adequately when the reservoir domain extends in the upstream direction three times the height of the dam.

Now, after $\underline{g}$ has been formed, using appropriate 13 to 20 node

3-D fluid elements and an adequate reservoir domain, we statically condense out those nodal degrees of freedom in the reservoir that are not on the dam-reservoir interface. The number of equations eliminated is NER as defined in Section 3.2, resulting in matrix $\underline{g}_s$ of dimension (NES x NES), where number NES is also defined in Section 3.2.

4.1.2.2 Formation of Matrix $\underline{h}_s$

The matrix $\underline{h}_s$ in Eq. (3.29) is the assembled form of $\underline{h}_s^{(i)}$ in Eq. (3.16). The integration of Eq. (3.16) is only appropriate to be carried out numerically as above. Therefore, let us recall

$$\underline{h}_s^{(i)} = \iint_{S^{(i)}} \underset{\sim}{N}_s^{(i)^T} \underset{\sim}{\lambda}^{(i)} \underline{\phi}_s^{(i)} \, dA^{(i)} \tag{3.16}$$

and apply Gaussian Quadrature integration to the integral, to obtain

$$\underline{h}_s^{(i)} = \sum_m \sum_n w_m \, w_n \, \underline{n}^{(i)}(r_m, s_n) \, |J_{mn}^{(i)}| \tag{4.6}$$

where

w_m, w_n = weighting functions of Gaussian Quadrature

(r_m, s_n) = Gaussian Quadrature integration points in natural coordinates (r,s)

$\underline{n}^{(i)}(r_m, s_m) = \underset{\sim}{N}_s^{(i)^T} \underset{\sim}{\lambda}_{mn}^{(i)} \underline{\phi}_s^{(i)}$ evaluated at the integration points (r_m, s_n)

$\underset{\sim}{\lambda}_{mn}^{(i)} = \langle \lambda_x^{(i)} \; \lambda_y^{(i)} \; \lambda_z^{(i)} \rangle_{mn}$, normal direction cosines at (r_m, s_n) of element i (Fig. I-4 and Appendix A)

$|J_{mn}^{(i)}| = |\underset{\sim}{\lambda}_{mn}^{(i)}| = (\lambda_x^{(i)^2} + \lambda_y^{(i)^2} + \lambda_z^{(i)^2})^{\frac{1}{2}}$ evaluated at (r_m, s_n)(Ref. 29).

After $\underline{h}_s^{(i)}$ in Eq. (4.6) has been numerically evaluated, it is assembled into the global matrix $\underline{h}_s$. These calculations and assembly operations are carried out for all 2-D interface elements on the dam-reservoir interface. Thus far we have not considered what kind of 2-D element should be used, but 6 to 8 nodes 2-D elements (Fig. I-5(a) and Appendix B) seem to be appropriate.

Now, after the matrices $\underline{g}_s$ and $\underline{h}_s$ have been formed as above, we can proceed to carry out the computations for the global added-mass matrix $\underline{M}_{a_s}$ of Eq. (3.29). Because inversion of a matrix is very inefficient, the computation of Eq. (3.29) is carried out as follows:

(a) Solve $\underline{g}_s\ \underline{Q} = \underline{h}_s$, for $\underline{Q}$ (4.7)

using any suitable equation solver;

(b) Form the matrix product $\underline{M}_{a_s} = \rho\ \underline{h}_s^T\ \underline{Q}$

thus, the global added-mass matrix $\underline{M}_{a_s}$ of Eq. (3.29) is obtained.

4.2 Hydrodynamic Pressure Solutions and Their Comparisons

Although the added-mass coefficient matrix is the most convenient way to account for the hydrodynamic effects, it is hard to tell whether a scheme is good or not just by looking at the added-mass matrix coefficients. In order to evaluate an added-mass matrix scheme, we have to examine it with respect to the hydrodynamic effects it produces.

If we recall the procedures to formulate the added-mass matrix, it is clear that the hydrodynamic pressures are the quantities of interest. The definition of added-mass coefficients can be termed as nodal resisting forces caused by unit nodal accelerations acting into the reservoir. Yet, the nodal accelerations actually cause distributed hydrodynamic pressures to act on the dam face, and the nodal forces are obtained through processes of lumping the pressures. Therefore, the hydrodynamic effects represented by the added-mass coefficient matrix can be evaluated by the studies on the pertinent hydrodynamic pressures.

Now, we can impose any pattern of accelerations on the upstream face of the dam and obtain, from Eq. (2.4) or Eq. (3.21), the hydrodynamic pressures distributed over the dam face. The simplest pattern of accelerations that can be applied is unit uniform motions in the upstream-downstream direction. Physically, this is just the rigid body motion of the dam with unit accelerations acting in the upstream-downstream direction, while the reservoir floor and canyon walls are fixed.

Figures I-6 through I- 9 show the hydrodynamic pressure distributions over the upstream face of dams of various geometries subjected to unit uniform acceleration in the upstream-downstream direction. The cases studied included a gravity dam with vertical upstream face, cylindrical arch dams, and a general doubly curved arch dam. Notice that in all cases, the y-dimensions of successive fluid elements have a ratio of 1.25 in the upstream direction.

4.2.1 Gravity Dams

Figure I-6(a) shows the reservoir of a gravity dam with vertical upstream face, discretized into 16-node 3-D fluid elements and 8-node 2-D interface elements. Since the geometry of the reservoir and the excitations of the interface boundary do not vary with x, this is a 2-D problem and the pressure solutions are independent of x. Actually, this is exactly the case Westergaard (1) studied, and the exact solution is available. As shown in Fig. I-6(b), the hydrodynamic pressure solutions from finite element method converges sufficiently when L/H = 3. Also, the figure indicates that both Westergaard approximate solution and the finite element solution with L/H = 3 are good approximations to the exact solution.

Due to the discretization error, it is seen that the finite element solution converges to a value lower than the exact result. It can be shown that 20-node 3-D fluid elements will yield a better solution because they are more flexible, but the additional computational cost may not be justified.

In this case study, the finite element method is demonstrated to be a reasonably accurate and efficient method to evaluate hydrodynamic effects; the Westergaard approximate solution is expected to be good for this case only, because it was derived from the closed form solution for this case.

4.2.2 Cylindrical Arch Dams

As a bridge from the study of gravity dams to the case of general arch dams, several cylindrical arch dams were studied. Fig. I-7(a) shows the reservoir of a cylindrical arch dam with vertical upstream face. The reservoir has parallel vertical side walls and horizontal bottom. Fig. I-7(b) shows the hydrodynamic pressure distributions at the crown section due to unit upstream acceleration. The finite element solution converges sufficiently when L/H = 3, and the Westergaard approximate solution is virtually identical to that for the gravity dam in Fig. I-6(b). Fig. I-7(c) shows that similar results are found halfway between the crown and abutment, although the finite element results are increased slightly while the modified Westergaard results are decreased. In Fig. I-7(d), the hydrodynamic pressure distribution at the vertical section next to abutment shows significant changes: increases for finite element and decreases for Westergaard. The latter results are unacceptable; the finite element results are effectively converged at L/H = 3. The underestimations of hydrodynamic pressures by the Westergaard approximate solutions can be attributed to the fact that it only recognizes the water depth and normal direction cosines of the dam face; it is not aware of the existence of the bank which forms sharp angle with the dam thus restricting the lateral direction flow of the reservoir water.

If we now enlarge the angle between the bank and the dam, by introducing diverging reservoir walls as shown in Fig. I-8(a), it can be seen from Fig. I-8(d) that the Westergaard approximate solution is again close to finite element solution. It should be noticed that in Figs. I-7(d) and I-8(d), the Westergaard approximate solutions do not change, but the finite element solution varies due to the boundary restrictions imposed by the bank. In general, the Westergaard approximate solution overestimates hydrodynamic pressures if the abutment angle between bank and dam is reasonably wide as shown in Figs. I-8(b) and (c). These figures also compare the effects of the reservoir bank flare angles for the finite element solutions.

4.2.3 General Arch Dams

In Fig. I-9(a) we present the reservoir of a general arch dam, where the reservoir has constant section (prismatic form) in the upstream direction. Because of the discretization approximation in the finite element method, the normal direction cosines for nodes at the face of the dam, may not be calculated accurately especially for the corner nodes. A general conclusion of this comparison as depicted in Fig. I-9 is that the Westergaard approximate solution is too conservative and overestimates hydrodynamic effects. Its chief advantage is that it is the least expensive means to represent hydrodynamic effects. However, by actually carrying out computations of hydrodynamic pressures by both methods on Techi Arch Dam, an existing nonsymmetric arch dam (Fig. I-10), we found that it was not very expensive to use Galerkin Finite Element Method. Results obtained by the two methods, shown in Fig. I-9(d), demonstrate the significant overestimation given by the Westergaard approach.

From the cases studied, it is evident that the Generalized Westergaard approximation can be used for crude preliminary analysis purposes taking advantages of its relative economy. The Galerkin Finite Element Method with its competitive low cost should be used to represent incompressible hydrodynamic effects for final design studies. The validity of this method will be strengthened by the correlation studies presented in the following chapter.

5. NUMERICAL CORRELATIONS WITH EXPERIMENTS ON TECHI ARCH DAM

5.1 Properties of Techi Arch Dam

The Techi Dam, located in the middle part of Taiwan in a moderately active seismic zone, was completed in September 1974. It is 180 m in height, with a crest 290 m long at an elevation of 1411 m above sea. The thickness of the dam is 4.5 m at the crest and 20 m at the base. It is a double curvature arch dam with total concrete volume of 430,000 m^3. A perimetral joint surface has been provided between the dam body and the pulvino block; the dam body has 22 vertical cantilever monoliths with a contraction joint between each monolith (Fig. I-10).

The mechanical properties of the dam and its foundation are as follows:

	Dam Body
Young's Modulus	$E = E_{dynamic} = 5.6774 \times 10^6$ psi
Poisson Ratio	$\nu = 0.21$ $(0.19 \sim 0.23)$
Thermal Coefficient	$\alpha = 5.6 \times 10^{-6}$
Mass Density	$\rho = 150$ lb/ft^3
Compressive Strength	$\sigma_c \approx 5365.15$ psi
Tensile Strength	$\sigma_t \approx 500$ psi

	Foundation
Young's Modulus	$E = 8.516 \times 10^6$ psi
Poisson Ratio	$\nu = 0.21$
Mass Density	$\rho = 162$ 16/ft^3
Compressive Strength	$\sigma_c \approx 2.1 \times 10^4$ psi
Tensile Strength	$\sigma_t \approx 930$ psi

In 1979, several sets of dynamic experiments were carried out on the dam, including measurements of both ambient vibrations and forced vibrations. Numerical modelling of the dynamic behavior of Techi Dam was carried out on the CDC 7600 machine at Lawrence Berkeley Laboratory. A certain volume of massless foundation rock was included (Fig. I-11, I-12) in the model, and both the dam body and foundation rock were discretized by 3-D finite elements. Thick shell elements, transition elements and 3-D shell elements as described in the computer program ADAP (23) were used for the dam body whereas 8-node brick elements were used for the foundation rock. (Figures I-11 through I-14). Various added-mass matrix representations of hydrodynamic effects were computed from the preprocessor RSVOIR (28), and assembled with the concrete mass matrix computed by the program ADAP. The added-mass matrices that were considered included the Generalized Westergaard approximation solution, a consistent added-mass matrix from Galerkin Finite Element Method, and a diagonalized added-mass matrix obtained by diagonalizing the consistent added-mass matrix. (22). Also, various different water levels were considered in the study (Appendix C).

The vibration frequencies and mode shapes were calculated by the ADAP program for each case including foundation and hydrodynamic effects. Also, stresses in the dam due to the static loads, namely hydrostatic and gravity, were evaluated. Because there was no information on temperature changes, no thermal load was included. Finally, a response spectrum dynamic analysis was carried out. The first 8 modes of the case considering the diagonalized added-mass matrix from Galerkin Finite Element Method were used in the dynamic response analysis, and stresses envelopes were obtained for the dam-foundation-reservoir system subjected to hydrostatic load, gravity load, plus the Design Base Earthquake excitations. Mode shape and frequency correlations with the experimental results are shown in Section 5.2, and the stress responses including earthquake effects are presented in Section 5.3.

5.2 Correlation of Frequencies and Mode Shapes

Because of heavy rainfall that occurred during the field measurement program, the vibration measurements were taken at different water levels. Therefore, numerical solutions were also calculated for various water levels using different methods of approximation; by curve-fitting we can interpolate frequency values at intermediate water levels.

5.2.1 Frequency Correlations

Various types of frequency correlations are presented in Figures I-15 through I-19. Fig. I-15 shows the variation of fundamental frequency of Techi Dam with changes of reservoir height, calculated with the modified Westergaard reservoir approximation and with the finite element model. Also shown is corresponding information on frequency changes in a typical gravity dam. This figure shows that the decrease in fundamental frequency of an arch dam is more rapid than that of a gravity dam when the water level in the reservoir increases. This shows that the added-mass which represents the hydrodynamic effects has a greater influence on the fundamental frequency of the arch dam than on that of the gravity dam. This is obvious because the arch dams are in general more flexible and have less concrete mass. The figure also shows that when the water level is close to the crest, the added-mass has similar influence on the fundamental frequency for both gravity dam and arch dam. However this cannot be taken as a general rule, because it depends on the geometry of the reservoir and of the dam being considered. If the reservoir cross-section is of a wide V-shape, it is expected that the influence of the added-mass upon the fundamental frequency will be much greater on arch dams. It is also interesting to see that the added-mass cause almost the same rate of change of fundamental frequency of the arch dam, whether it was computed from Generalized Westergaard approximate solution or from the Galerkin Finite Element Method, but the significant overestimate of reservoir effects given by the Westergaard model is obvious.

The correlations between the analytical procedures and also with the experimental results are presented in a different form in Fig. I-16, where the changes due to water level are based on the full reservoir condition. The similar slopes among all 3 curves, i.e., the rates of increase in the fundamental frequency per unit decrease in water depth show that the analytical procedures for taking account of hydrodynamic effects are fairly accurate. The sharp drop on the curve of the finite element solution shows that the hydrodynamic effect has negligible influence on the fundamental frequency of the dam when the water level is below 40% of the height of the dam. The increase in fundamental frequency of the dam without water over that of the dam with full reservoir, is approximately 35% when the added-mass is computed by finite element method. Expressed in the context of Fig. I-16, if the fundamental frequency of the dam without water is 100%, the fundamental frequency of the dam with full reservoir is about 74%. In general, a full reservoir will reduce the fundamental frequency of an arch dam by 20% to 30%.

Figure I-17 shows comparisons between results of the two numerical representation of added-mass for the frequencies of first 4 modes of vibration of the reservoir-dam system when the water level varies. This figure again shows that the rate of change of frequencies with water level is similar for both numerical representations of added-mass. But obviously the added-mass obtained by Generalized Westergaard solution is greatly overestimated compared to that computed by Galerkin Finite Element Method. The difference between different schemes is greater than between different water levels for the same scheme.

The correlation with forced vibration experimental results shown in Fig. I-18, demonstrates that the hydrodynamic effects evaluated by Finite Element Method in the form of diagonalized added-mass matrix gives better agreement than the Westergaard procedure. Although the finite element analysis underestimates the added-mass effect for the fundamental mode, it overestimates it for the second mode and gives quite good agreement for the third and fourth modes. Therefore, as a whole, it may be concluded that hydrodynamic effects are well evaluated by Finite Element Method.

A final comparison of all experimental and analytical results for the various water levels that have been studied is presented in Fig. I-19. On this comparison the question has to be raised as to how to identify the mode number corresponding to a given frequency. Because of the possibility of missing modes in the experiments, as will be seen in the following section, we have to be sure that the frequency correlations actually apply to the same mode number. We know that in solution of an eigenproblem, any errors in the computational procedure affects eigen-vectors more than eigenvalues; that is, the computed eigenvalues tend to be more accurate than the computed eigenvectors. However, because the frequency errors also may be due to inaccurate material properties, in this study it was necessary to identify the mode number by similarity in mode shape; i.e., if the associated frequencies are different, it is presumed to be because the material properties are not modelled accurately. In the following section, mode numbers are identified by mode shapes, considering both radial and tangential components; in this way some missing modes in the experiments were discovered. On this basis the correlations of frequencies associated with the same mode number are proven to be valid.

5.2.2 Mode Shape Correlations

The correlations of mode shapes are illustrated in Figures I-20 and I-21. Fig. I-20 shows the correlations between experiments (34) and numerical solutions using the Galerkin Finite Element Method for the case when water level is at 90% of dam height. Fig. I-21 presents the correlations for the case when water level is at 85% of the dam height, except that the analysis in this case used the Generalized Westergaard reservoir model.

As mentioned above, the correlations should be done for the same mode number as identified by similar mode shapes (because some tangential components were not measured, only radial components are compared in the figures). Some different modes, as shown by Figures I-20(b) and (c), may have similar radial components of the mode shapes; but they are indeed different modes because displacement shapes on vertical sections are different. This is far more evident for higher modes. In Figures I-20 and I-21 we only show the mode shapes of the crest, but for the higher modes it may be necessary also to show the mode shapes of selected sections below the crest in order to differentiate mode numbers.

In Fig. I-20, we see that the correlations of mode shapes are very good for the first several modes, but some modes were missed in the experimental results. The measured frequencies associated with those missing modes are listed on the figures, although the mode shapes were not measured. The measured and calculated frequencies for the similar mode shapes are within 5%, indicating the hydrodynamic effects represented by the added-mass matrix computed by Galerkin Finite Element Method are reasonable, while also considering the uncertainties in the concrete material modelling. It is interesting to see that the 3rd mode shape may not be easy to obtain in the forced vibration test because its crest nodes are so close to those of the 2nd mode. In general, because the behavior of a structure is normally dominated by its lower modes, Fig. I-20 shows that the hydrodynamic effects represented by the diagonalized added-mass matrix computed from the Galerkin Finite Element Method are certainly adequate for engineering purposes. Although they are not shown, it is worthwhile to mention that the mode shapes given by the consistent added-mass matrix are almost identical to those according to the diagonalized added-mass matrix for both radial and tangential components, except for mode numbers above the 9th.

Fig. I-21 shows that the correlations of mode shapes for 85% water depth are good up to 4th mode with the 3rd mode missing from experimental results. This indicates that the added-mass matrix computed according to the Generalized Westergaard Formula has good relative distribution on the dam face. However, frequencies of similar mode shapes have errors of up to 20%; thus, the added-mass matrix according to the Generalized Westergaard Formula overestimates the hydrodynamic effects in magnitude. One may notice from Figures I-21(d) and (e) that the crest mode shapes are similar for modes 4 and 5 of the numerical solution in both radial and tangential components. If only the crest mode shapes were compared in this case they would appear to represent the same mode number. But they are truly different modes because the vertical crown section shapes (not shown) are completely different from each other. When we examine correlations of mode shapes and their associated frequencies of mode 9, in Fig. I-21(i) we can only say that this is a beautiful note in the melody played by Generalized Westergaard Formula.

From the correlation studies on frequencies and mode shapes present in this section, it may be concluded that the hydrodynamic effects represented by the diagonalized added-mass matrix from the Galerkin Finite Element Method can be considered as a good approximation of the true behavior. Nevertheless, the Generalized Westergaard approximate solution still can be useful for crude preliminary studies.

5.3 Stress Response Representations

Stresses calculated in a structure subjected to specified loadings provide the basis for the design of the structure. According to the assumed mechanical properties of the structural material, the structure is designed so that when subjected to the design loads, it won't develop excessive stresses that will lead to damage. Because of the potential disaster associated with the failure of a dam, it is very important to analyze the stresses in the dam accurately, when it is subjected to the maximum expected loadings. For arch dams, two critical stresses may be represented conveniently in terms of normal components in the horizontal and vertical directions, usually called arch and cantilever stresses.

Three intensity loads of earthquakes often are used in the design of a dam:

(1) Maximum Credible Earthquake (MCE): This is the maximum possible earthquake that might occur at the site of the dam. When subjected to the MCE, the dam may suffer damages, but must retain the reservoir.

(2) Design Base Earthquake (DBE): This is an earthquake intensity corresponding to a return period of 100 years, (Fig. I-25(b) and (c)), the expected life of the structure. When subjected to the DBE, the dam should sustain only repairable damages, and its equipment should be able to operate normally.

(3) Operation Base Earthquake (OBE): This is an earthquake intensity corresponding to a return period of 25 years. (Fig. I-25(b) and (c)); it is very likely to occur during the life of the structure. When subjected to the OBE, the dam should not sustain any damage.

The Design Base Earthquake was used for this study. Figures I-22 to I-24 present the stress responses of Techi Dam when subjected to various types of loadings. In the figures, SIG-XX denotes horizontal normal stress (arch stress) while SIG-YY denotes vertical normal stress (cantilever stress). All cases presented in Figures I-22 to I-24 are discussed in the following sections.

5.3.1 Stress Response to Static Loadings

Because no temperature change data was available, the only static loads considered were hydrostatic and gravity. Figs.I-22 shows the static stress results in the form of contour plots; all the tension zones are shaded. Four separate plots are presented (Figs.I-22(a),(b), (c), and (d)), showing arch and cantilever stresses on the upstream and downstream faces. Obviously, all the tensile stresses, either cantilever or arch, due to the static loads, are well below the tensile strength of the concrete (which is assumed to be 500 psi here, see Section 5.1).

The compressive stresses are also well below the material strength. The static compressive cantilever stresses shown on the downstream face at the foot of the dam in Fig. I-22(d) while it is subjected to static loads are beneficial because they compensate for dynamic tensile stresses which may be quite high in this region.

5.3.2 Stress Response to Combined Static Loads and Design Base Earthquake (DBE) Excitation

The response spectra for the DBE are shown in Fig. I-25(a). From Fig. I-19, the fundamental frequency of Techi Arch Dam, with 90% reservoir depth, is approximately 2.7 Hz according to finite element solution with diagonalized added-mass matrix, it corresponds to approximately 2 g of the pseudo-acceleration intensity on the response spectra for the DBE in Fig. I-25(a). If we consider pseudo-acceleration intensity of 0.2 g and above as significant (10% of the intensity of fundamental mode), then the DBE has important intensity associated with excitation frequencies up to 7 Hz, which will excite the first 8 modes of the Techi Dam considering hydrodynamic effects (see Fig. I-19). Thus, the first 8 modes were included in the response spectrum dynamic analysis. Because the dynamic stresses resulting from the response spectrum dynamic analysis are in absolute value, we present the stress response due to combined static and dynamic loadings in terms of maximum and minimum stress envelopes.

The stress envelopes have minimum values obtained by subtracting response spectrum dynamic stresses from corresponding static stresses, and the maximum values are evaluated by adding response spectrum dynamic stresses to the corresponding static stresses. Fig. I-23 illustrates the stress envelope contours on the upstream face while Fig. I-24 presents the stress envelope contours on the downstream face. As before, SIG-XX indicates arch stresses and SIG-YY represents cantilever stresses; and here, minimum stresses show the largest possible compressive stresses whereas maximum stresses show the largest possible tensile stresses.

From Figures I-23 (a),(b),(e) and (f), it is evident that the maximum arch and cantilever compressive stresses on the upstream face due either to upstream-downstream excitations or cross-canyon excitations, are all well below the compressive strength of the concrete, which is about 5000 psi.

Similarly, Figures I-23(d) and (h) show that the maximum tensile cantilever stresses are well below the tensile strength of the material; hence, no cantilever cracking will occur. However, in Figures I-23(c) and (g), it is clear that the tensile arch stresses indicated near the crest are beyond the tensile strength of the material; thus cracks are expected to be formed there. But it must be remembered that vertical contraction joints were built into the structures; thus the tensile arch stresses will merely open these joints. Therefore, no cracking is expected from these indicated tensile stresses in the crest region and the dam will be able to withstand the earthquake without significant damage.

Figures I-24(a) to (h) present the corresponding stress results for the downstream face. Figs. I-24(c) and (g) indicate that tensile arch stresses on the downstream face also exceed the tensile strength of the material, and again it may be assumed that the contraction joints will open to release the tensile arch stresses. Figs. I-24(d) and (h) show that cantilever cracking also is unlikely on the downstream face, and Figs. I-24(a), (b), (e) and (f) show that the compressive stresses are well within the compressive strength of the concrete.

Thus, the discussions in this section have shown that Techi Dam will not have significant damage when it is subjected to hydrostatic load and gravity load combined with the Design Base Earthquake excitations, taking account of incompressible hydrodynamic effects and foundation flexibility. However, one other aspect of the dynamic behavior should be considered: the nonlinear response mechanism associated with the opening of the contraction joints due to the action of dynamic tensile arch stresses. It is evident that such joint opening on one face of the arch dam will be accompanied by the modification of the arch stresses on the other face (and vice versa), and also the possibility of changes in the state of stresses in the cantilever direction. This type of nonlinear response mechanism is the subject of the second part of this thesis.

6. CONCLUSIONS AND REMARKS

The hydrodynamic effects represented by an added-mass matrix associated with incompressible fluid reservoir of arch dams are reported here. Two basically different computational procedures, namely Generalized Westergaard Formula and Galerkin Finite Element Method, are described in detail, and pressure solutions obtained with each are compared. Rigorous vibration frequency and mode shape analyses are carried out, and based on their comparisons with field measurements, a best suitable standard procedure is proposed, i.e., Galerkin Finite Element Method with diagonalized added-mass matrix.

Safety evaluations of Techi Dam, that subjected to either static loads alone or to combined static and dynamic earthquake loads, are discussed. It is shown that Techi Dam won't sustain major damages due to these loading conditions, but that minor damages might occur near the crest spillway. This condition may need further study that includes joint opening nonlinear response, it nevertheless should not prohibit the normal operation of the gates.

It was found that hydrodynamic effects of an incompressible liquid reservoir were represented adequately by a reservoir model that extends in upstream direction 3 times the height of the dam. This greatly reduces the cost of the finite element analysis of the reservoir interaction, but the corresponding conclusion may not apply to compressible water. Inclusion of the water compressibility greatly complicates the reservoir analysis, and it is not known at present whether or not the results neglecting water compressibility conservative. Further reserach is needed to verify the significance of the influence of water compressibility on the real time response of an arch dam, especially when superposition procedure is not valid.

However, the results of the analyses and of the correlations with field measurements contained in this report have shown that the hydrodynamic effects represented by added-mass of incompressible water should be satisfactory for engineering purpose in the analysis and design of an arch dam.

In view of nonlinear dynamic response analysis of arch dams, diagonalization of the full added-mass matrix was deemed necessary to reduce the computational cost. This diagonalization has nevertheless destroyed the coupling effectsof added-mass, whether these coupling effects are important or not require further research.

APPENDIX A: COMPUTATIONS OF NORMAL DIRECTION COSINES

The normal direction cosines at any point on a curvilinear surface, as on the 2-D interface elements, can be found (29) from the intrinsic property of finite element interpolation functions which use the natural coordinates as curvilinear coordinates.

Figures I-4(b) and (c) show 2 kinds of possible 2-D interface element (2-D in natural coordinates, but 3-D in RCC space), where points p are regular points and point q is a degenerate corner point. The computations of normal direction cosines for points p are different from that for point q.

A.1: Normal Direction Cosines for a Regular Point p

From basic finite element property, we have,

$$\underset{\sim}{x}_p = \sum_i N_i(r,s)\underset{\sim}{X}_i \qquad (A.1)$$

where

$\underset{\sim}{x}_i = \langle x_i \; y_i \; z_i \rangle$, the coordinates of node i of the element

The unit normal vector at point p, $\underset{\sim}{n}_p$ can be found as,

$$\underset{\sim}{n}_p = \frac{\dfrac{\partial \underset{\sim}{x}_p}{\partial r} \times \dfrac{\partial \underset{\sim}{x}_p}{\partial s}}{\left| \dfrac{\partial \underset{\sim}{x}_p}{\partial r} \times \dfrac{\partial \underset{\sim}{x}_p}{\partial s} \right|} \qquad (A.2)$$

where

$\dfrac{\partial \underset{\sim}{x}_p}{\partial r} = \sum_i N_{i,r}(r,s)\underset{\sim}{X}_i$, vector tangent to r-curve at point p

$\dfrac{\partial \underset{\sim}{x}_p}{\partial s} = \sum_i N_{i,s}(r,s)\underset{\sim}{X}_i$, vector tangent to s-curve at point p

or, in finite element formulation,

$$\underset{\sim}{n}_p = \frac{1}{\left|\frac{\partial \underset{\sim}{x}_p}{\partial r} \times \frac{\partial \underset{\sim}{x}_p}{\partial s}\right|} \begin{bmatrix} \hat{i} & \hat{j} & \hat{k} \\ \sum_i N_{i,r}(r,s)x_i & \sum_i N_{i,r}(r,s)y_i & \sum_i N_{i,r}(r,s)z_i \\ \sum_i N_{i,s}(r,s)x_i & \sum_i N_{i,s}(r,s)y_i & \sum_i N_{i,s}(r,s)z_i \end{bmatrix} \quad (A.3)$$

Thus,

$$\underset{\sim}{n}_p = \frac{1}{\left|\frac{\partial \underset{\sim}{x}_p}{\partial r} \times \frac{\partial \underset{\sim}{x}_p}{\partial s}\right|} (n_{xp}\ \hat{i} + n_{yp}\ \hat{j} + n_{zp}\ \hat{k}) \quad (A.4)$$

and

$$\left|\frac{\partial \underset{\sim}{x}_p}{\partial r} \times \frac{\partial \underset{\sim}{x}_p}{\partial s}\right| = (n_{xp}^2 + n_{yp}^2 + n_{zp}^2)^{\frac{1}{2}} \quad (A.5)$$

A.2: Normal Direction Cosines for a Degenerate Corner Point q

Because $\frac{\partial \underset{\sim}{x}_q}{\partial r} = 0$ at the degenerate corner point q (Fig. I-4(b)), we cannot find $\underset{\sim}{n}_q$ as above.

Instead,the unit normal vector $\underset{\sim}{n}_q$ can be found most conveniently as follows:

$$\underset{\sim}{x}_q = \sum_i N_i(r,s)\underset{\sim}{X}_i \quad (A.6)$$

$$\underset{\sim}{m}_q = \left.\frac{\partial \underset{\sim}{x}_q}{\partial s}\right|_{r = 1.0} \times \left.\frac{\partial \underset{\sim}{x}_q}{\partial s}\right|_{r = -1.0} \quad (A.7)$$

and

$$\underset{\sim}{n}_q = \frac{1}{|\underset{\sim}{m}_q|}\ \underset{\sim}{m}_q \quad (A.8)$$

The sequence of the cross-product is expressed in Eq. (A.7) according to the convention that the connectivity of the element is defined in the counterclockwise direction (Appendix B). In finite element formulation, Eq. (A.7) becomes

$$\underset{\sim}{m}_q = \begin{bmatrix} \hat{i} & \hat{j} & \hat{k} \\ \sum_i N_{i,s}(1.0,s)x_i & \sum_i N_{i,s}(1.0,s)y_i & \sum_i N_{i,s}(1.0,s)z_i \\ \sum_i N_{i,s}(-1.0,s)x_i & \sum_i N_{i,s}(-1.0,s)y_i & \sum_i N_{i,s}(-1.0,s)z_i \end{bmatrix} \tag{A.9}$$

and,

$$\underset{\sim}{n}_q = \frac{1}{|\underset{\sim}{m}_q|} (m_{xq}\,\hat{i} + m_{yq}\,\hat{j} + m_{zq}\,\hat{k}) \tag{A.10}$$

where

$$|\underset{\sim}{m}_q| = (m_{xq}^2 + m_{yq}^2 + m_{zq}^2)^{\frac{1}{2}} \tag{A.11}$$

APPENDIX B: FINITE ELEMENT INTERPOLATION FUNCTIONS AND THEIR DERIVATIVES (21,22)

Variable node finite elements are used in the analysis described in this report; the convention of their connectivities is shown in Fig. I-5.

B.1: Interface Elements (Fig. I-5(a))

For interface elements, 2-D in natural coordinates and 3-D in RCC space, their interpolation functions and the derivatives of their interpolation functions with respect to the natural coordinates are as follows:

$$\phi_1 = \zeta_1 - \frac{1}{2}(\zeta_5 + \zeta_8)$$

$$\phi_i = \zeta_i - \frac{1}{2}(\zeta_{i+3} + \zeta_{i+4}) \quad i=2\sim4$$

$$\phi_j = \zeta_j \qquad j=5\sim8$$

where $\zeta_k = 0$ if node k is not included

$$\zeta_k = G(r,r_k)G(s,s_k)$$

$$G(\beta,\beta_k) = \frac{1}{2}(1+\beta_k\beta),\ \beta_k = \pm 1,\ \beta = r,s$$

$$G(\beta,\beta_k) = 1-\beta^2 \qquad ,\ \beta_k = 0$$

and derivatives

$$\zeta_{k,\beta} = G,_\beta(r,r_k)G(s,s_k) + G(r,r_k)G,_\beta(s,s_k)$$

$$G,_\beta(\beta,\beta_k) = \frac{1}{2}\beta_k,\ \beta_k = \pm 1$$

$$G,_\beta(\beta,\beta_k) = -2\beta\ ,\ \beta_k = 0$$

For degenerate elements, if several nodes are degenerated into one node, their associated interpolation functions also have to be degenerated into one function, and similarly the derivatives of the interpolation functions.

B.2 3-D Fluid Elements (Fig. I-5(b))

For 3-D fluid elements, the suggested interpolation functions and the derivatives of the interpolation functions with respect to natural coordinates are as follows:

$$N_1 = \zeta_1 - \frac{1}{2}(\zeta_9 + \zeta_{12} + \zeta_{17})$$

$$N_i = \zeta_i - \frac{1}{2}(\zeta_{i+7} + \zeta_{i+8} + \zeta_{i+16}) \qquad i = z\sim 4$$

$$N_5 = \zeta_5 - \frac{1}{2}(\zeta_{13} + \zeta_{16} + \zeta_{17})$$

$$N_j = \zeta_j - \frac{1}{2}(\zeta_{j+7} + \zeta_{j+8} + \zeta_{j+12}) \qquad j = 6\sim 8$$

$$N_k = \zeta_k \qquad k = 9\sim 20$$

where

$$\zeta_m = 0, \text{if node m is not included}$$

$$\zeta_m = G(r,r_m)G(s,s_m)G(t,t_m)$$

$$G(\beta,\beta_m) = \frac{1}{2}(1 + \beta_m\beta) \quad ,\beta_m = \pm 1, \ \beta = r,s,t$$

$$G(\beta,\beta_m) = 1-\beta^2 \qquad ,\beta_m = 0$$

and derivatives

$$\zeta_{m,\beta} = G,_\beta(r,r_m)G(s,s_m)G(t,t_m) + G(r,r_m)G_\beta(s,s_m)G(t,t_m) + G(r,r_m)G(s,s_m)G,_\beta(t,t_n)$$

$$G,_\beta(\beta,\beta_m) = \frac{1}{2}\beta_m \ , \ \beta_m = \pm 1$$

$$G,_\beta(\beta,\beta_m) = -2\beta \quad , \ \beta_m = 0$$

For degenerate elements, if several nodes are degenerated into one node, their associated interpolation functions also have to be degenerated into one function, and similarly for the derivatives of the interpolation functions.

APPENDIX C: VARIABLE WATER LEVELS

When the dam is discretized in such a way that its element boundaries on the upstream interface do not match the boundaries of the fluid elements at the interface, the added-mass matrix found by the methods presented in Chapter 3 cannot be assembled directly with the concrete mass matrix of the dam. This is because different nodal points or degrees of freedom apply to the water and the concrete elements. This is most likely to occur when the dam is discretized so that the water surface is located between the horizontal boundaries of the dam element.

This problem presents no difficulty for the added-mass matrix formed by Generalized Westergaard Formula. But in using Galerkin Finite Element Method, the difficulty arises in the integration of Eq. (3.16):

$$\underline{h}_{s(ND \times 3ND)}^{(i)} = \iint_{S^{(i)}} \underset{\sim}{N}_s^{(i)T} \underset{\sim}{\lambda}^{(i)} \underline{\phi}_s^{(i)} \, dA^{(i)} \tag{3.16}$$

The shape functions $\underset{\sim}{N}_s^{(i)}$ and $\underline{\phi}_s^{(i)}$, in this case, does not reside in the same domain, rather the domain of $\underset{\sim}{N}_s^{(i)}$ is included in the domain of $\underline{\phi}_s^{(i)}$ (Fig. I-26). The integration only can be carried out for in the domain of $\underset{\sim}{N}_s^{(i)}$ and cannot be in the domain of $\underline{\phi}_s^{(i)}$, because $\underset{\sim}{N}_s^{(i)}$ are discontinuous functions in the domain of $\underline{\phi}_s^{(i)}$ (they vanish above the water level, see Fig. I-26). Therefore, Eq. (3.16) can be written, in this case, as follows:

$$\underline{h}_s^{(i)} = \iint_{S^{(i)}} \underset{\sim}{N}_s^{(i)T}(r,s) \, \underset{\sim}{\lambda}^{(i)}(r,s) \, \underline{\phi}_s^{(i)}(\xi(r,s), \eta(r,s)) \, dA^{(i)} \tag{C.1}$$

or, in the form of quadrature integrations:

$$\underline{h}_s^{(i)} = \sum_j \sum_k w_j w_k \underset{\sim}{N}_s^{(i)T}(r_j,s_k)\ \underset{\sim}{\lambda}^{(i)}(r_j,s_k)\ \underline{\phi}_s^{(i)}(\xi(r_j,s_k),\eta(r_j,s_k))|J^{(i)}(r_j,s_k)| \tag{C.2}$$

All the terms in Eq. (C.2) are defined similarly to those in Eq. (4.6).

The task is in evaluating values of $\underline{\phi}_s^{(i)}$ at integration points (r_j,s_k), while $\underline{\phi}_s^{(i)}$ are functions of (ξ,η). Naturally, we have to find coordinates (ξ,η) at points where (r_j,s_k) locates, and they are only related through the RCC coordinates of the nodes that associate with each element respectively.

Therefore, firstly we denote the RCC coordinates of fluid element nodes as x, y, z and RCC coordinates of concrete elements as X, Y, Z. Then, we can have the expression:

$$x_n = \underset{\sim}{\phi}_s \underset{\sim}{X} \tag{C.3}$$

where

x_n = x-coordinate of node n of the fluid element at the interface

$\underset{\sim}{X}$ = vector of X-coordinates of nodal points of concrete elements at interface

$\underset{\sim}{\phi}_s$ = vector of shape functions associated with nodes of the concrete elements.

x_n and $\underset{\sim}{X}$ are known, and if we position x_n properly, that is, at the locations where ξ values are -1, 0, +1, then, Eq. (C.3) will reduce to a simple form of a quadratic equation with η as unknown. Then if we solve η_n for the corresponding x_n, knowing $-1 \leq \eta_n \leq 1$, we can find the coordinates (ξ,η) for all nodes of the fluid element on the interface. Furthermore, the integration points (r_j,s_k) has an x-coordinate, x_a, given by

$$x_a = \underset{\sim}{N}_s(r_j,s_k)\ \underset{\sim}{x} \qquad (C.4)$$

where $\underset{\sim}{x}$ = vector of x-coordinates of nodal points of the fluid element at interface (i.e., x_n's).

relating Eq. (C.4) to Eq. (C.3), we have,

$$x_a = \underset{\sim}{N}_s(r_j,s_k)\ \underline{\Phi}_s\ \underset{\sim}{X} = \underset{\sim}{E}_{sx}\ \underset{\sim}{X} \qquad (C.5)$$

where $\underline{\Phi}_{s(ND\ x\ ND)}$ = collection of $\underset{\sim}{\phi}_s$ in Eq. (C.3) with known (ξ,η)'s

By Eq. (C.5) we can find RCC coordinates of integration points (r_j,s_k) in terms of RCC nodal coordinates of the concrete element.

Now, refering back to Eq. (C.2) with Eq. (C.5), we have

$$\underline{\phi}_s^{(i)} = \begin{bmatrix} \underset{\sim}{E}_{sx}^{(i)} & 0 & 0 \\ 0 & \underset{\sim}{E}_{sy}^{(i)} & 0 \\ 0 & 0 & \underset{\sim}{E}_{sz}^{(i)} \end{bmatrix} \qquad (C.6)$$

which corresponds to the nodal degrees of freedom of element i arranged according to $<\underset{\sim}{X}^T\ \underset{\sim}{Y}^T\ \underset{\sim}{Z}^T>^T$.

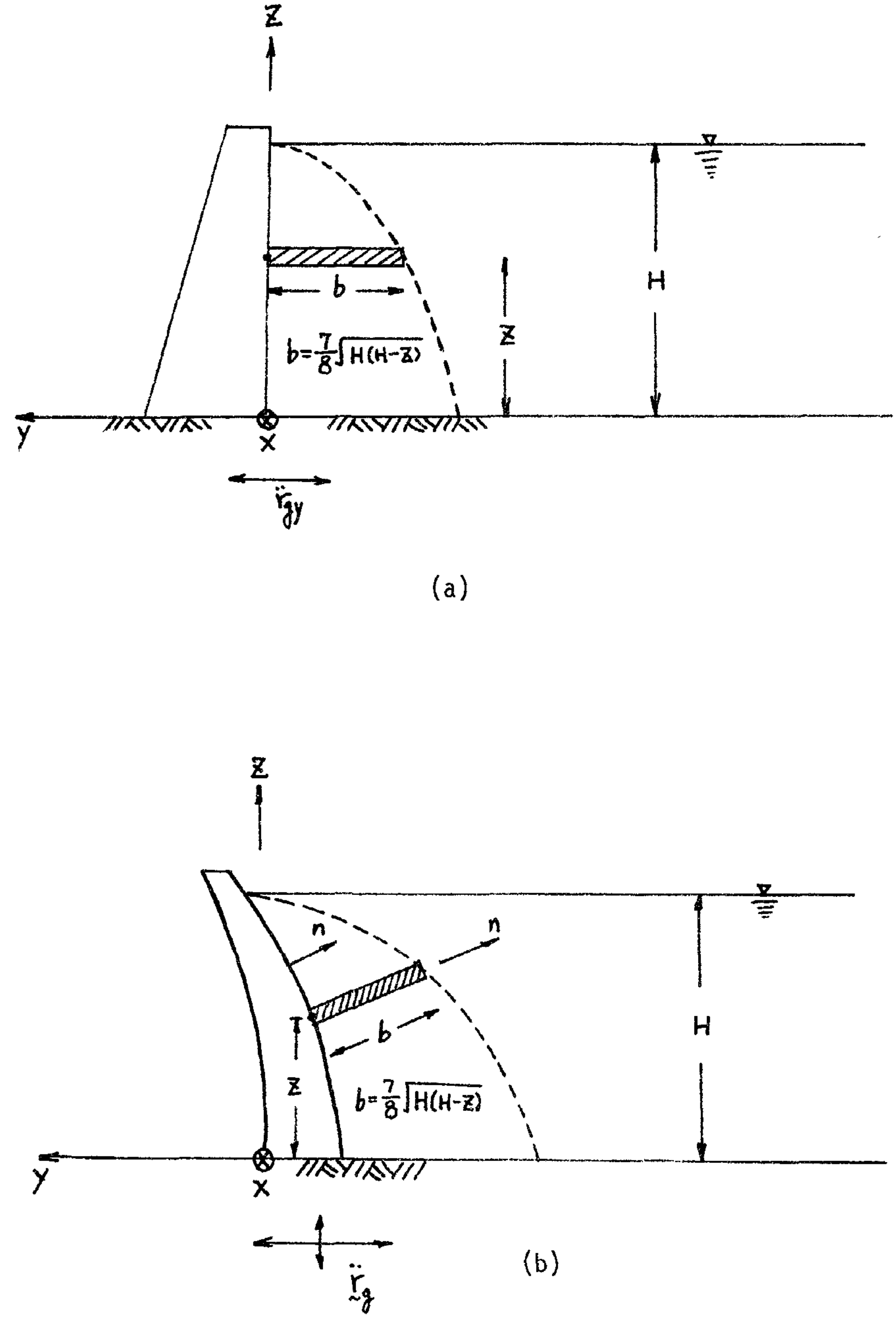

FIG. I-1 PICTORIAL ADDED-MASS ACCORDING TO WESTERGAARD

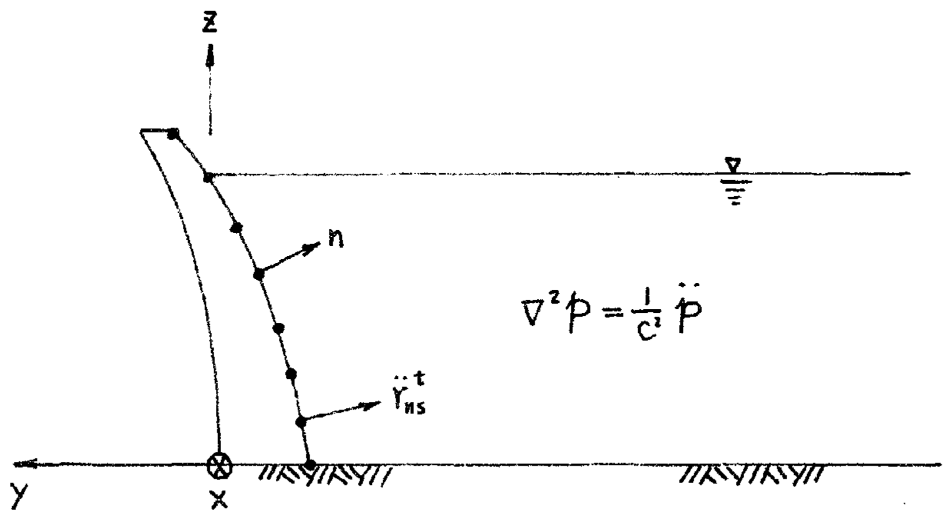

(a)

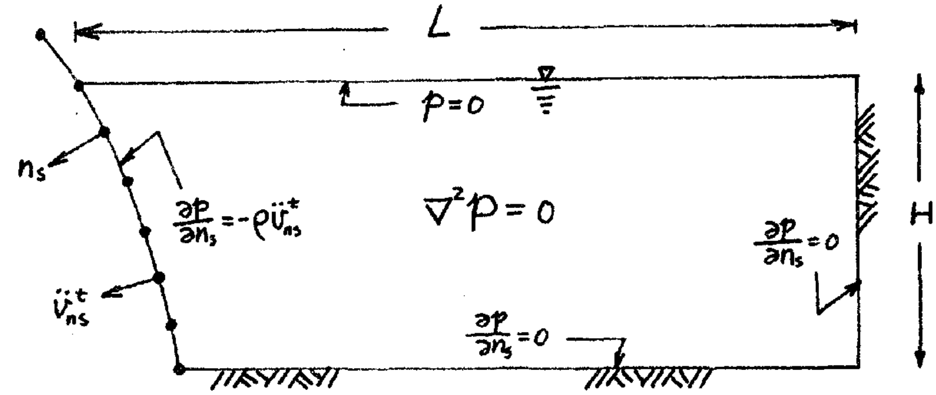

(b)

FIG. I-2 GALERKIN DISCRETIZATION OF THE RESERVOIR

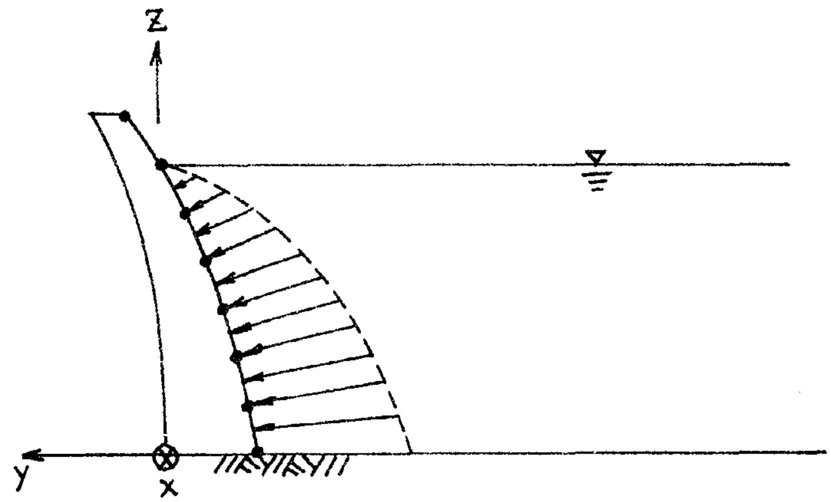

(a) HYDRODYNAMIC PRESSURES

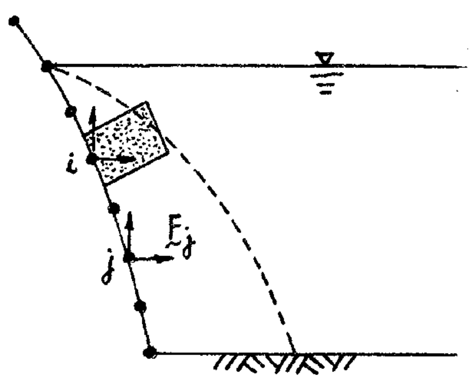

(b) TRIBUTARY AREA LUMPING PROCESS

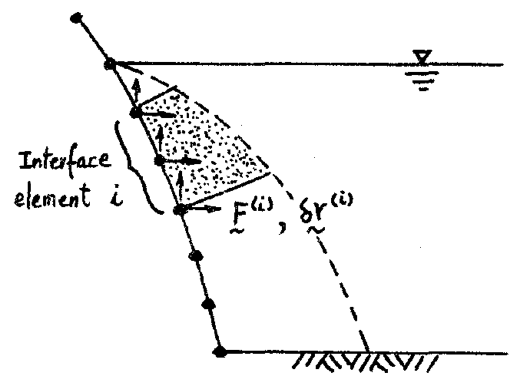

(c) CONSISTENT LUMPING PROCESS

FIG. I-3 LUMPING HYDRODYNAMIC PRESSURES INTO EQUIVALENT HYDRODYNAMIC NODAL FORCES

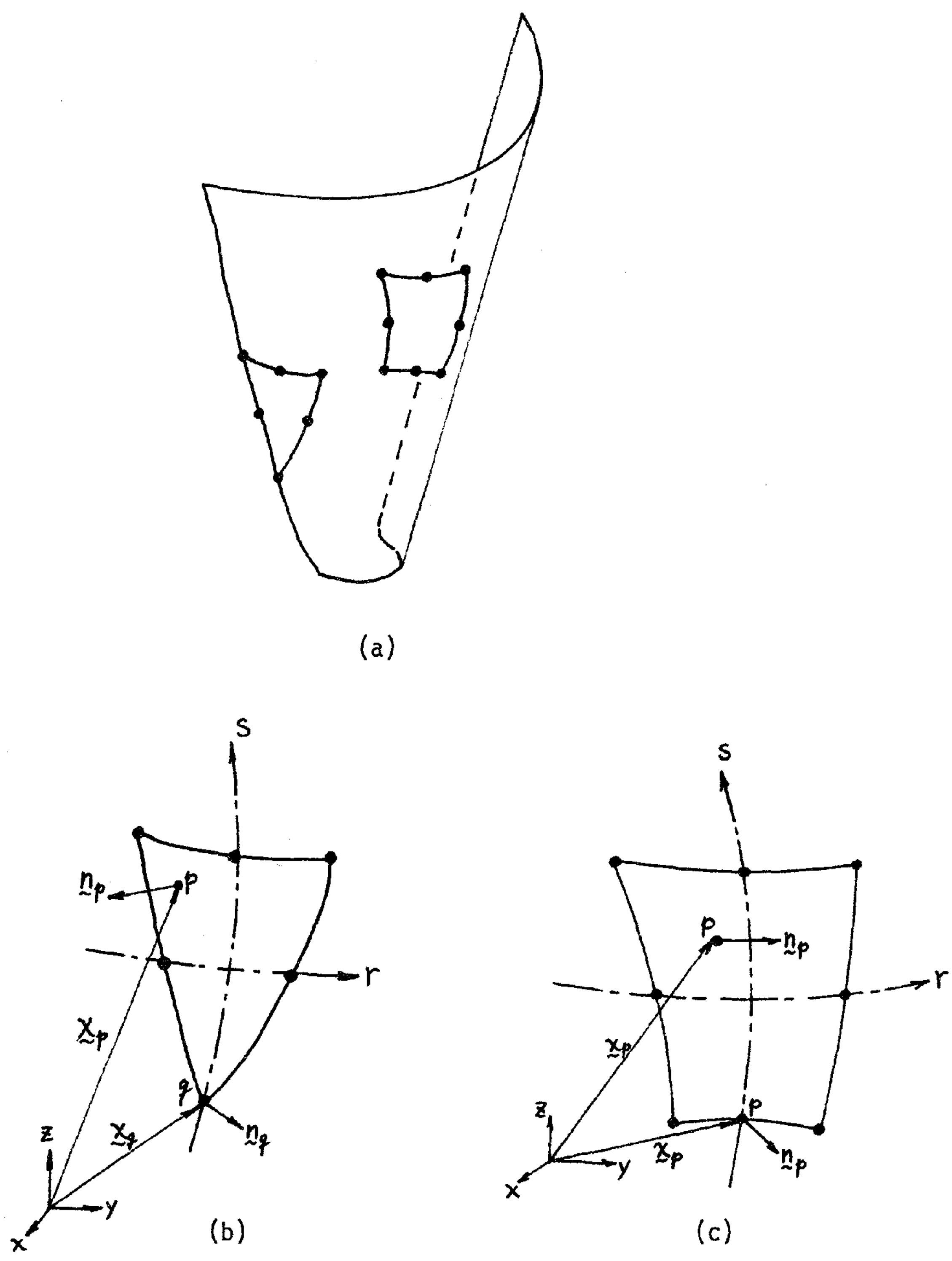

FIG. I-4 NORMAL DIRECTION COSINES OF CURVILINEAR SURFACE

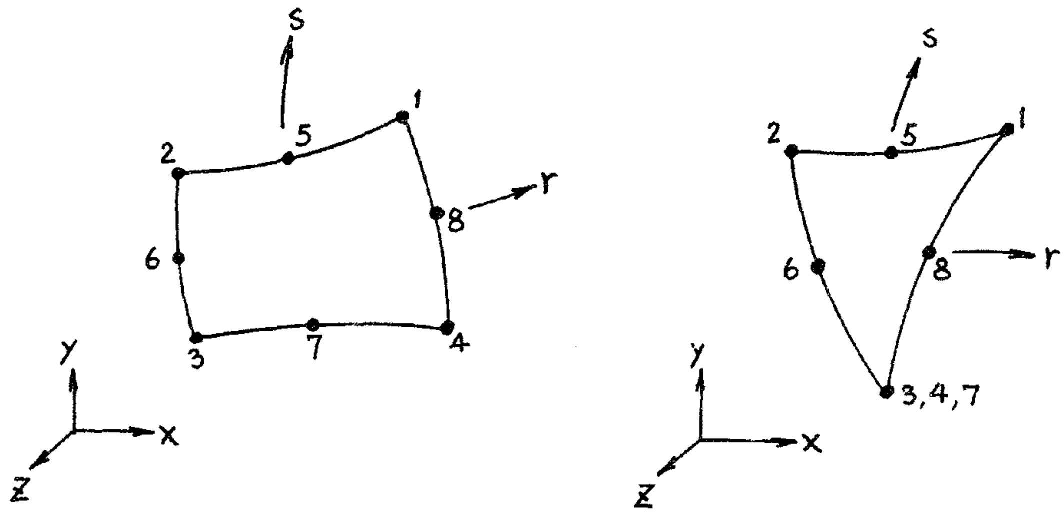

(a) INTERFACE ELEMENTS

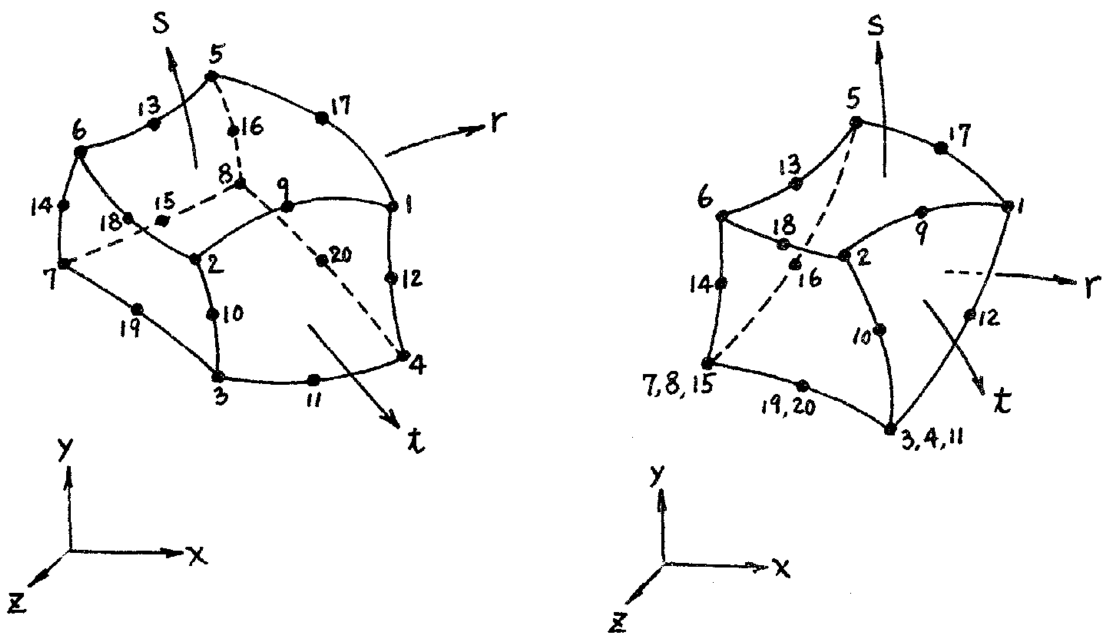

(b) FLUID ELEMENTS

FIG. I-5 FINITE ELEMENTS : 2-D AND 3-D IN NATURAL COORDINATES

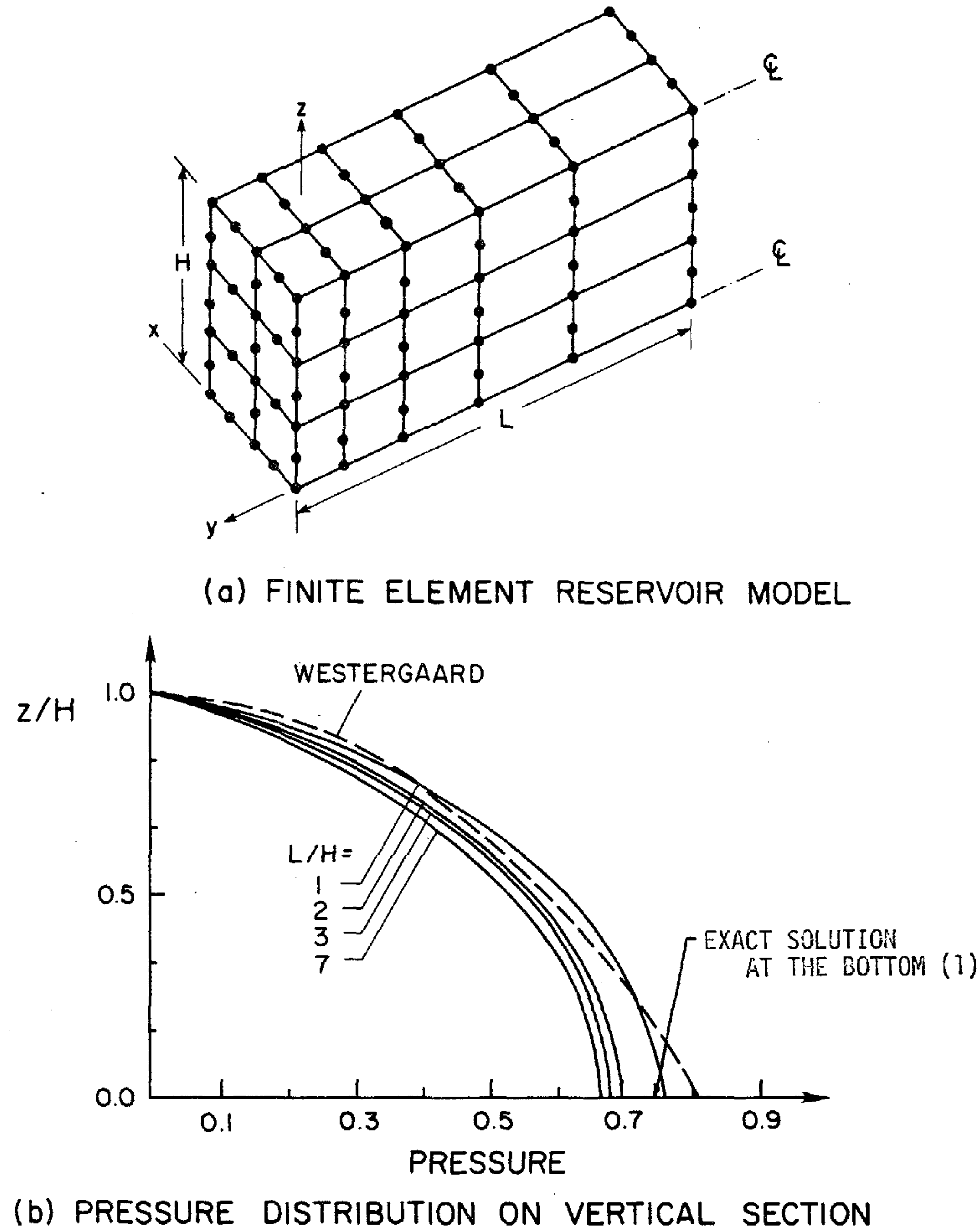

FIG. I-6 GRAVITY DAM WITH VERTICAL UPSTREAM FACE

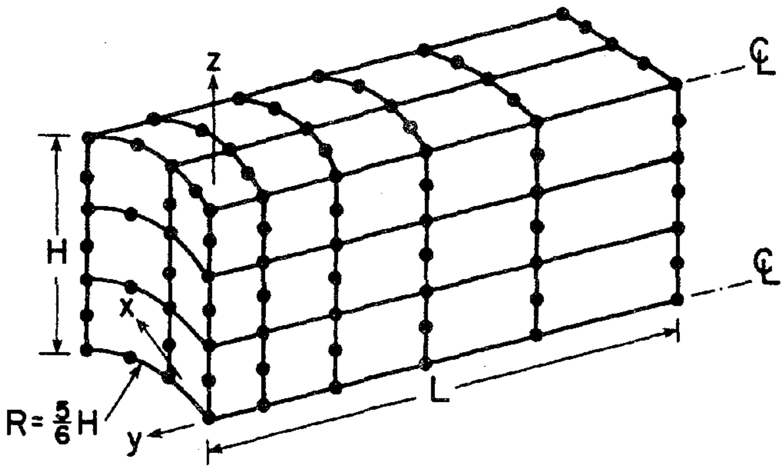

(a) FINITE ELEMENT RESERVOIR MODEL

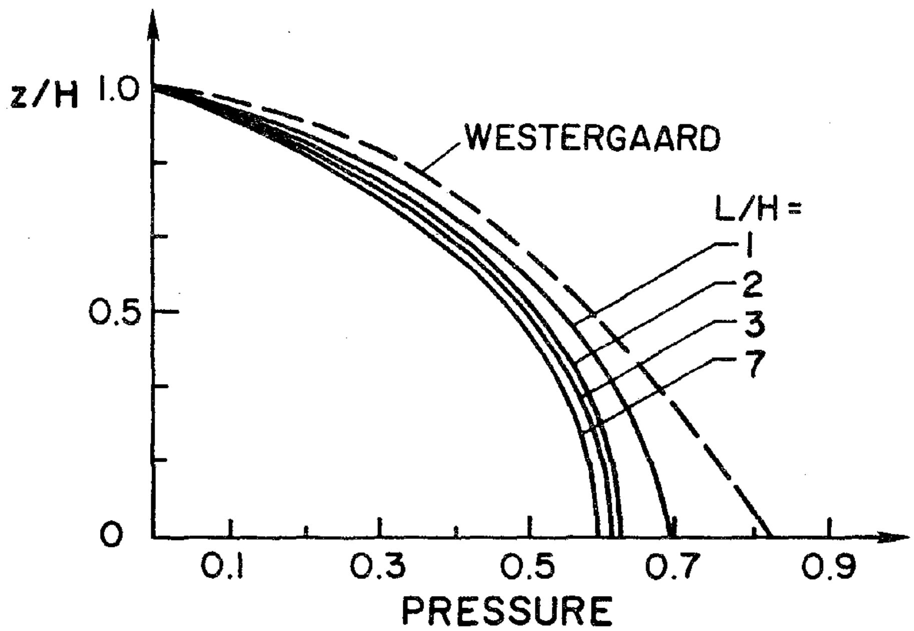

(b) PRESSURE DISTRIBUTION AT CROWN SECTION

FIG. I-7 ARCH DAM WITH CYLINDRICAL UPSTREAM FACE

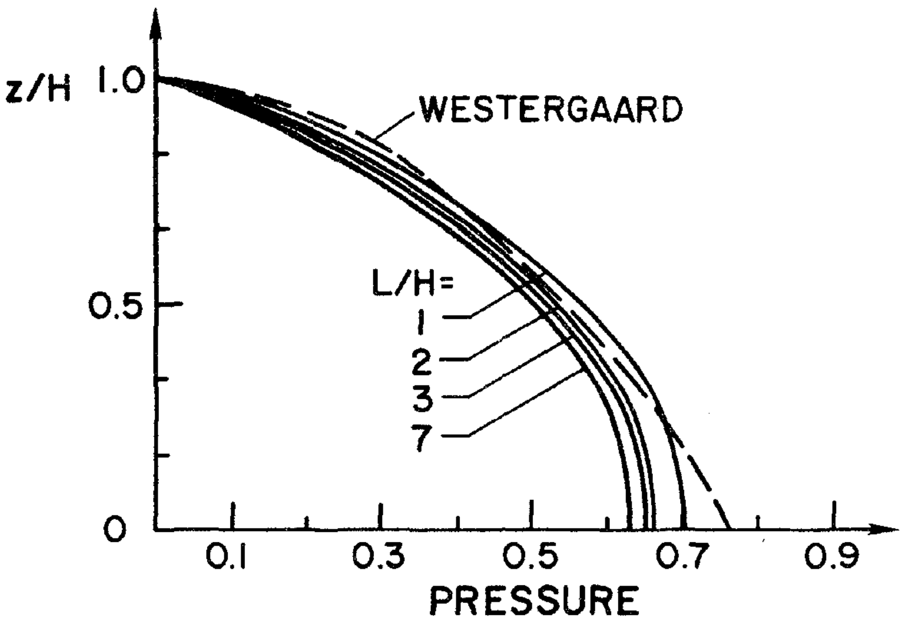

(c) PRESSURE DISTRIBUTION AT QUARTER ARC

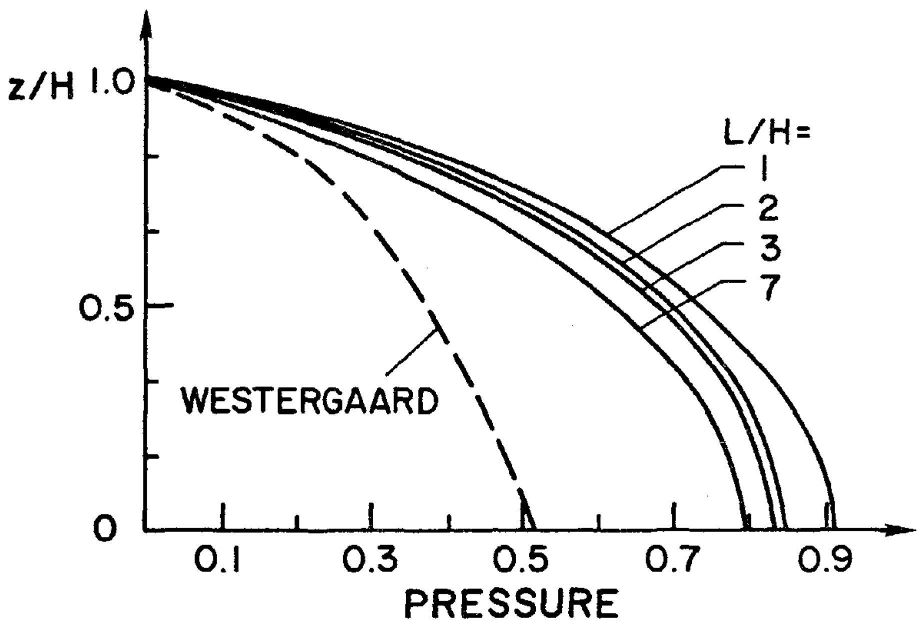

(d) PRESSURE DISTRIBUTION AT ABUTMENT SECTION

FIG. I-7 (Cont.) ARCH DAM WITH CYLINDRICAL UPSTREAM FACE

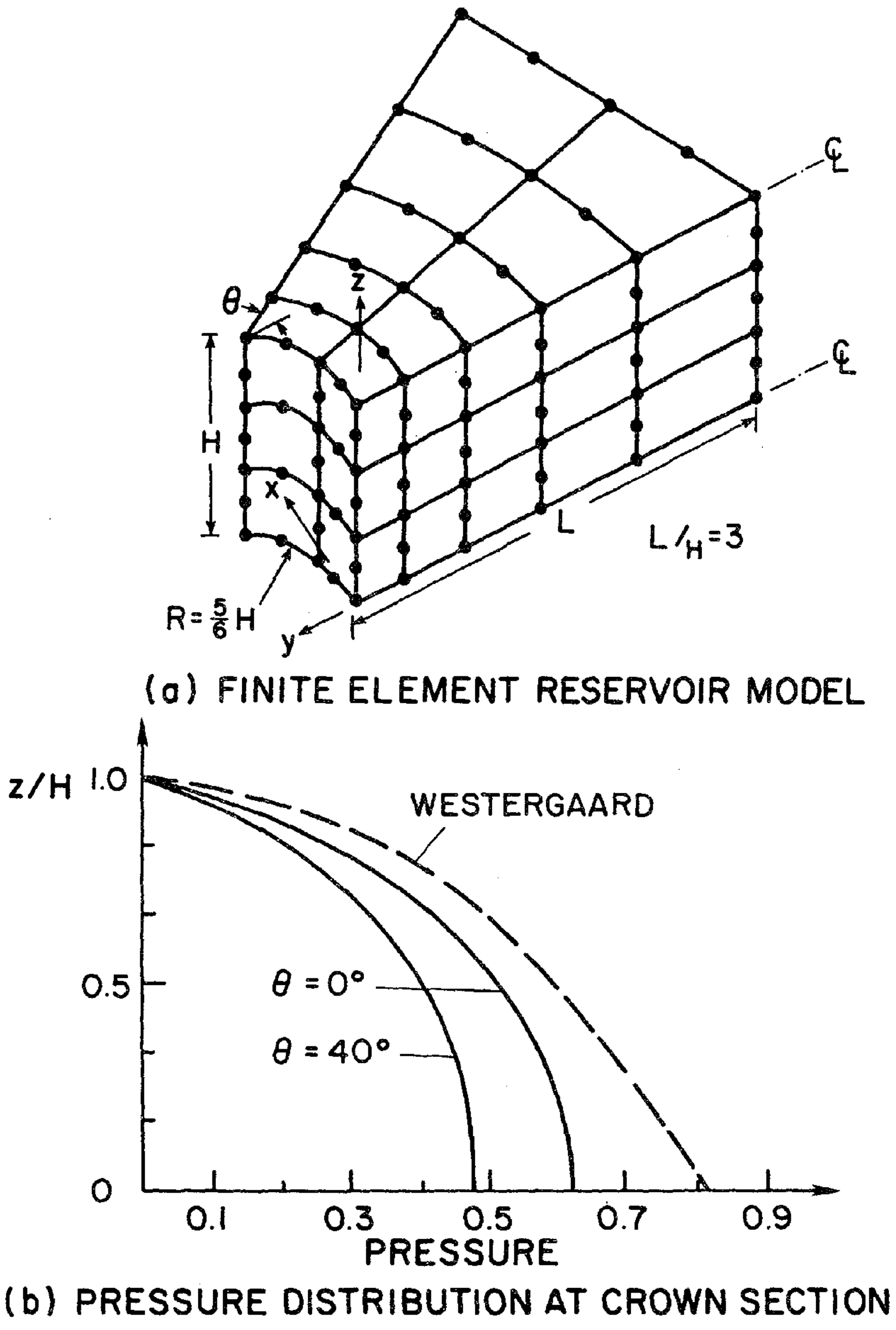

FIG. I-8 ARCH DAM WITH CYLINDRICAL UPSTREAM FACE AND DIFFERENT ABUTMENT ANGLES

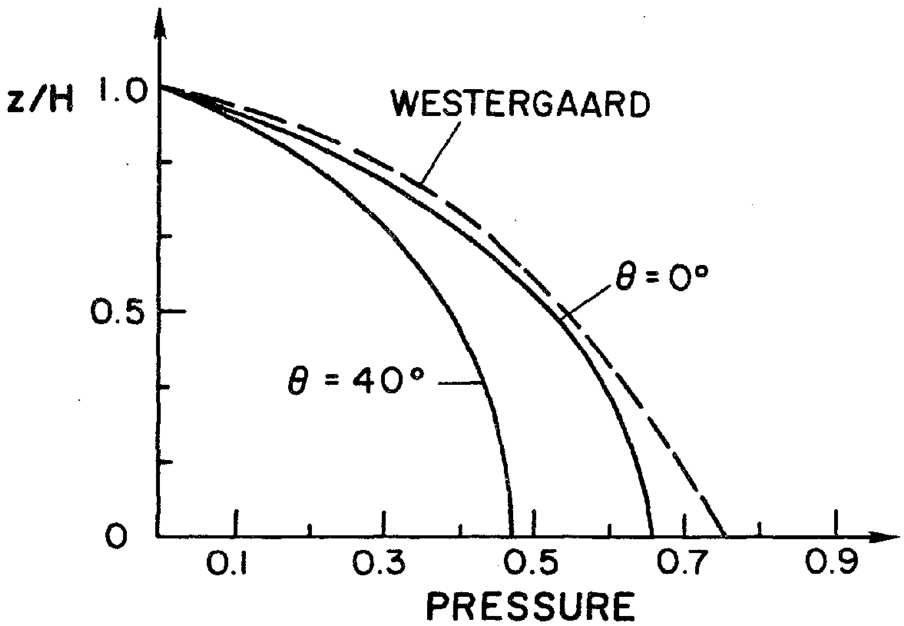

(c) PRESSURE DISTRIBUTION AT QUARTER ARC

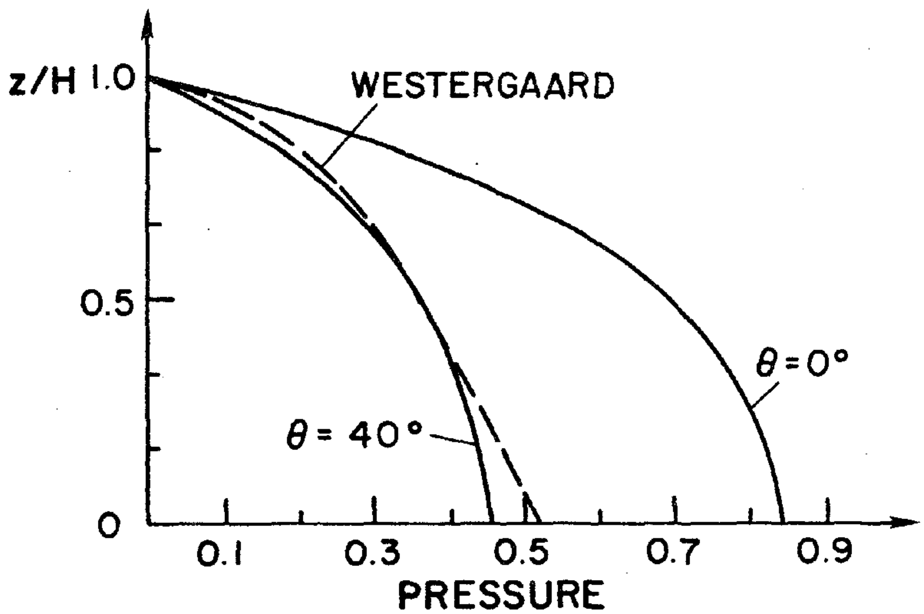

(d) PRESSURE DISTRIBUTION AT ABUTMENT SECTION

FIG. I-8 (Cont.) ARCH DAM WITH CYLINDRICAL UPSTREAM FACE AND DIFFERENT ABUTMENT ANGLES

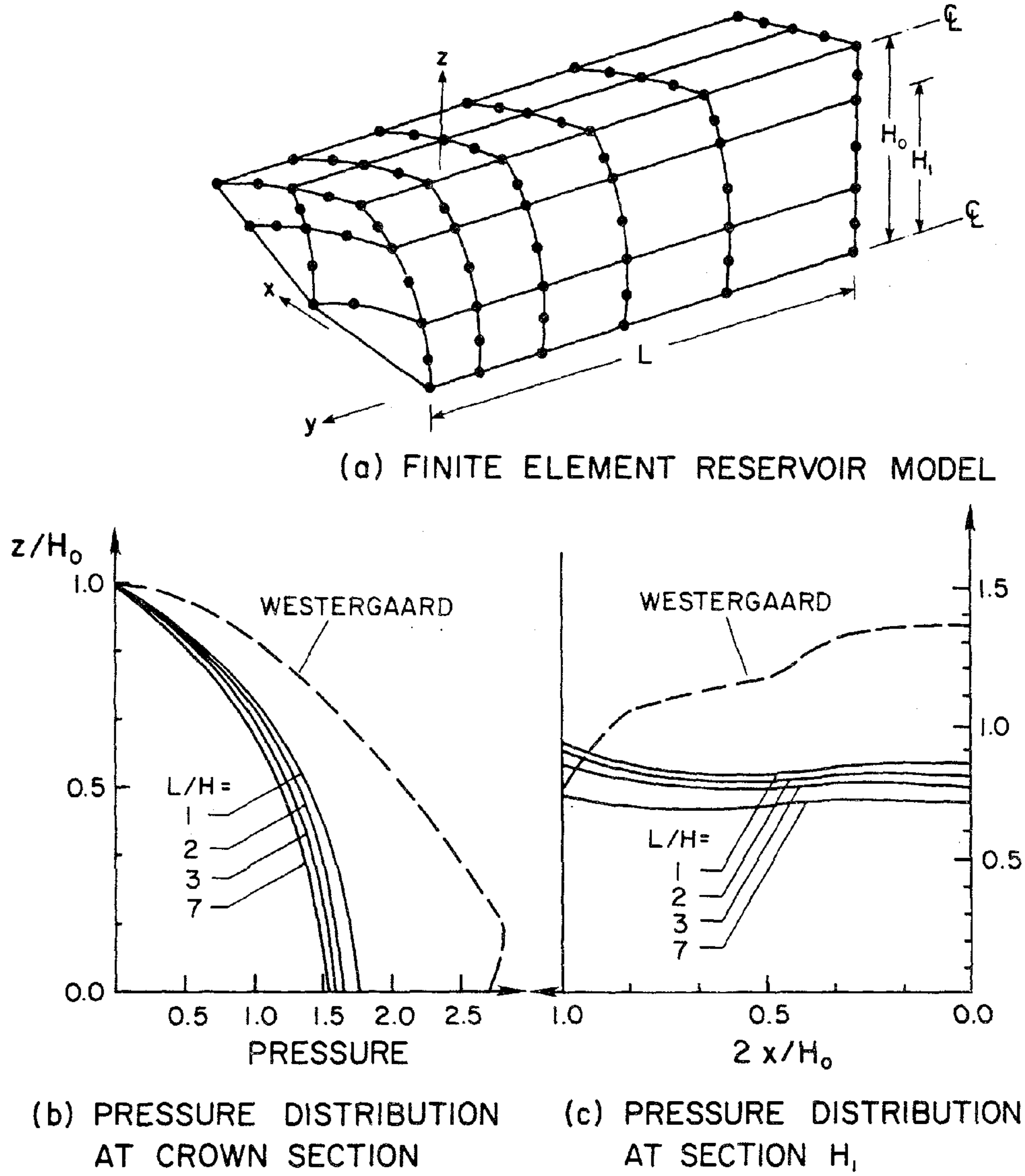

(a) FINITE ELEMENT RESERVOIR MODEL

(b) PRESSURE DISTRIBUTION AT CROWN SECTION

(c) PRESSURE DISTRIBUTION AT SECTION H_1

FIG. I-9 ARCH DAM WITH GENERAL GEOMETRY UPSTREAM FACE

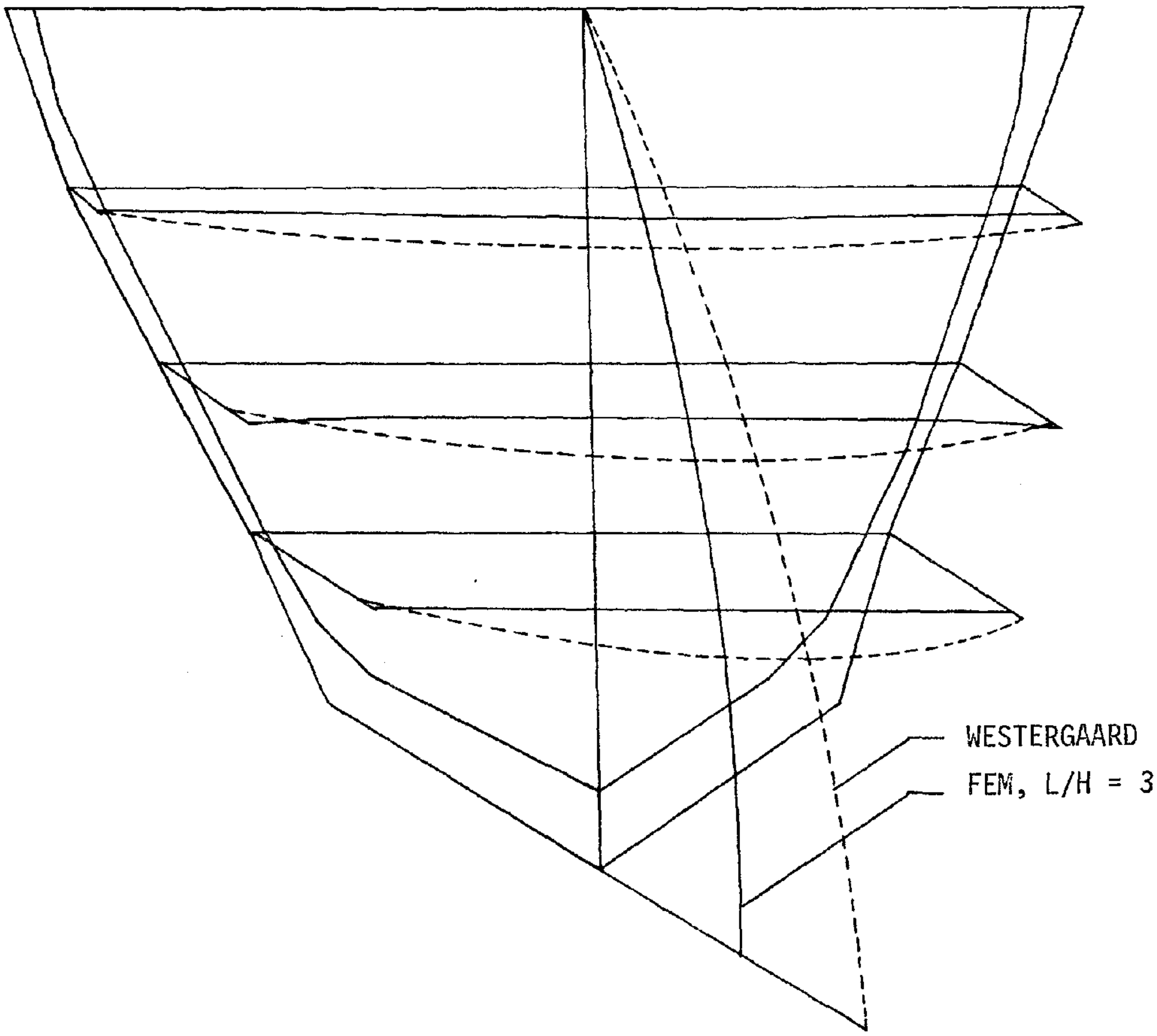

(d) PRESSURE DISTRIBUTION OVER THE DAM FACE

FIG. I-9 (Cont.) ARCH DAM WITH GENERAL GEOMETRY UPSTREAM FACE

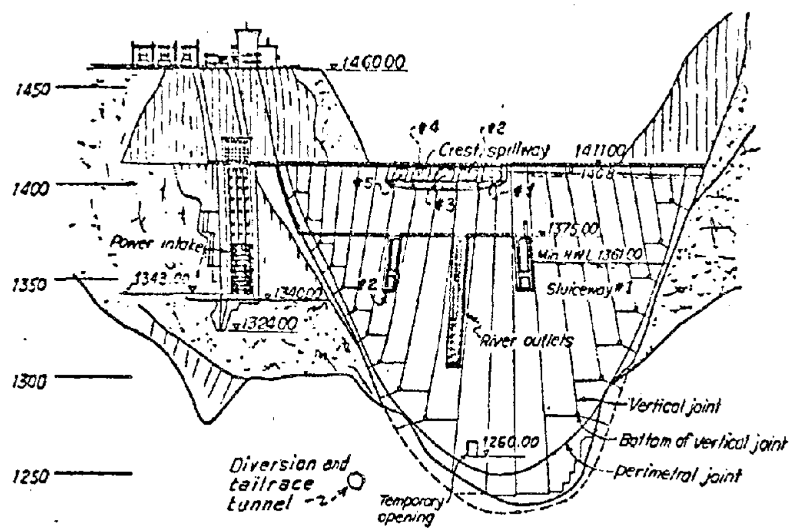

(a) *UPSTREAM VIEW*

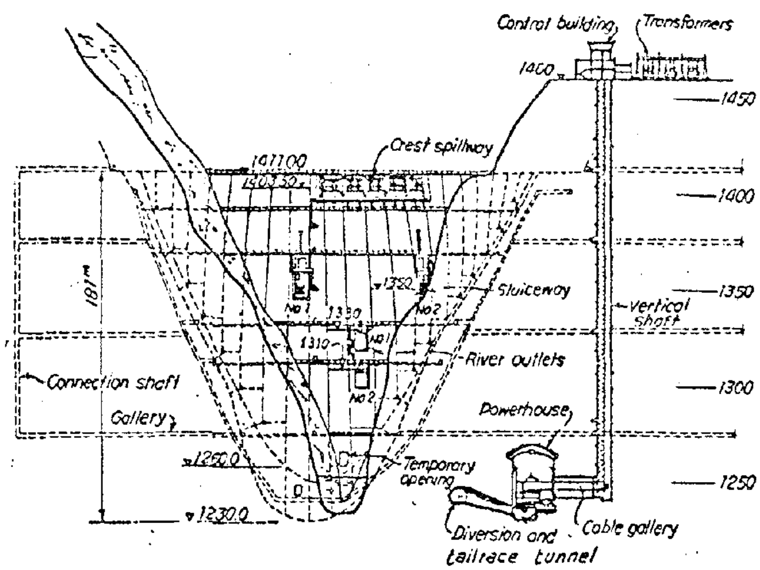

(b) *DOWNSTREAM VIEW*

FIG. I-10 TECHI ARCH DAM

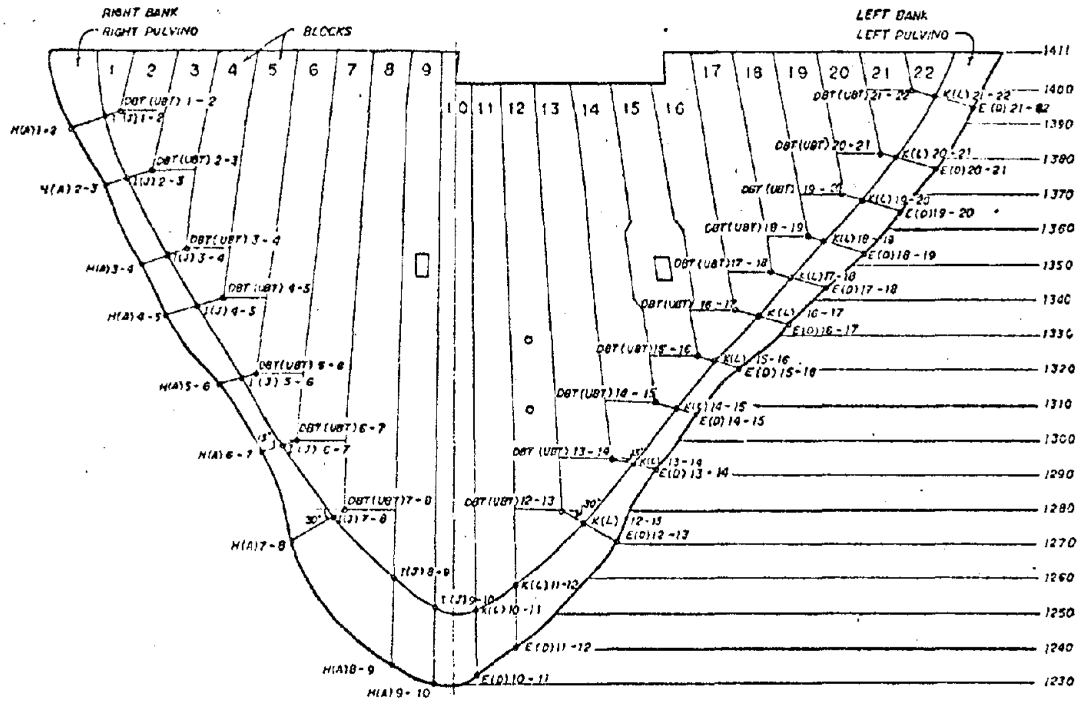

(c) KEY PLAN
(INCLINED CONTRACTION JOINTS)

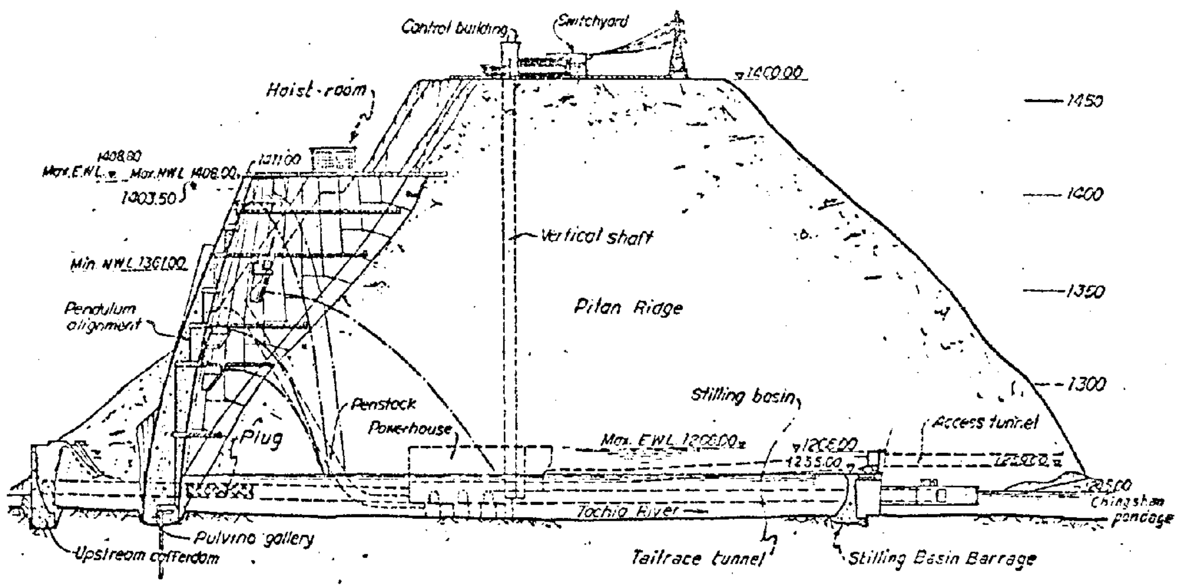

(d) MAIN SECTION AND LATERAL VIEW

FIG. I-10 (Cont.) TECHI ARCH DAM

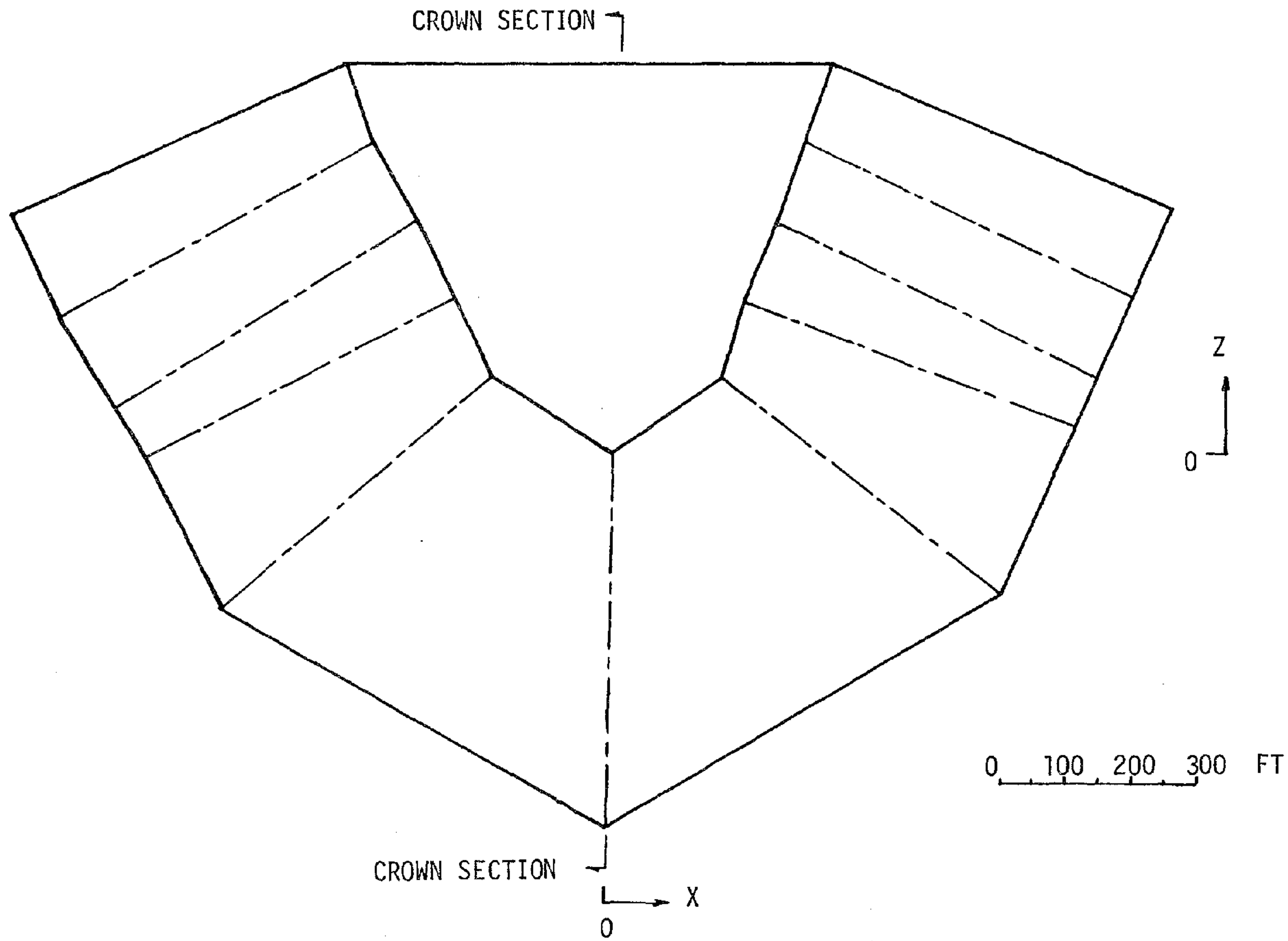

FIG. I-11 FOUNDATION ROCK AND DAM BODY OF TECHI DAM MODEL (XZ-PROJECTION)

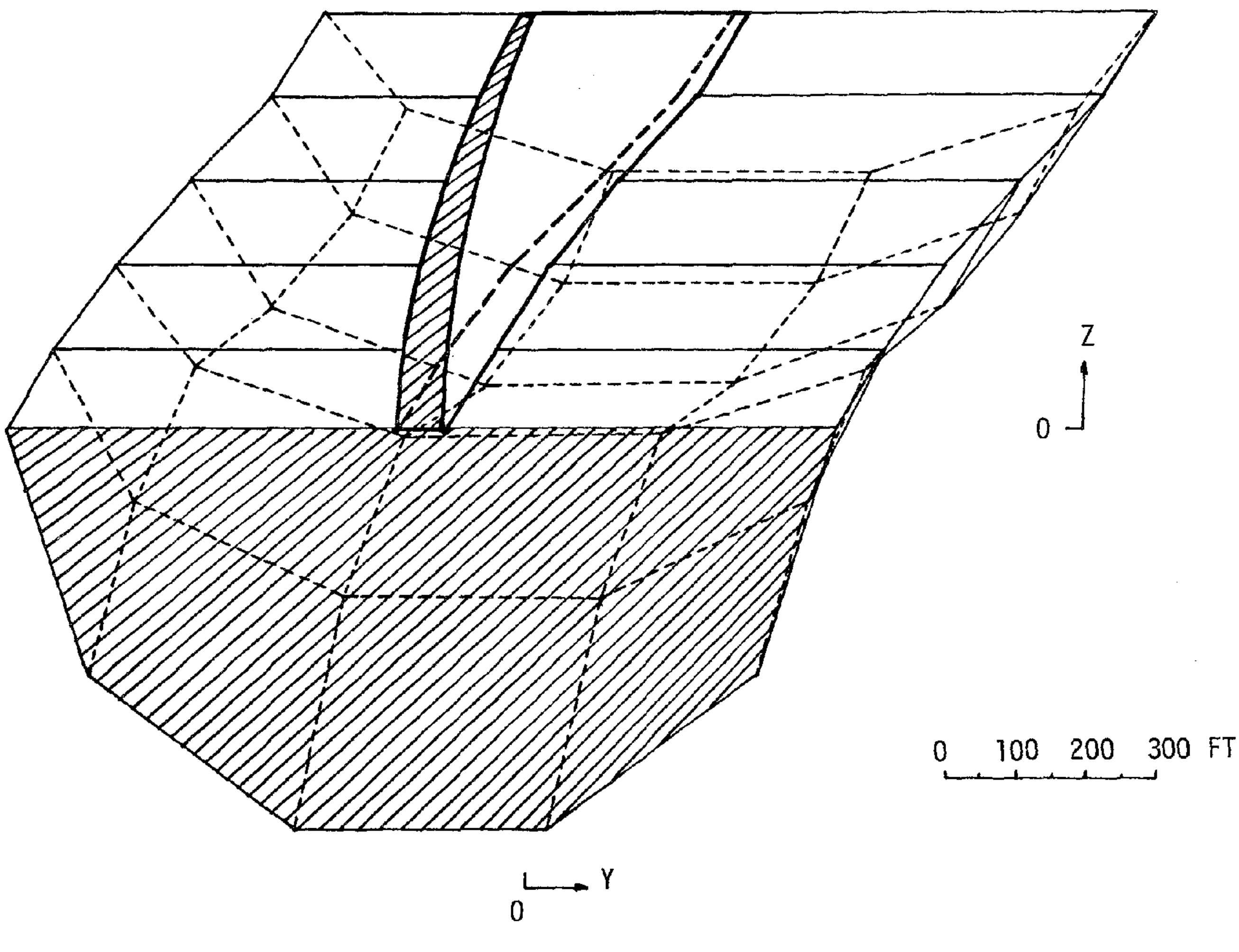

FIG. I-12 FOUNDATION ROCK AND DAM BODY OF TECHI DAM MODEL
(YZ-PROJECTION AT CROWN SECTION CUT)

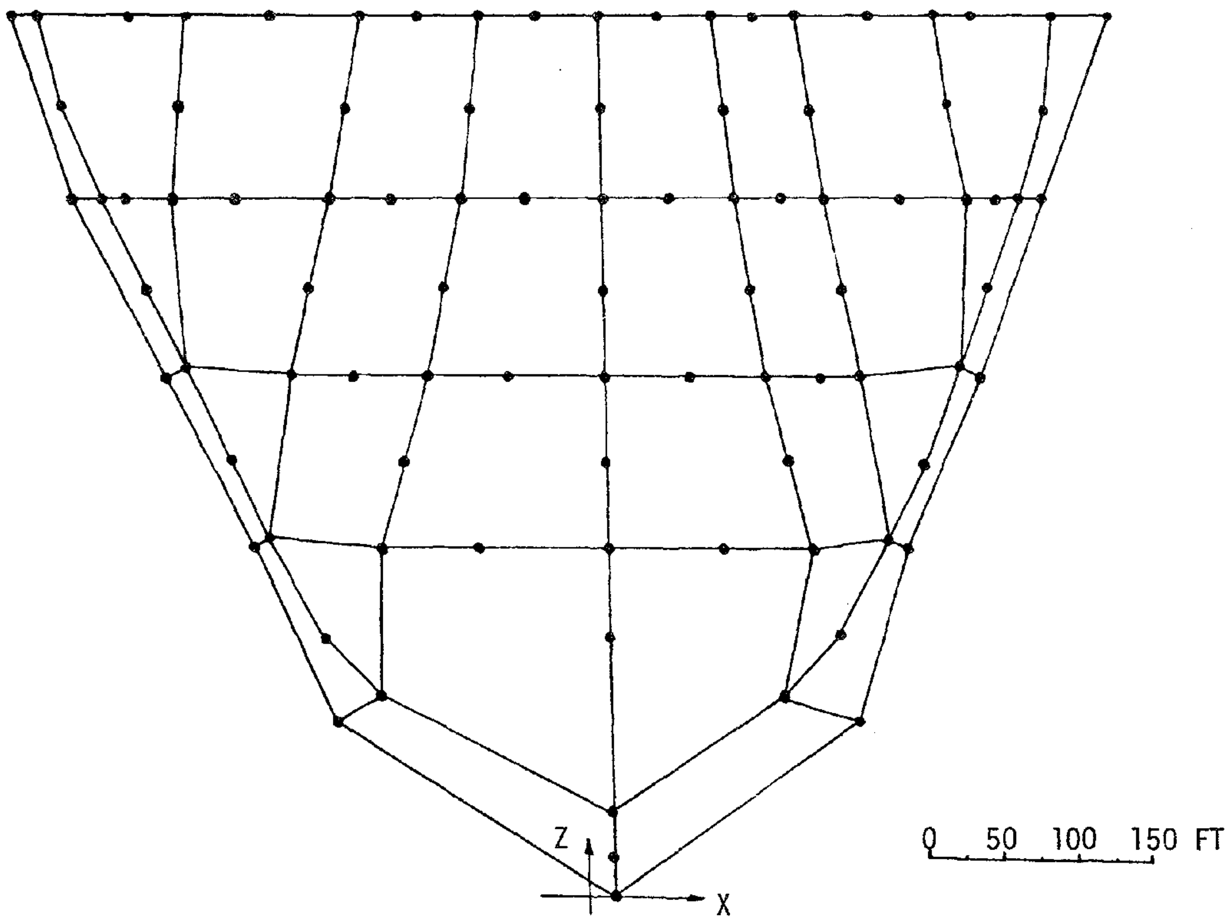

FIG. I-13 FINITE ELEMENT MESH OF DAM BODY (TECHI DAM)
UPSTREAM FACE PROJECTED ON XZ-PLANE

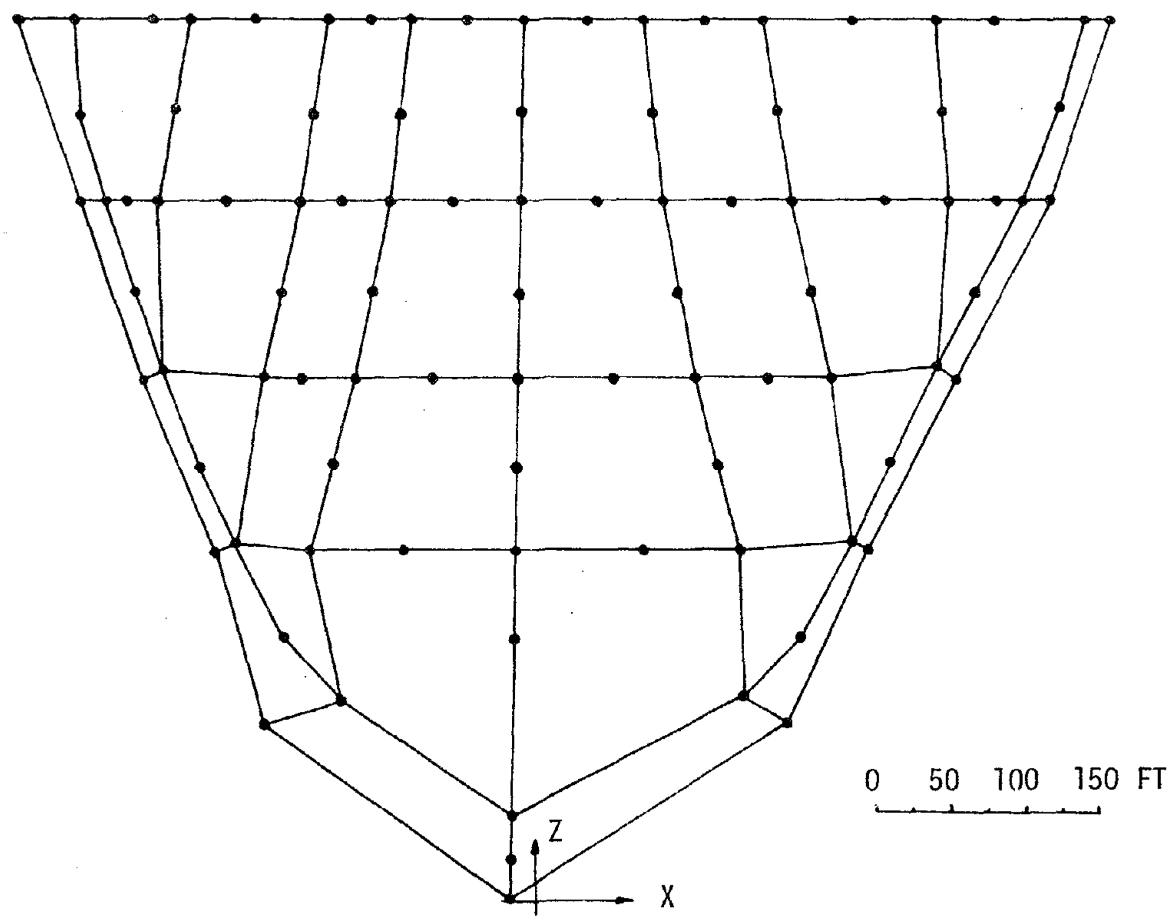

FIG. I-14 FINITE ELEMENT MESH OF DAM BODY (TECHI DAM)
DOWNSTREAM FACE PROJECTED ON XZ-PLANE

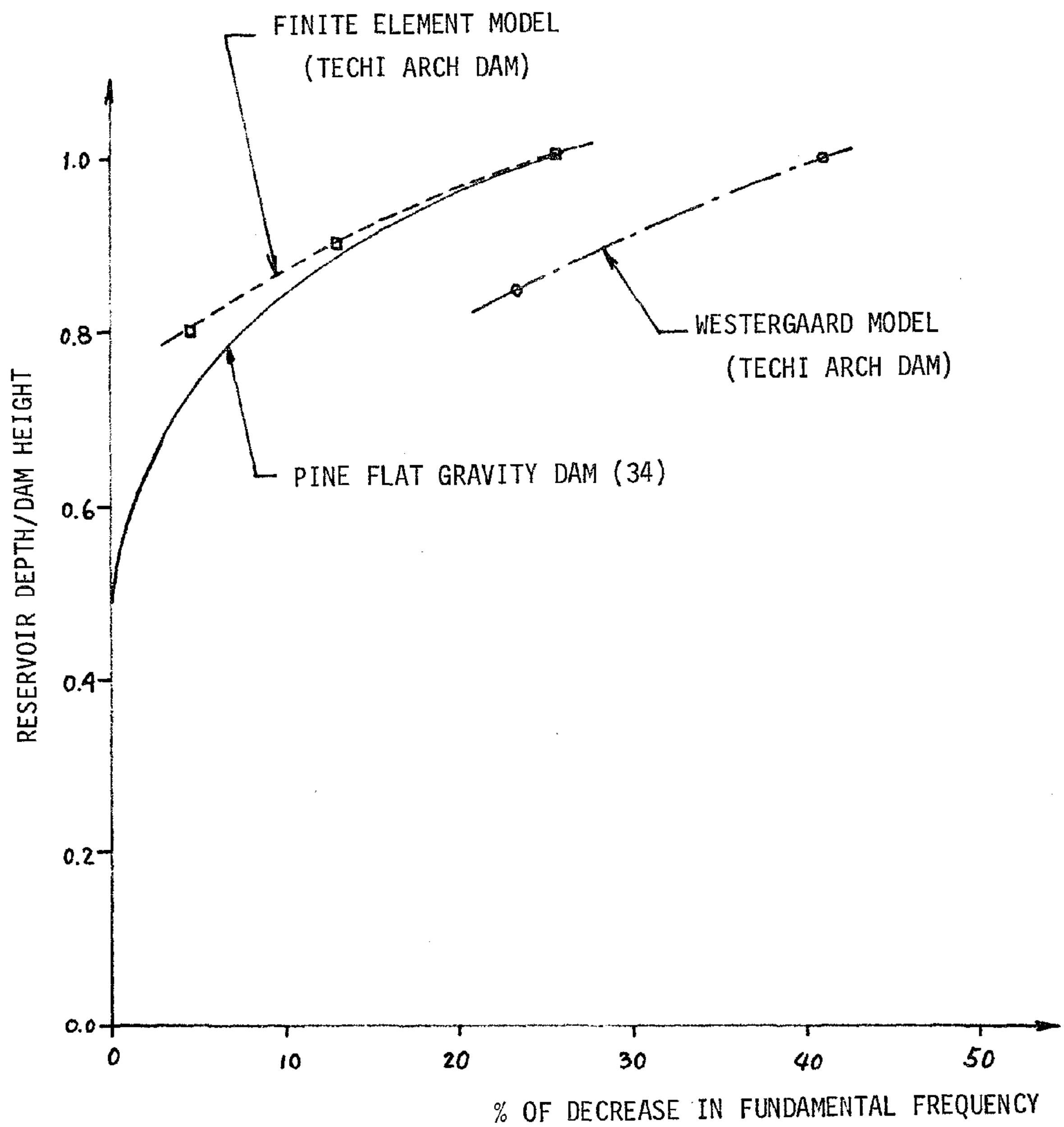

FIG. I-15 EFFECT OF INCOMPRESSIBLE RESERVOIR ON THE FUNDAMENTAL FREQUENCY OF VIBRATION OF THE DAM-RESERVOIR SYSTEMS

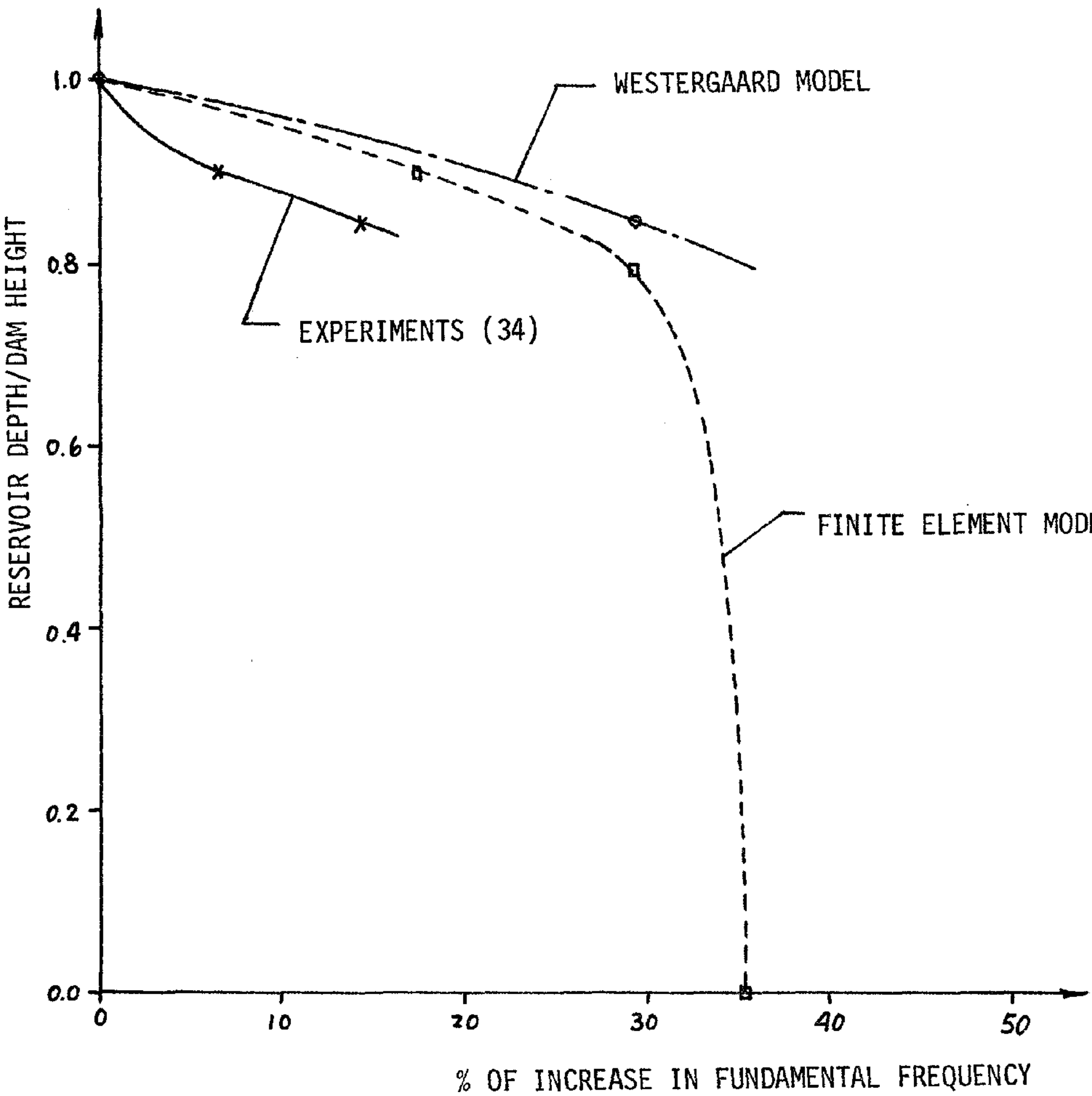

FIG. I-16 COMPARISON OF EFFECTS OF INCOMPRESSIBLE RESERVOIR ON THE FUNDAMENTAL FREQUENCY OF VIBRATION OF TECHI DAM-RESERVOIR SYSTEM

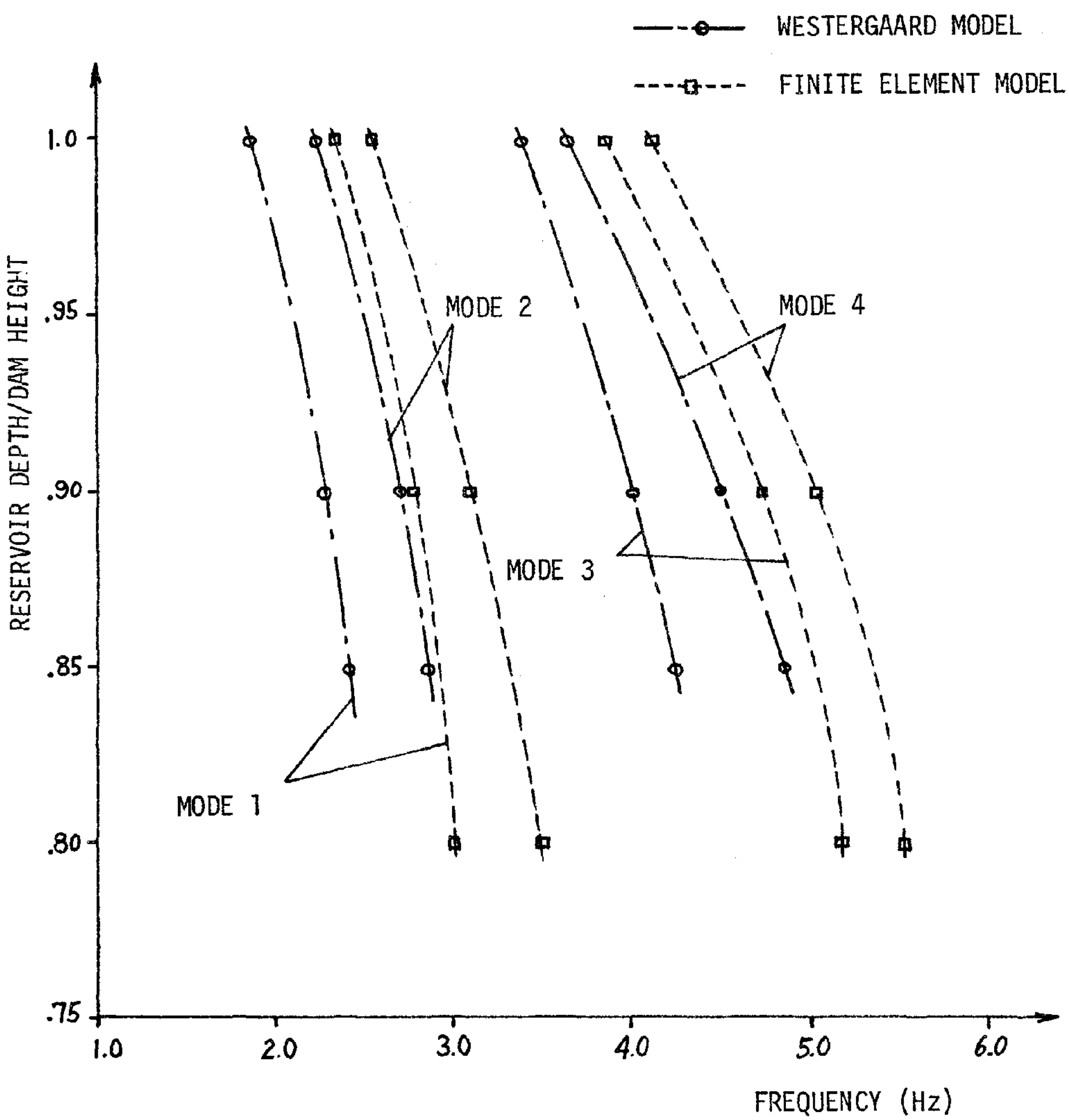

FIG. I-17 FREQUENCIES OF FIRST FOUR MODES OF TECHI DAM ACCORDING TO DIFFERENT RESERVOIR MODEL FOR VARIOUS WATER LEVELS

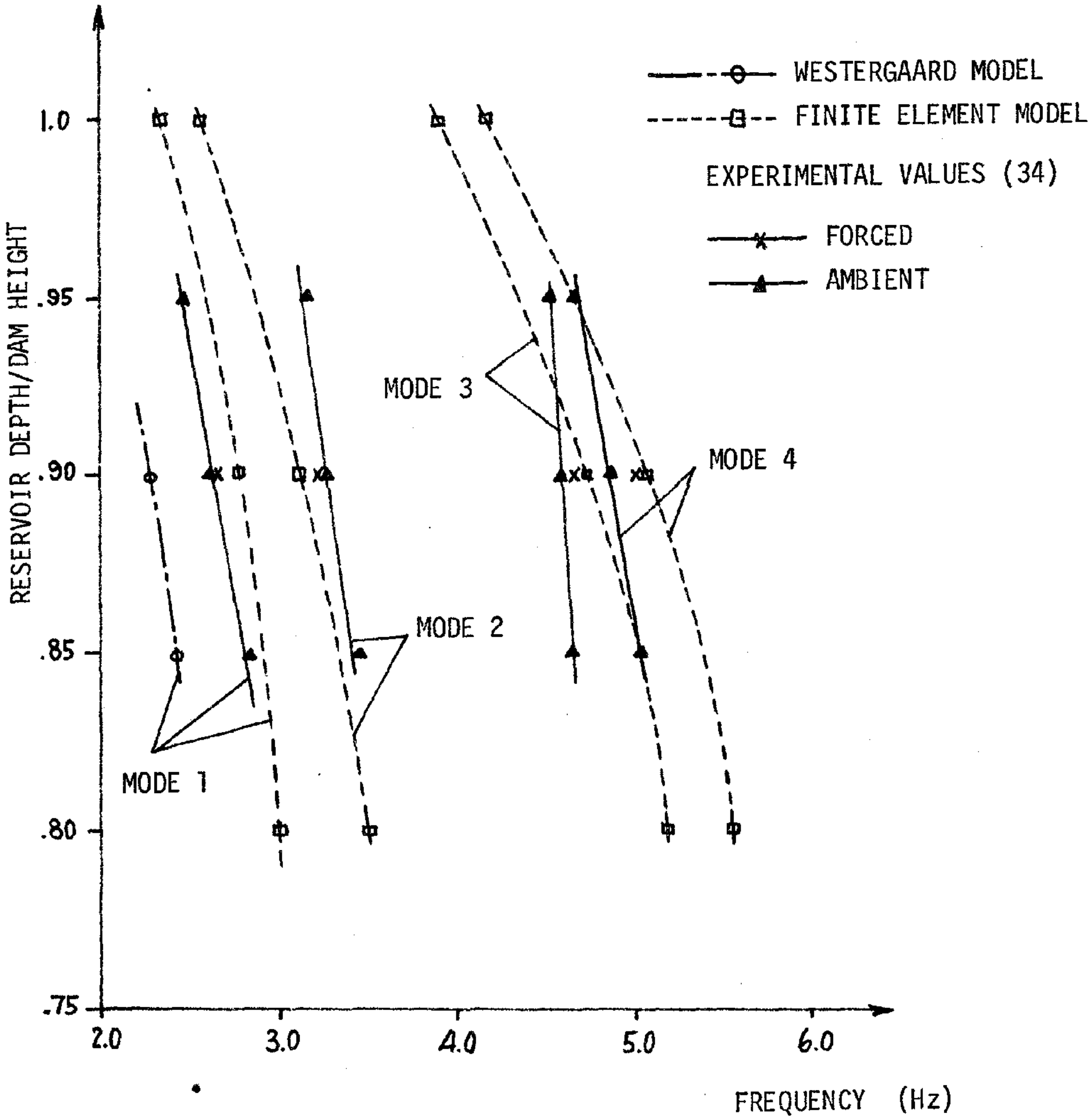

FIG. I-18 FREQUENCY CORRELATIONS OF EXPERIMENTS WITH NUMERICAL ANALYSES

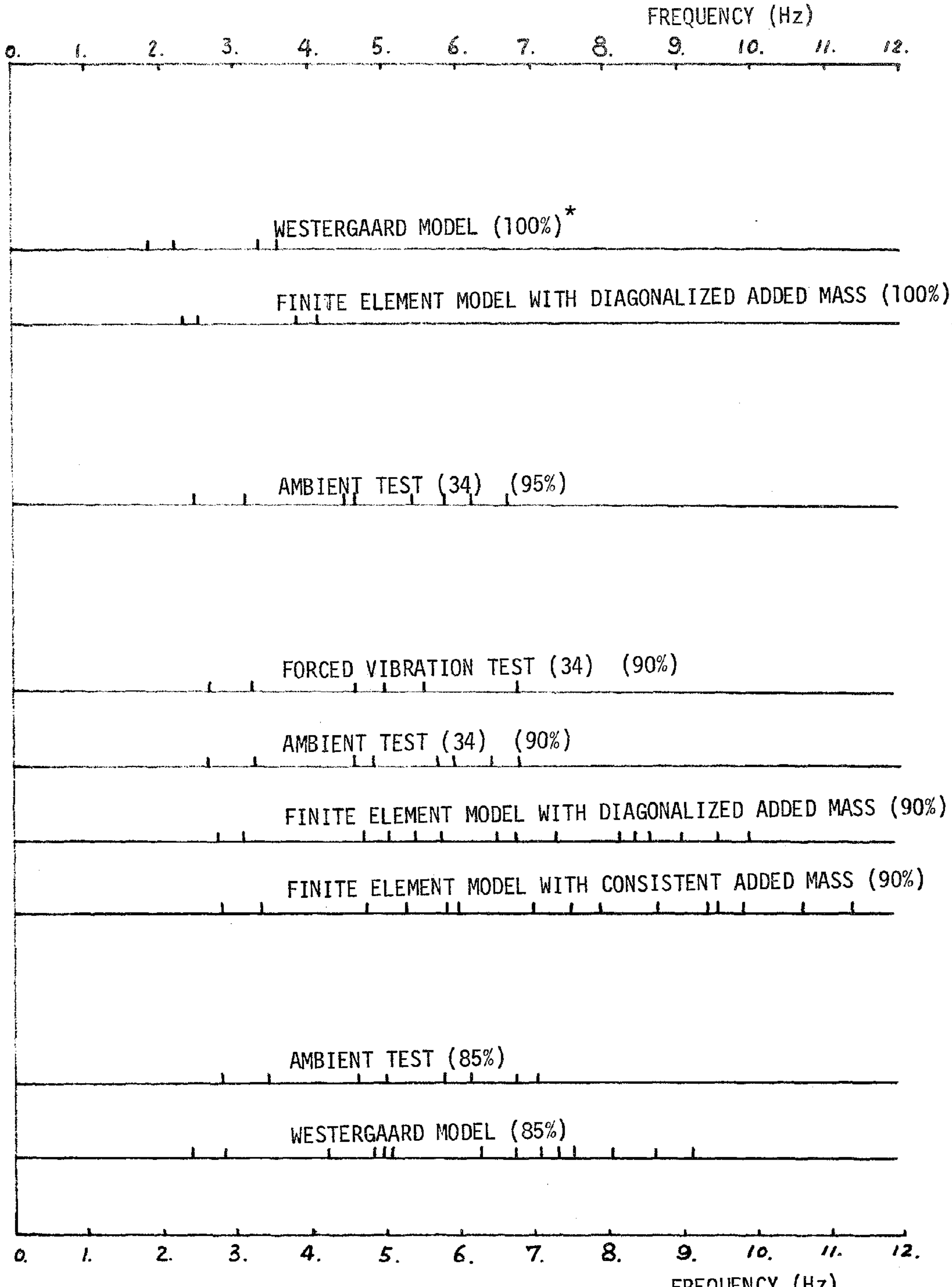

(*Reservoir water level in percentage of dam height)

FIG. I-19 FREQUENCY SPECTRA CORRELATIONS OF VARIOUS WATER LEVELS (TECHI DAM)

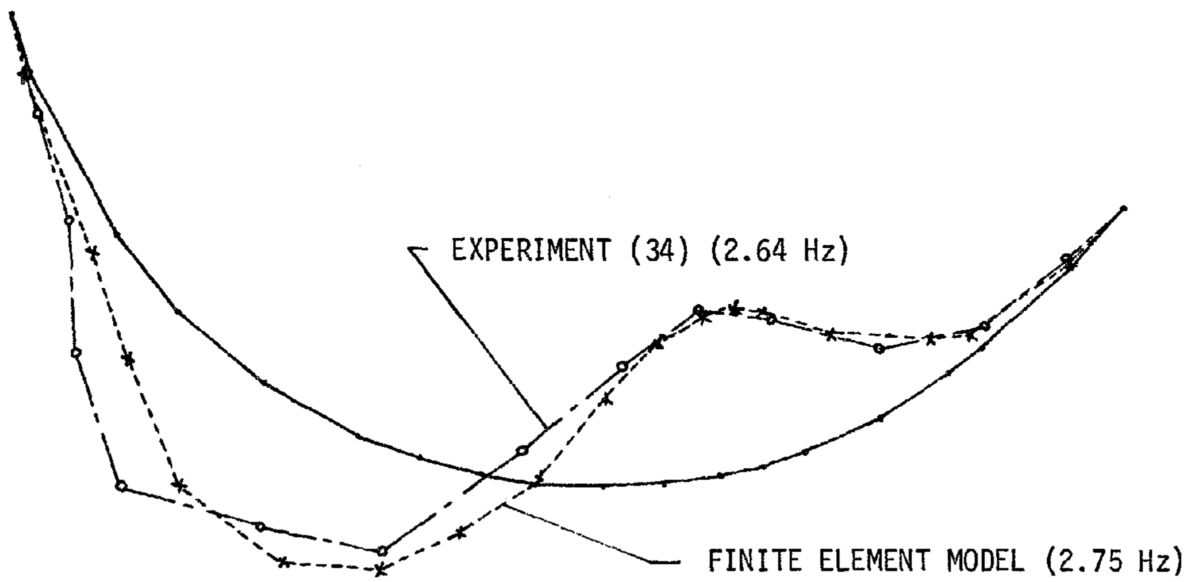

(a) MODE 1

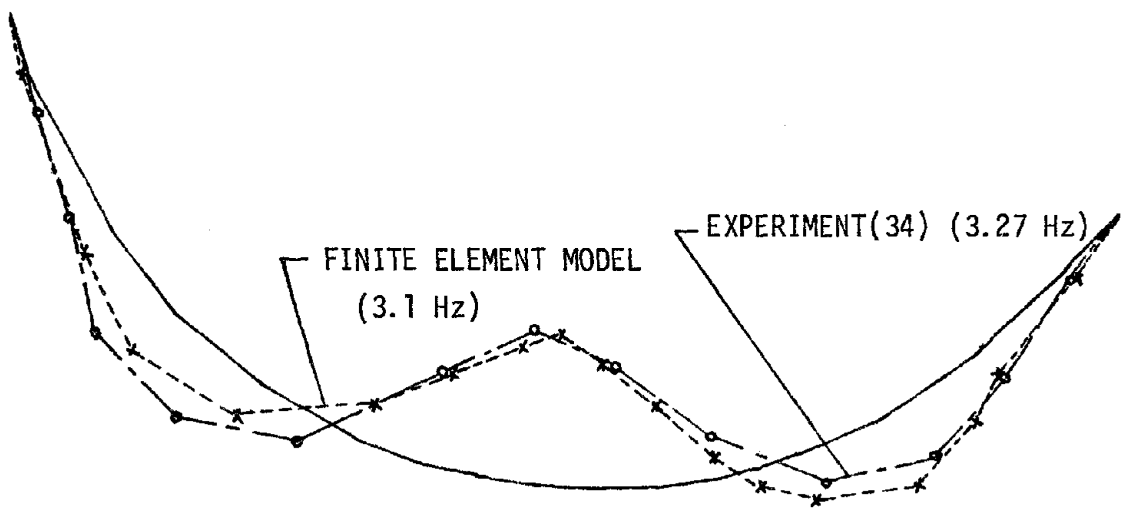

(b) MODE 2

FIG. I-20 MODE SHAPE (RADIAL) CORRELATIONS FOR 90% RESERVOIR DEPTH

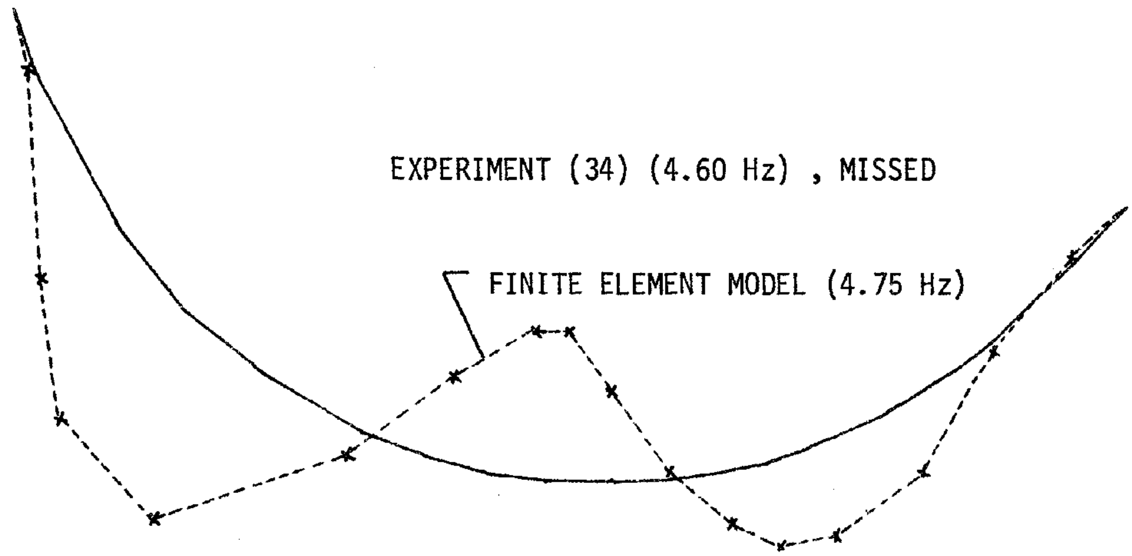

(c) MODE 3

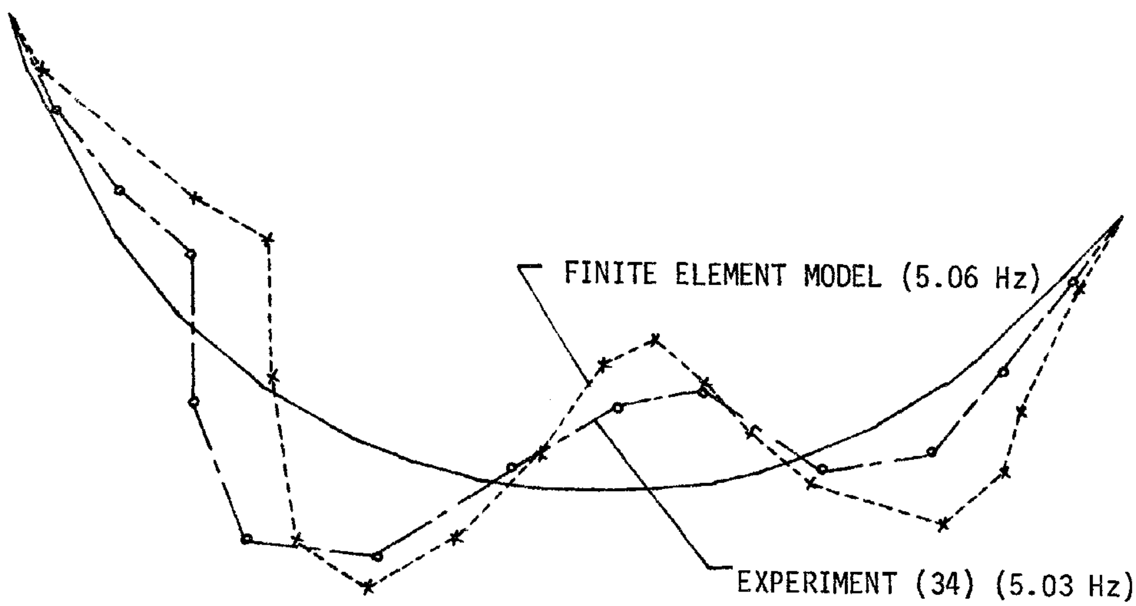

(d) MODE 4

FIG. I-20 (Cont.)

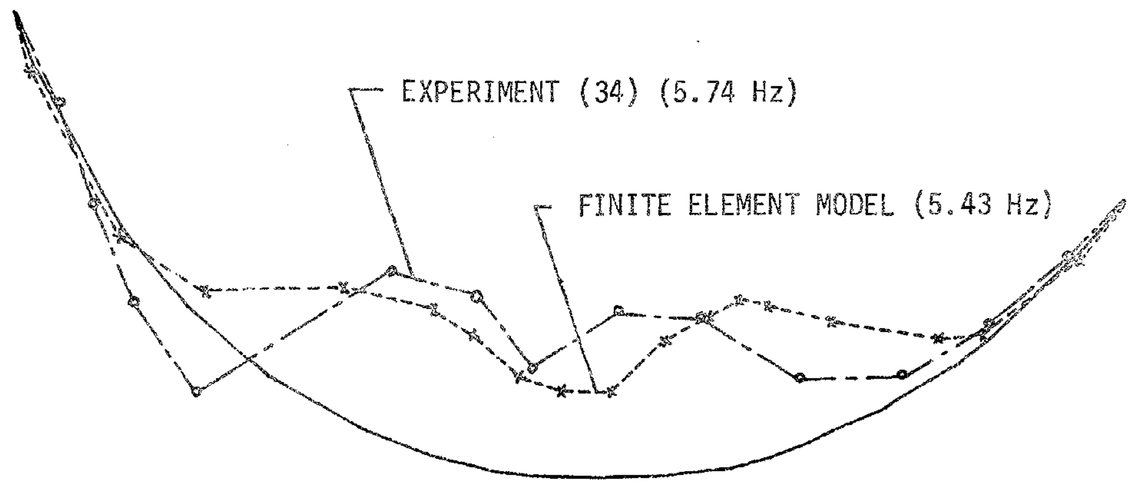

(e) MODE 5

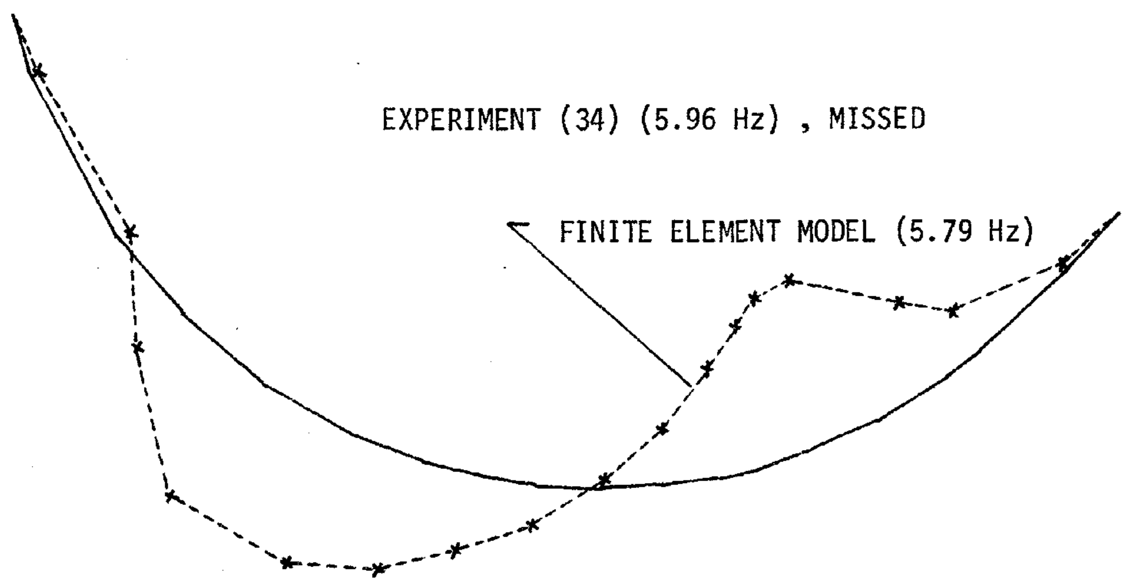

(f) MODE 6

FIG. I-20 (Cont.)

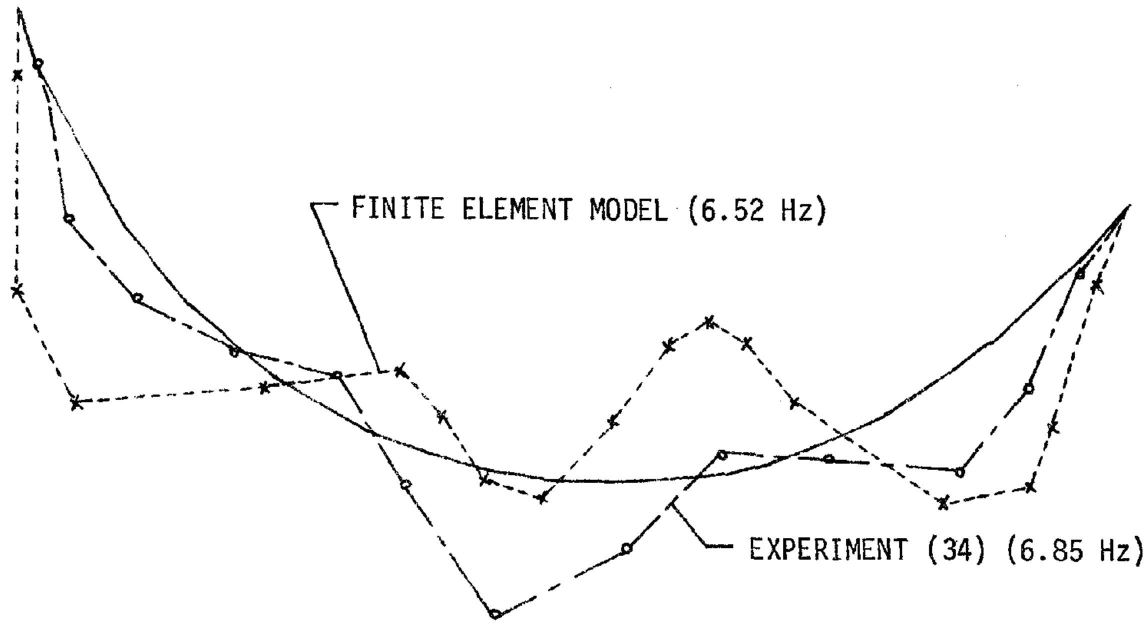

(g) MODE 7

FIG. I-20 (Cont.)

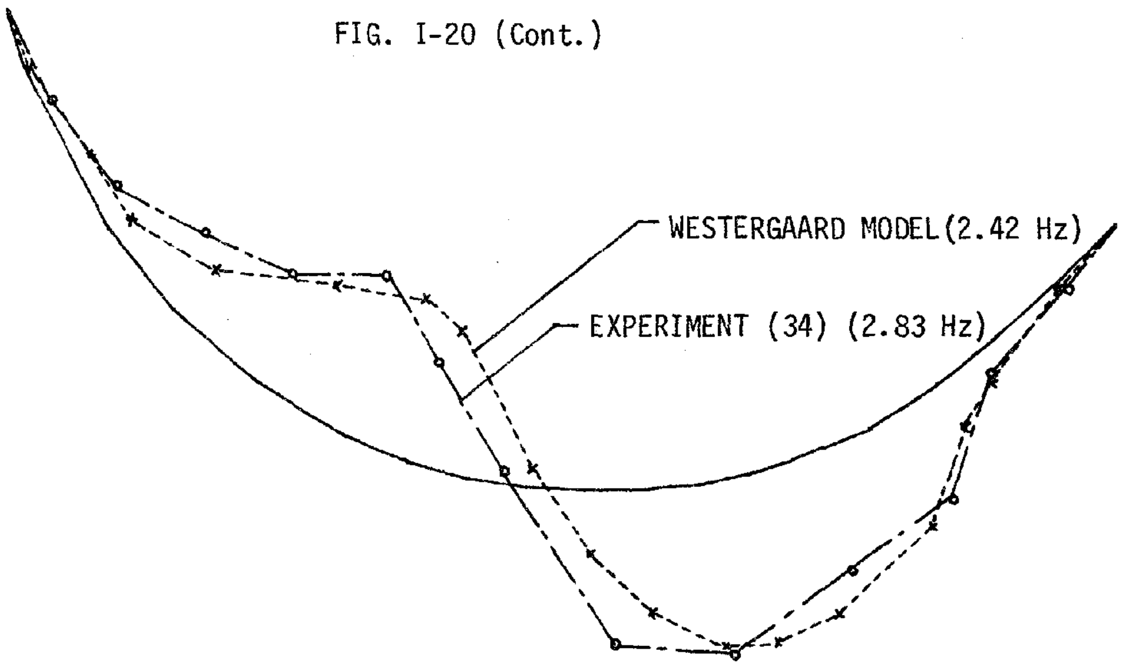

(a) MODE 1

FIG. I-21 MODE SHAPE (RADIAL) CORRELATIONS FOR 85% RESERVOIR DEPTH

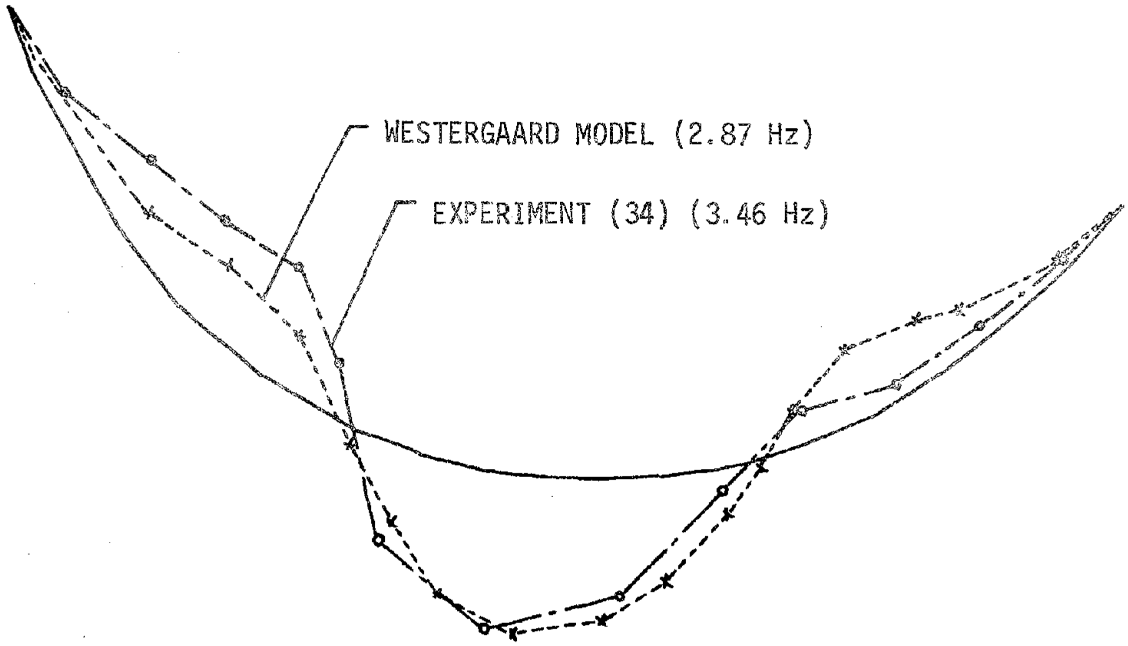

(b) MODE 2

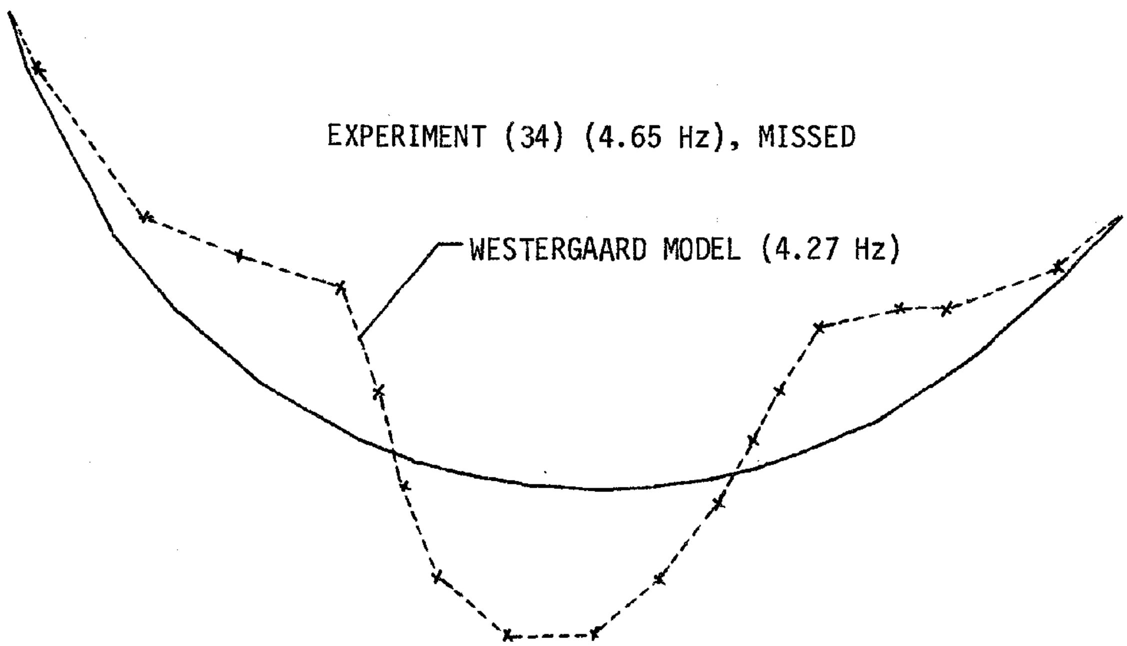

(c) MODE 3

FIG. I-21 (Cont.)

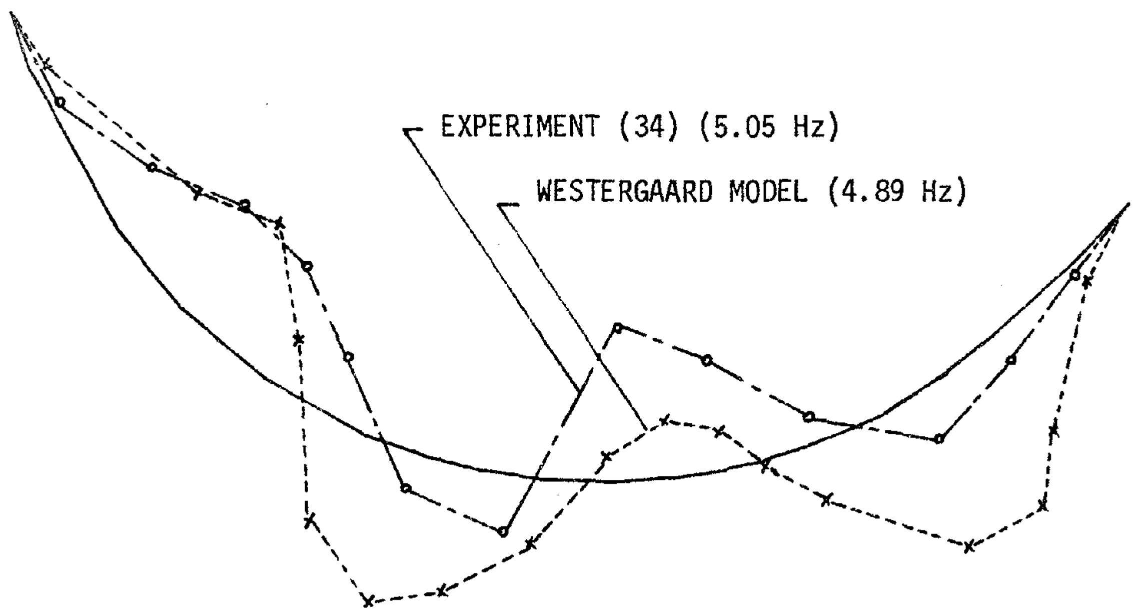

(d) MODE 4

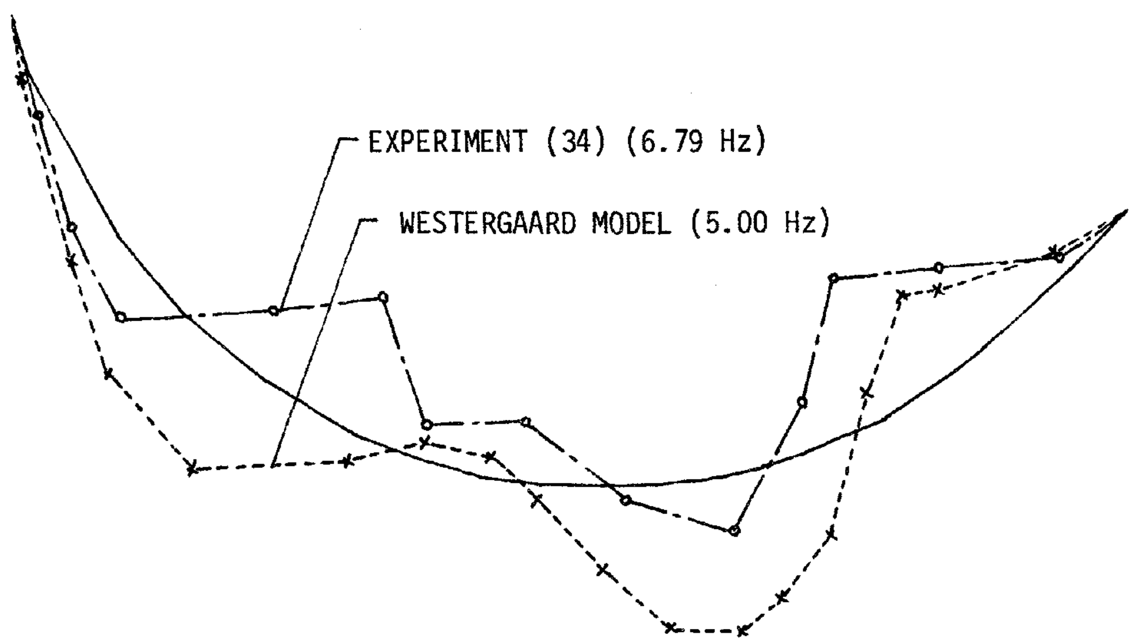

(e) MODE 5

FIG. I-21 (Cont.)

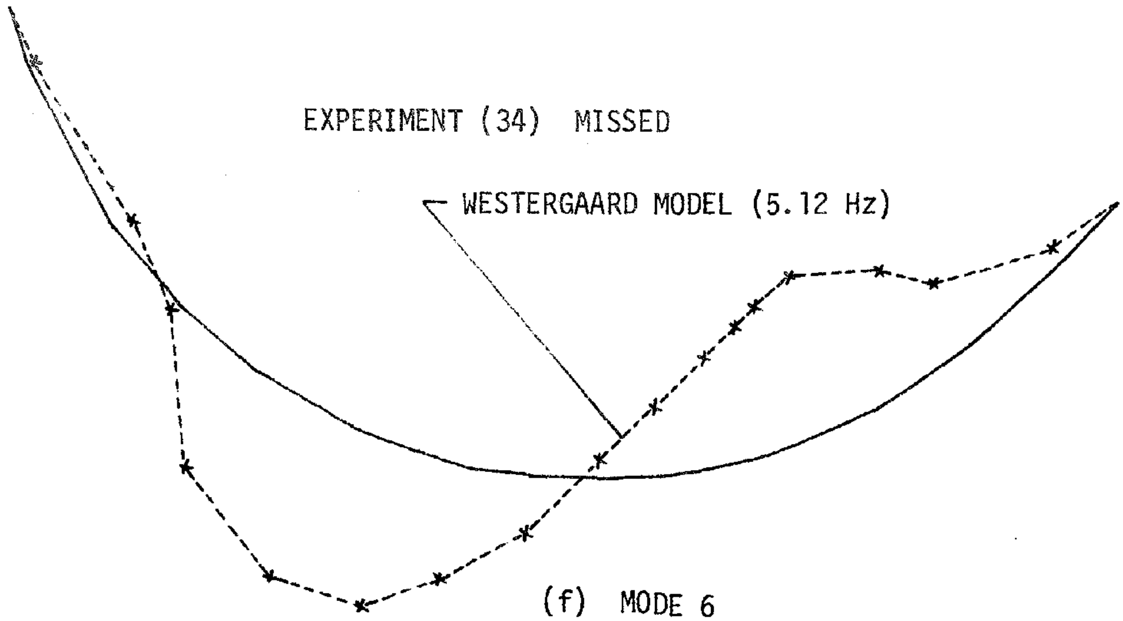

(f) MODE 6

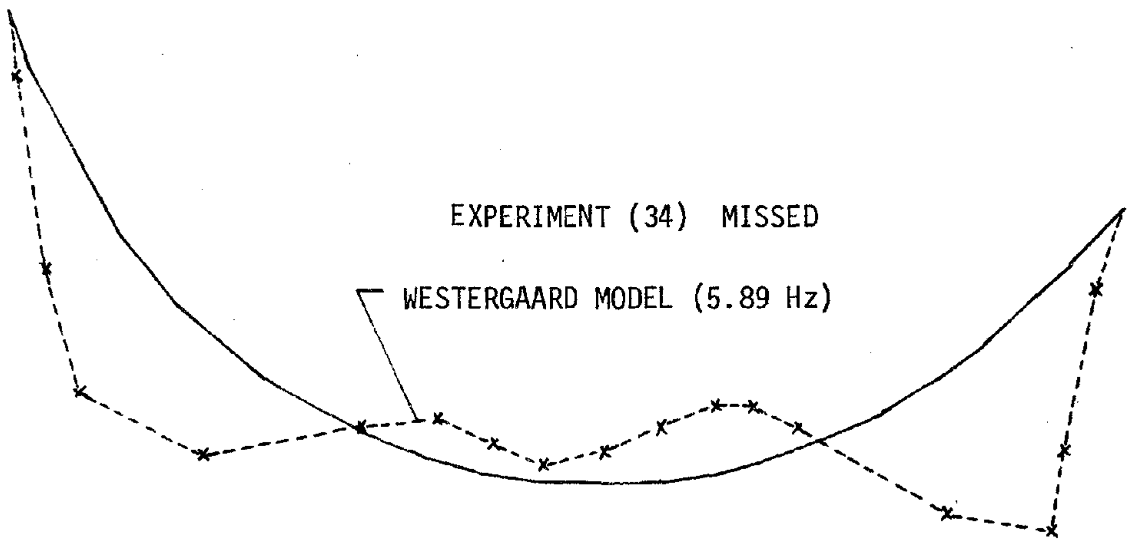

(g) MODE 7

FIG. I-21 (Cont.)

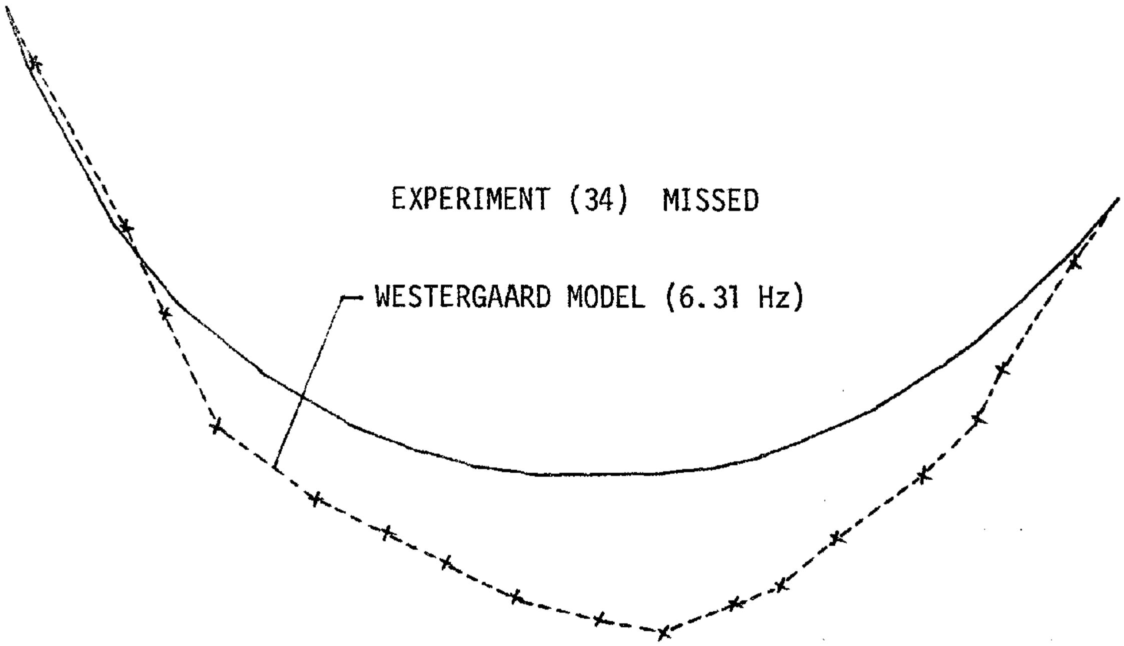

(h) MODE 8

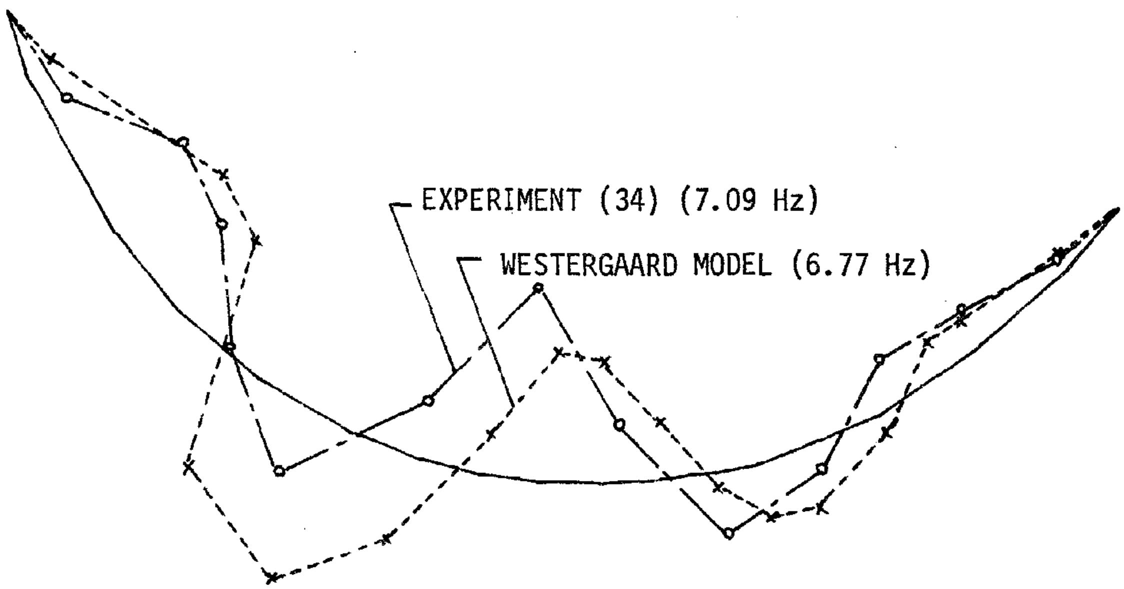

(i) MODE 9

FIG. I-21 (Cont.)

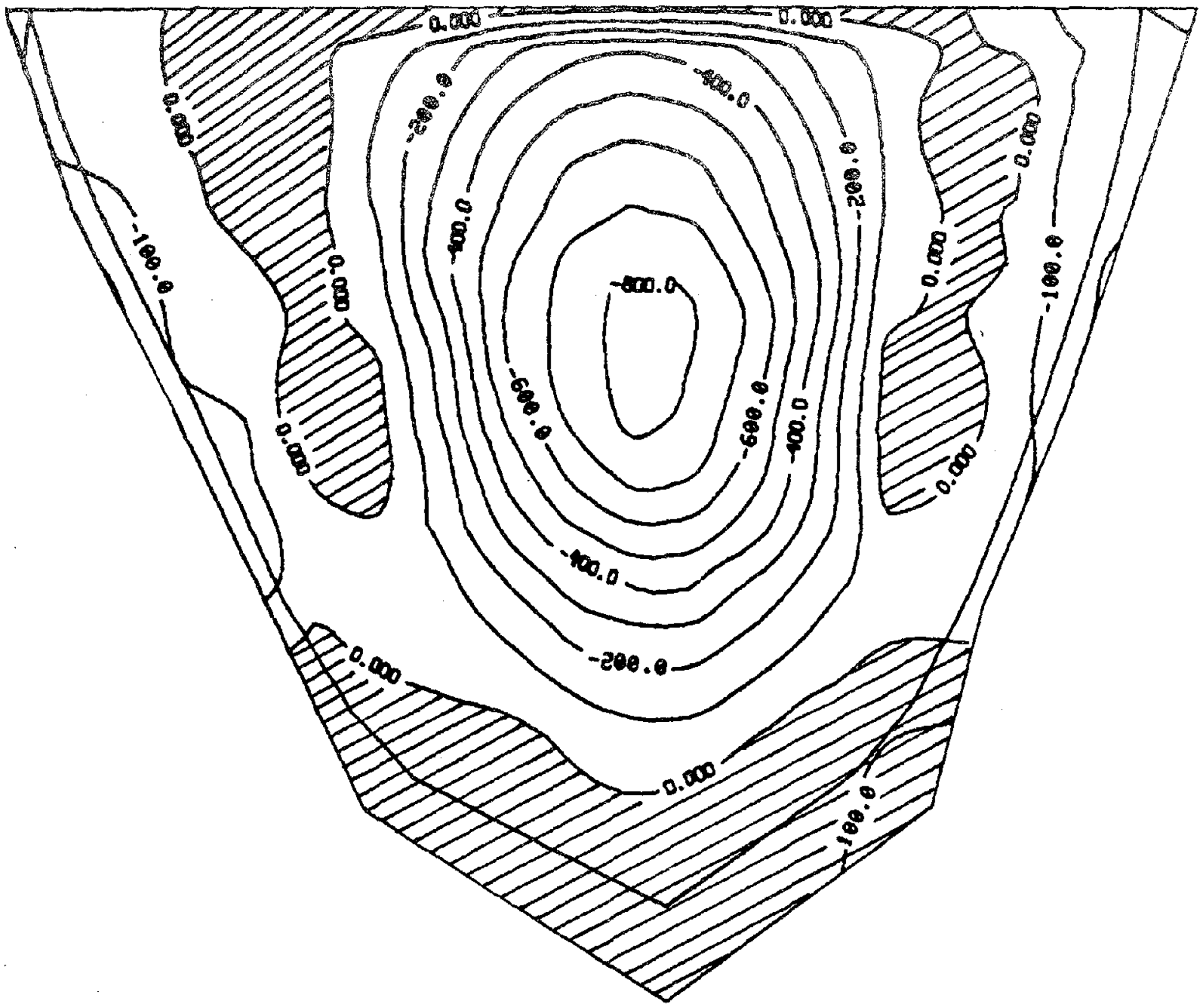

UPSTREAM FACE

SIG-XX

UNIT : PSI

CONTOUR INTERVAL= 100.0

HYDROSTATIC + GRAVITY LOADS ONLY

(a)

FIG. I-22 CANTILEVER STRESS AND ARCH STRESS IN TECHI DAM
DUE TO STATIC LOADS

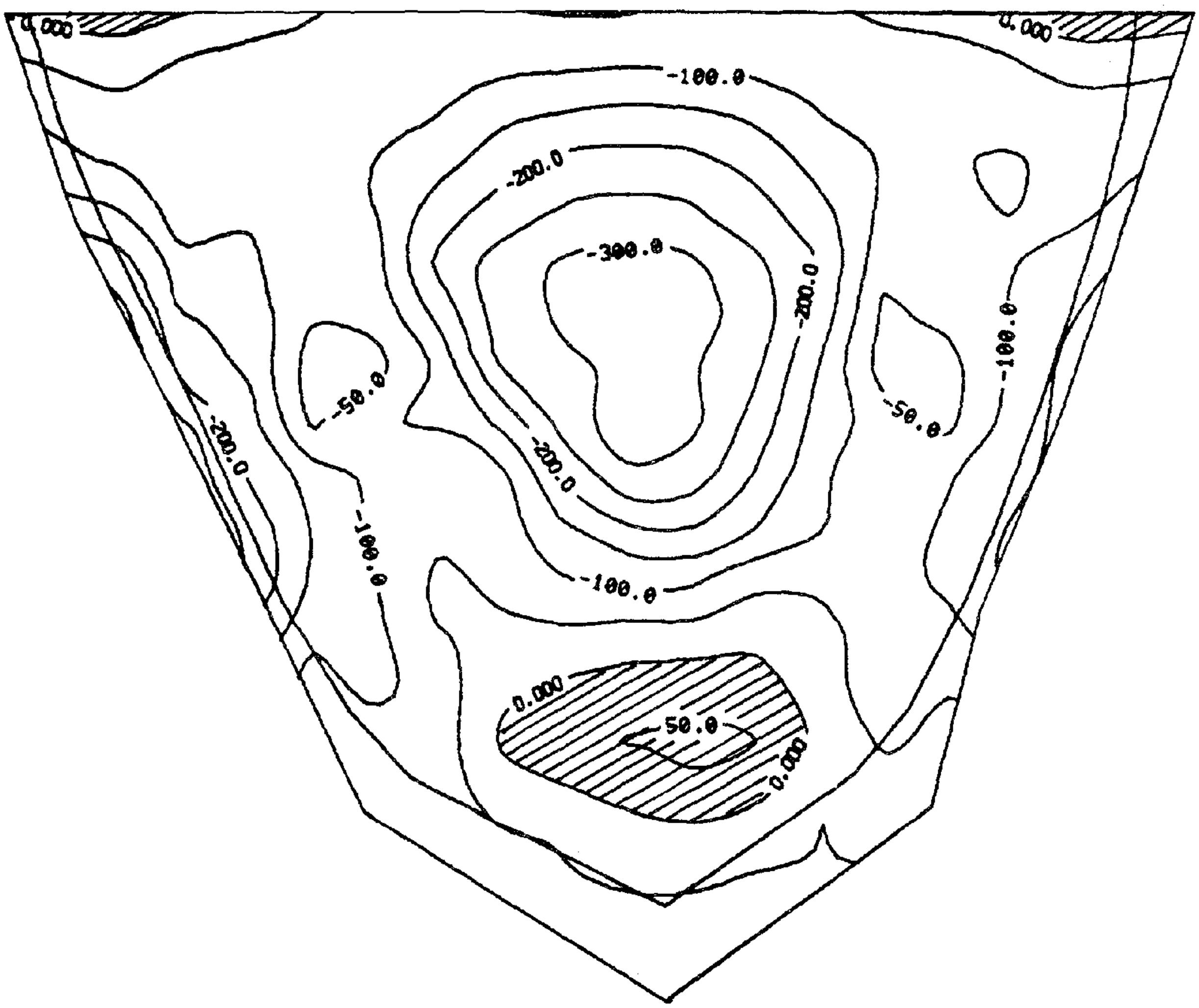

UPSTREAM FACE

SIG-YY

UNIT : PSI

CONTOUR INTERVAL= 50.0

HYDROSTATIC + GRAVITY LOADS ONLY

(b)

FIG. I-22 (Cont.)

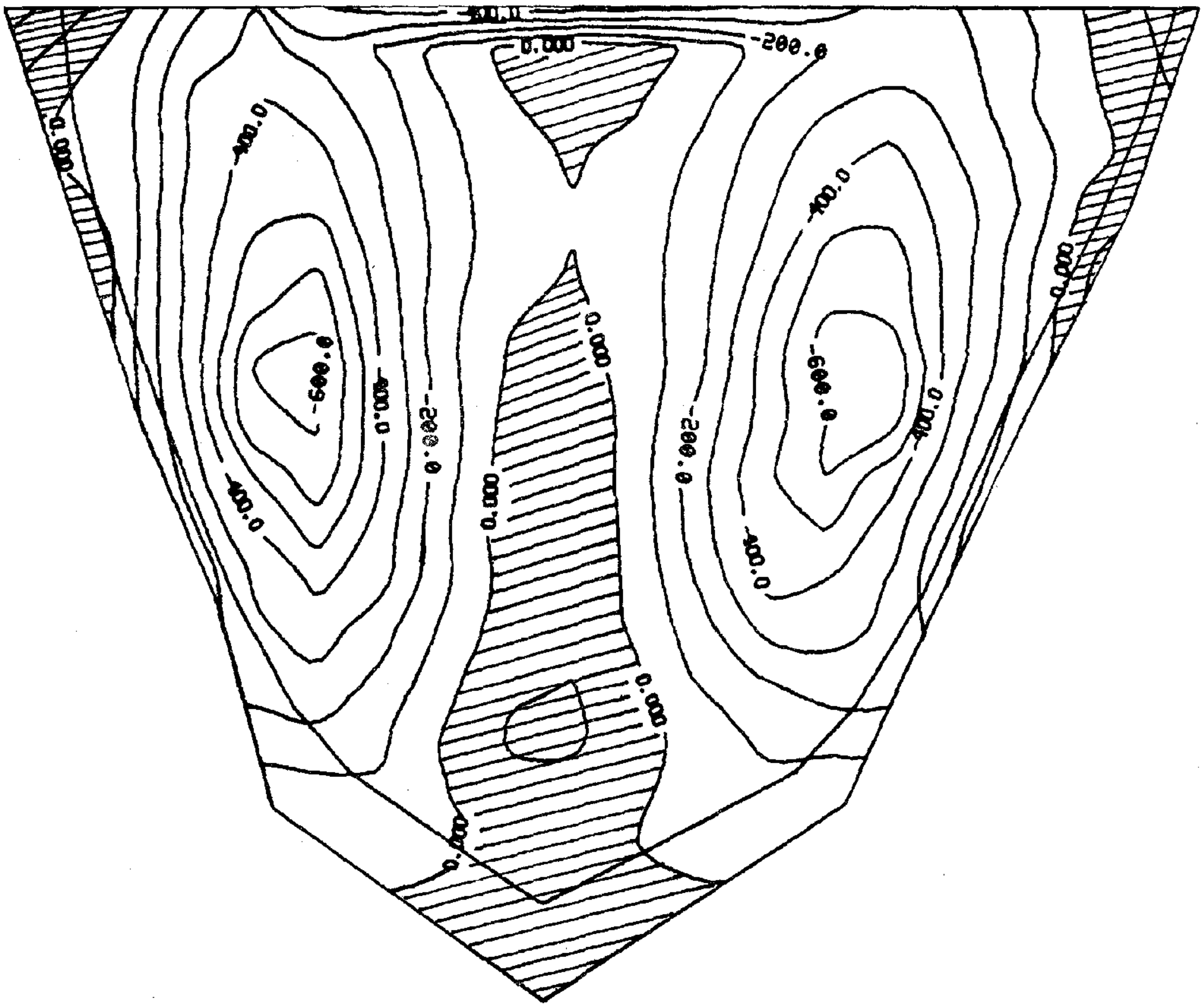

DOWNSTREAM FACE

SIG-XX

UNIT : PSI

CONTOUR INTERVAL= 100.0

HYDROSTATIC + GRAVITY LOADS ONLY

(c)

FIG. I-22 (Cont.)

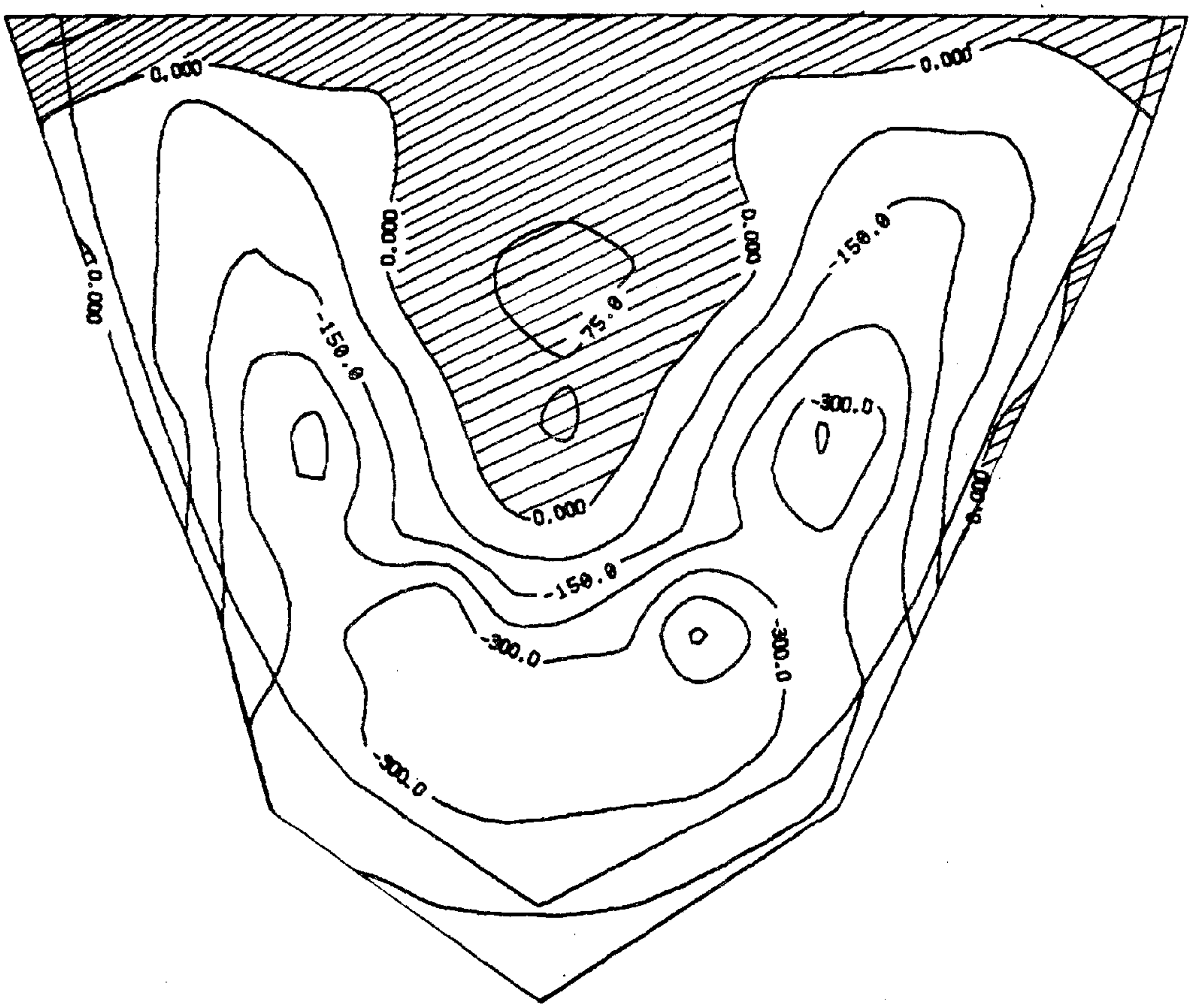

DOWNSTREAM FACE

SIG-YY

UNIT : PSI

CONTOUR INTERVAL= 75.0

HYDROSTATIC + GRAVITY LOADS ONLY

(d)

FIG. I-22 (Cont.)

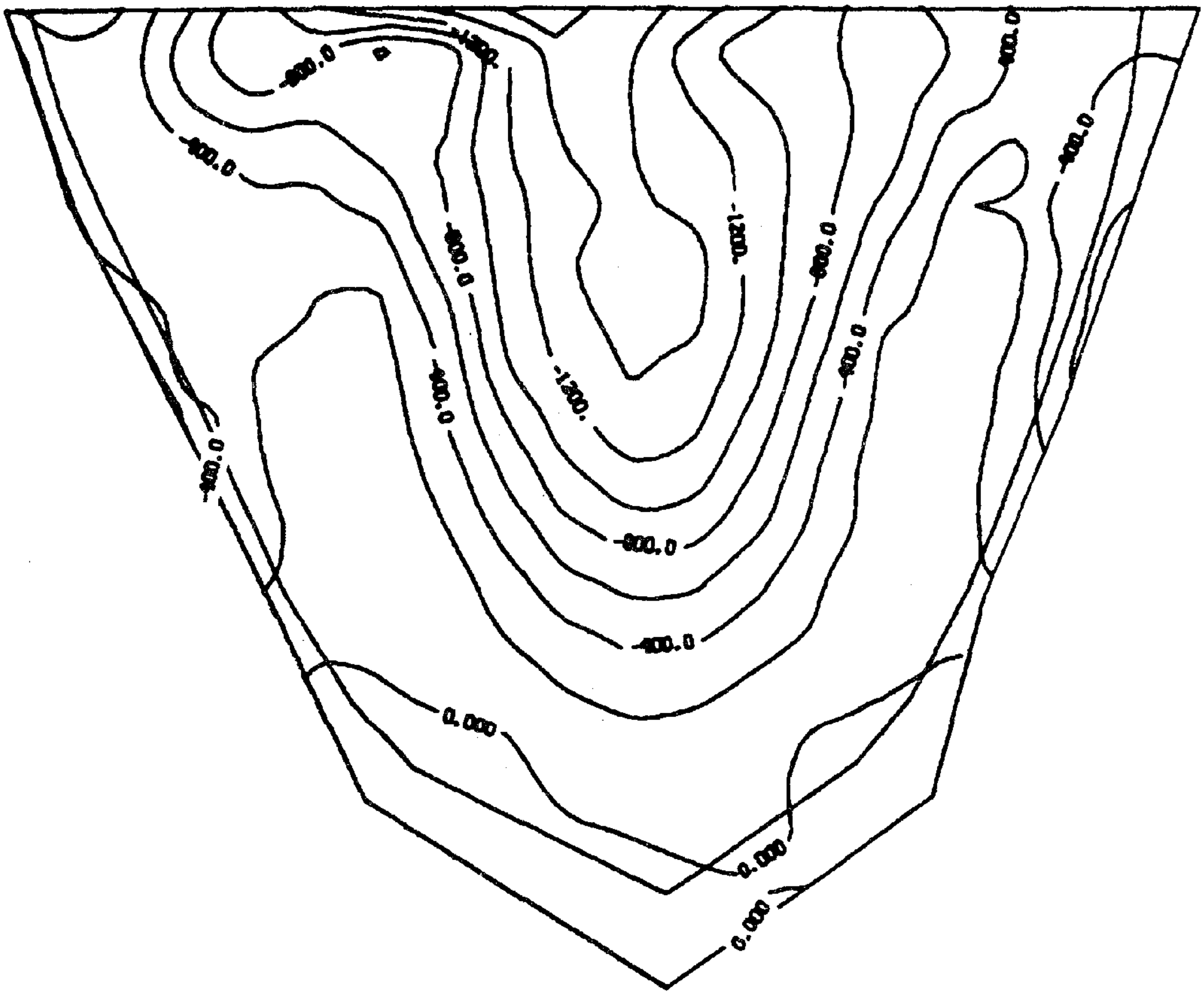

UPSTREAM FACE

MINIMUM SIG-XX

UNIT : PSI

CONTOUR INTERVAL= 200.0

UPSTREAM-DOWNSTREAM EXCITATIONS

AND HYDROSTATIC + GRAVITY LOADS

(a)

FIG.I-23 CANTILEVER STRESS AND ARCH STRESS ENVELOPES FOR UPSTREAM FACE OF TECHI DAM DUE TO STATIC LOADS AND DESIGN BASE EARTHQUAKE

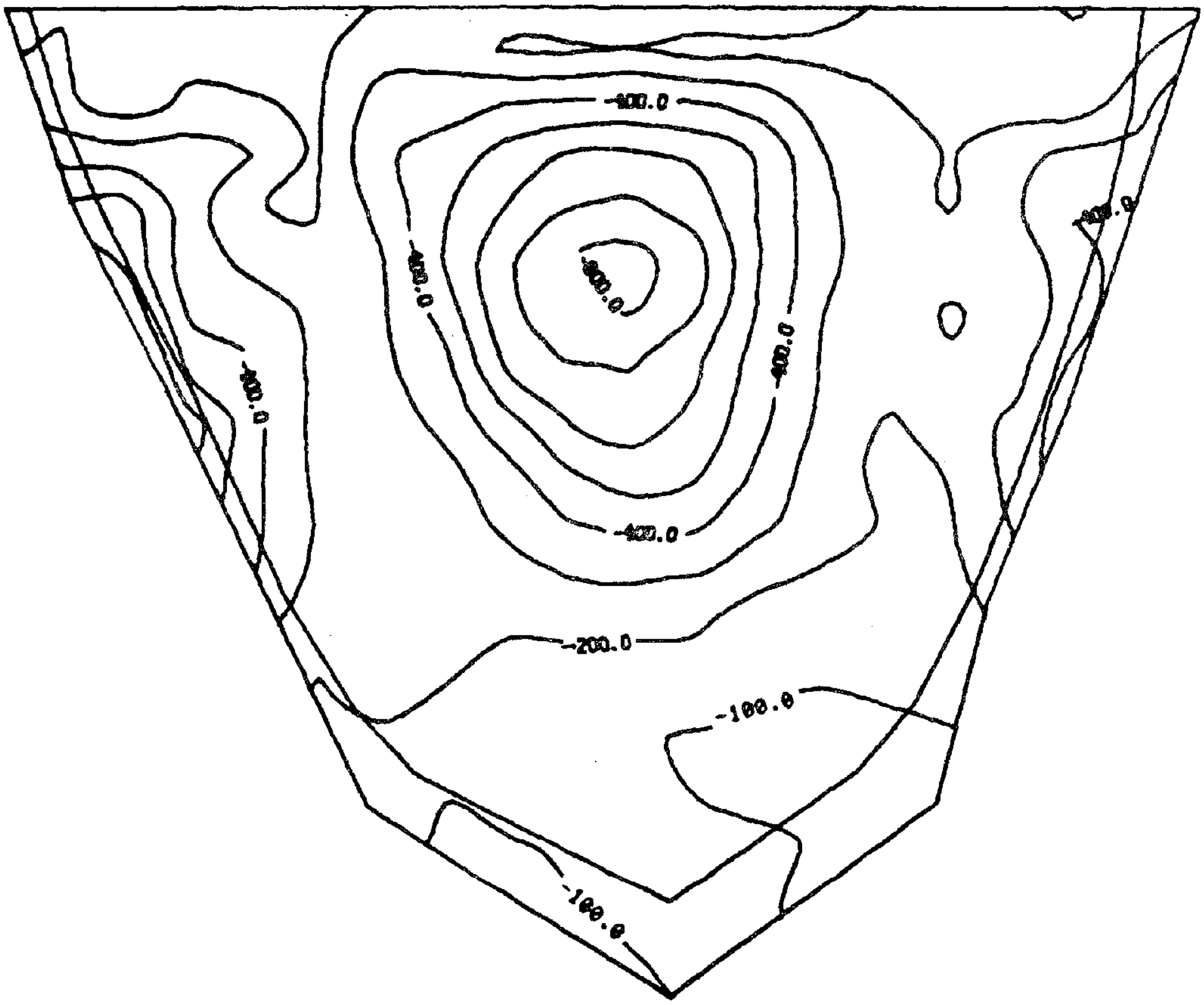

UPSTREAM FACE

MINIMUM SIG-YY

UNIT : PSI

CONTOUR INTERVAL= 100.0

UPSTREAM-DOWNSTREAM EXCITATIONS

AND HYDROSTATIC + GRAVITY LOADS

(b)

FIG. I-23 (Cont.)

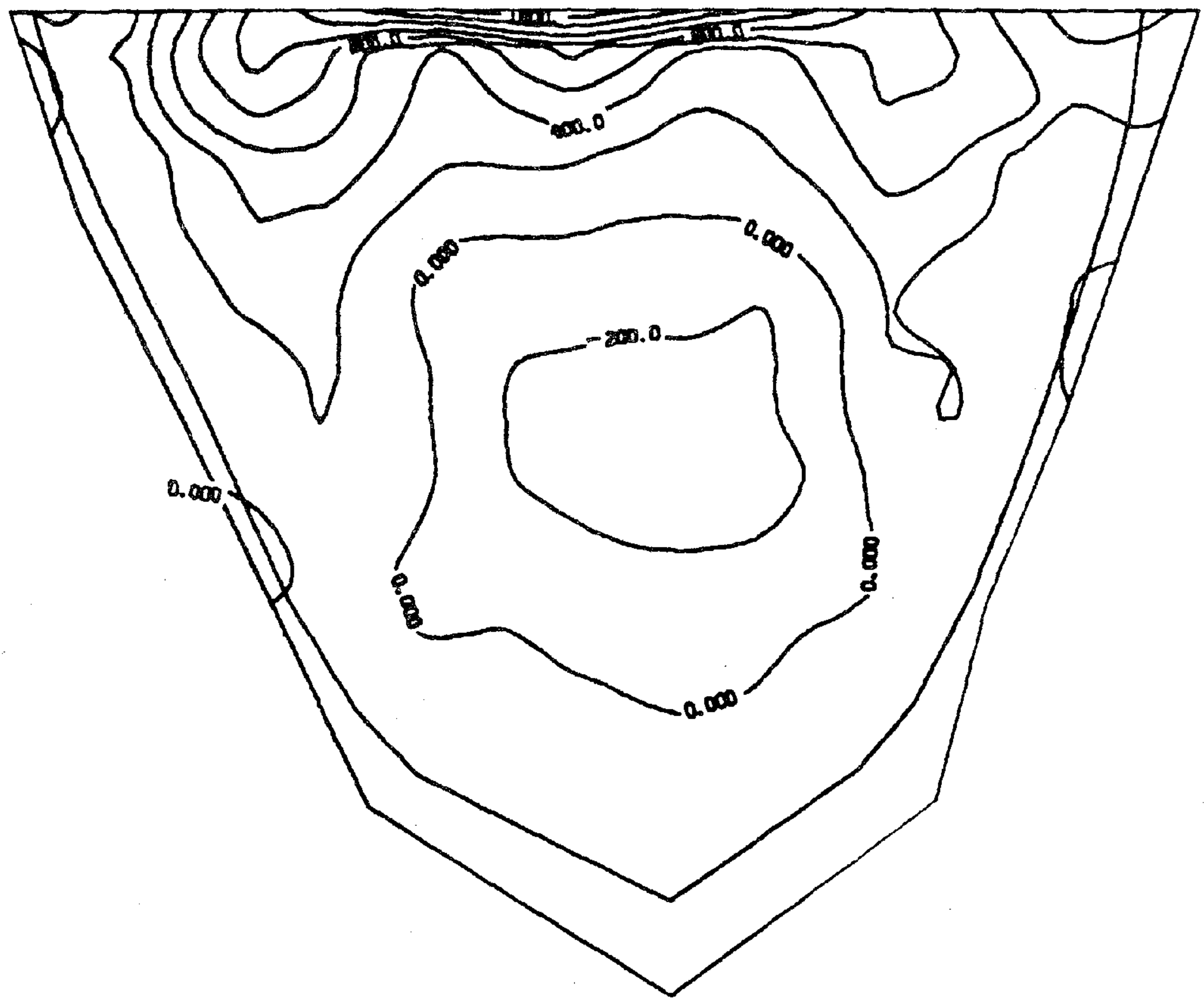

UPSTREAM FACE

MAXIMUM SIG-XX

UNIT : PSI

CONTOUR INTERVAL= 200.0

UPSTREAM-DOWNSTREAM EXCITATIONS

AND HYDROSTATIC + GRAVITY LOADS

(c)

FIG. I-23 (Cont.)

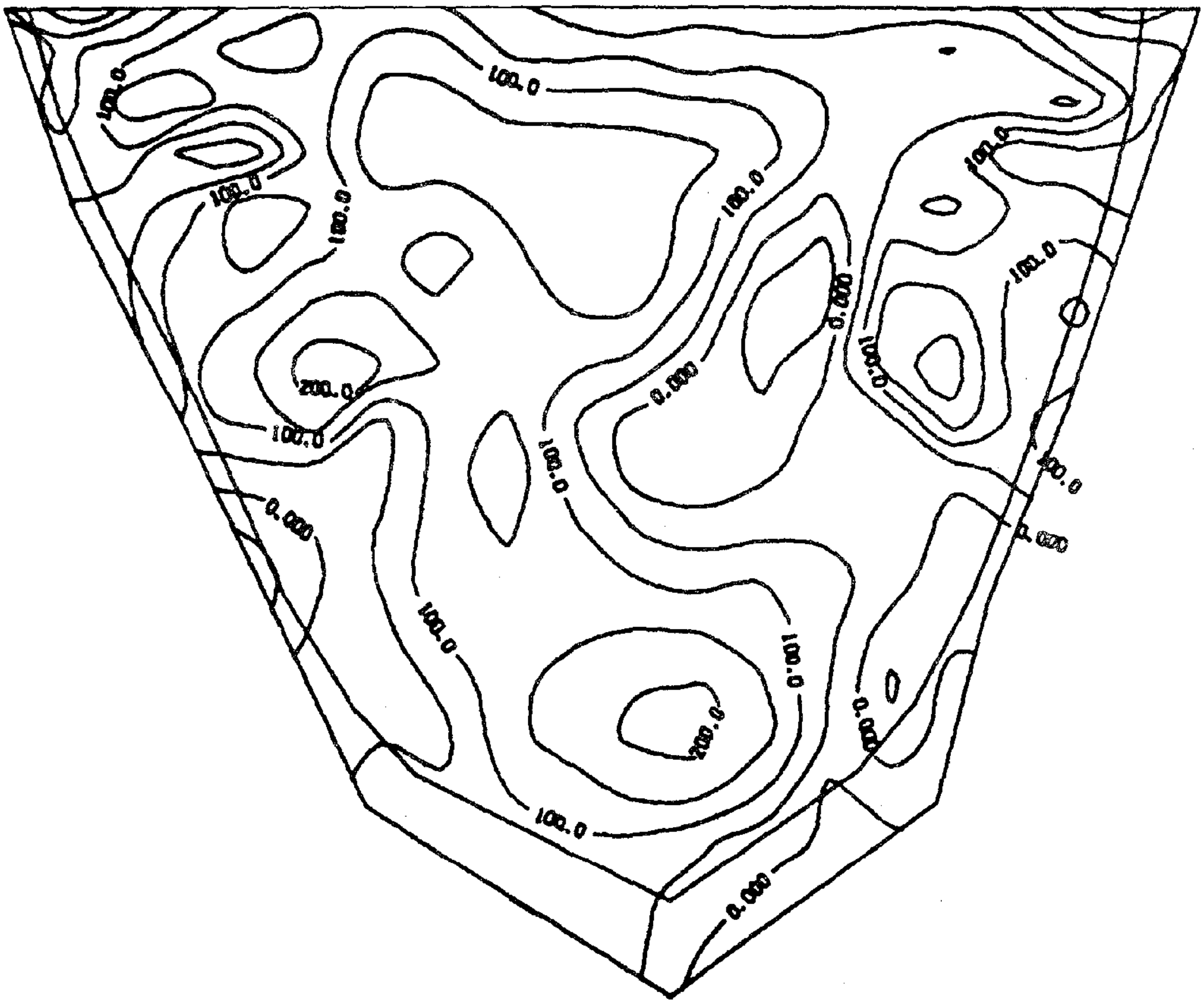

UPSTREAM FACE

MAXIMUM SIG-YY

UNIT : PSI

CONTOUR INTERVAL= 50.0

UPSTREAM-DOWNSTREAM EXCITATIONS

AND HYDROSTATIC + GRAVITY LOADS

(d)

FIG. I-23 (Cont.)

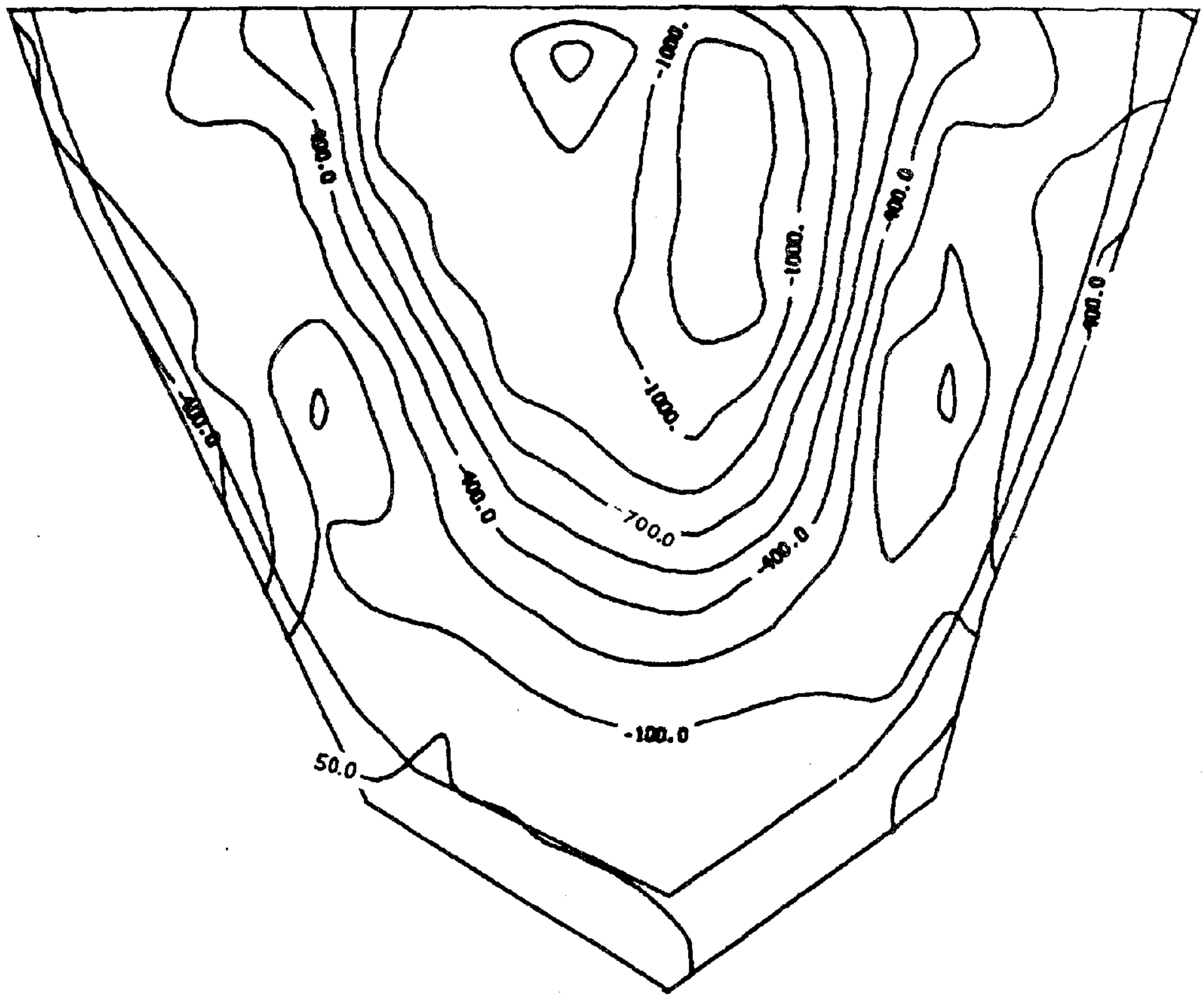

UPSTREAM FACE

MINIMUM SIG-XX

UNIT : PSI

CONTOUR INTERVAL= 150.0

CROSS-CANYON EXCITATIONS

AND HYDROSTATIC + GRAVITY LOADS

(e)

FIG. I-23 (Cont.)

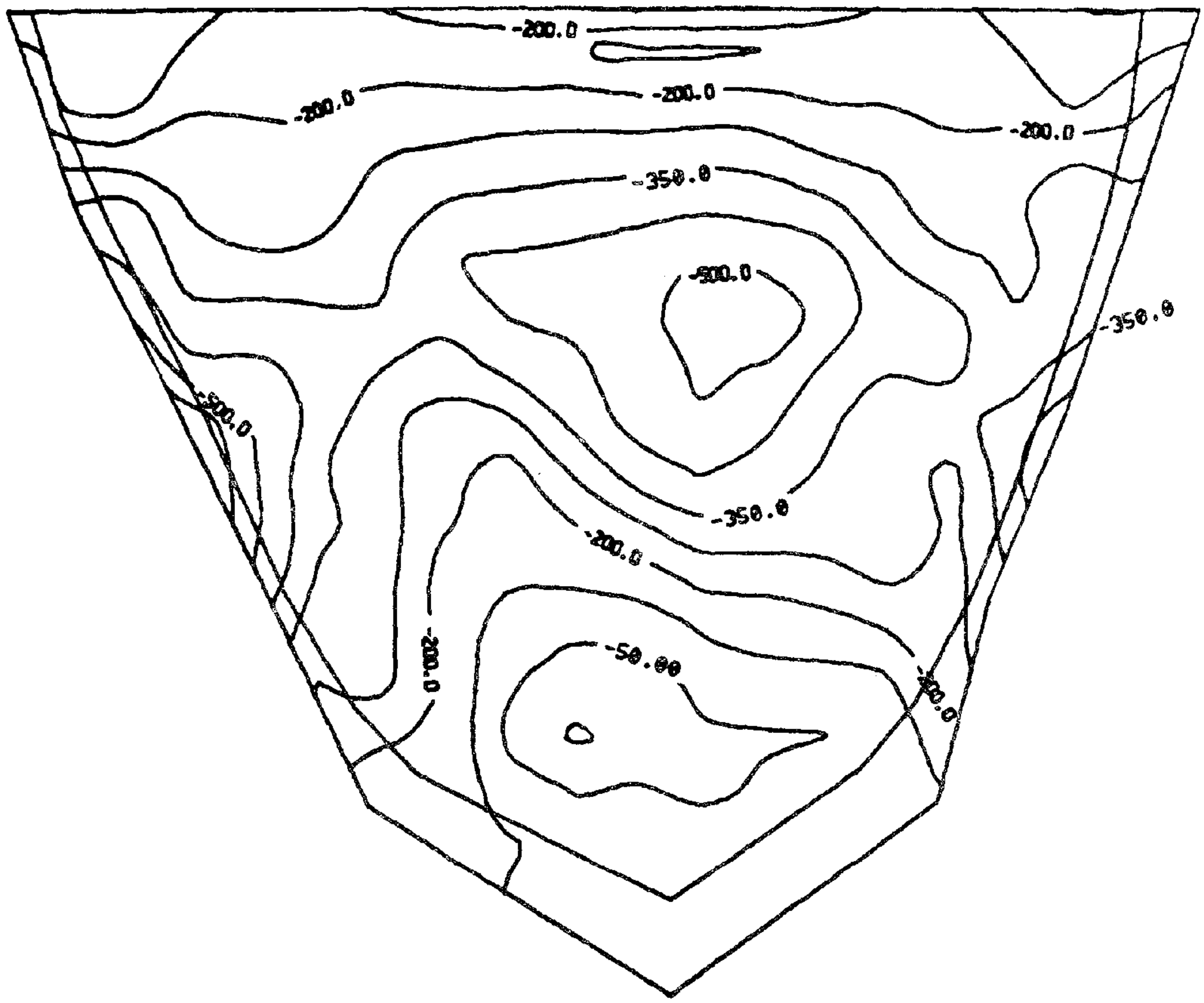

UPSTREAM FACE

MINIMUM SIG-YY

UNIT : PSI

CONTOUR INTERVAL= 75.0

CROSS-CANYON EXCITATIONS

AND HYDROSTATIC + GRAVITY LOADS

(f)

FIG. I-23 (Cont.)

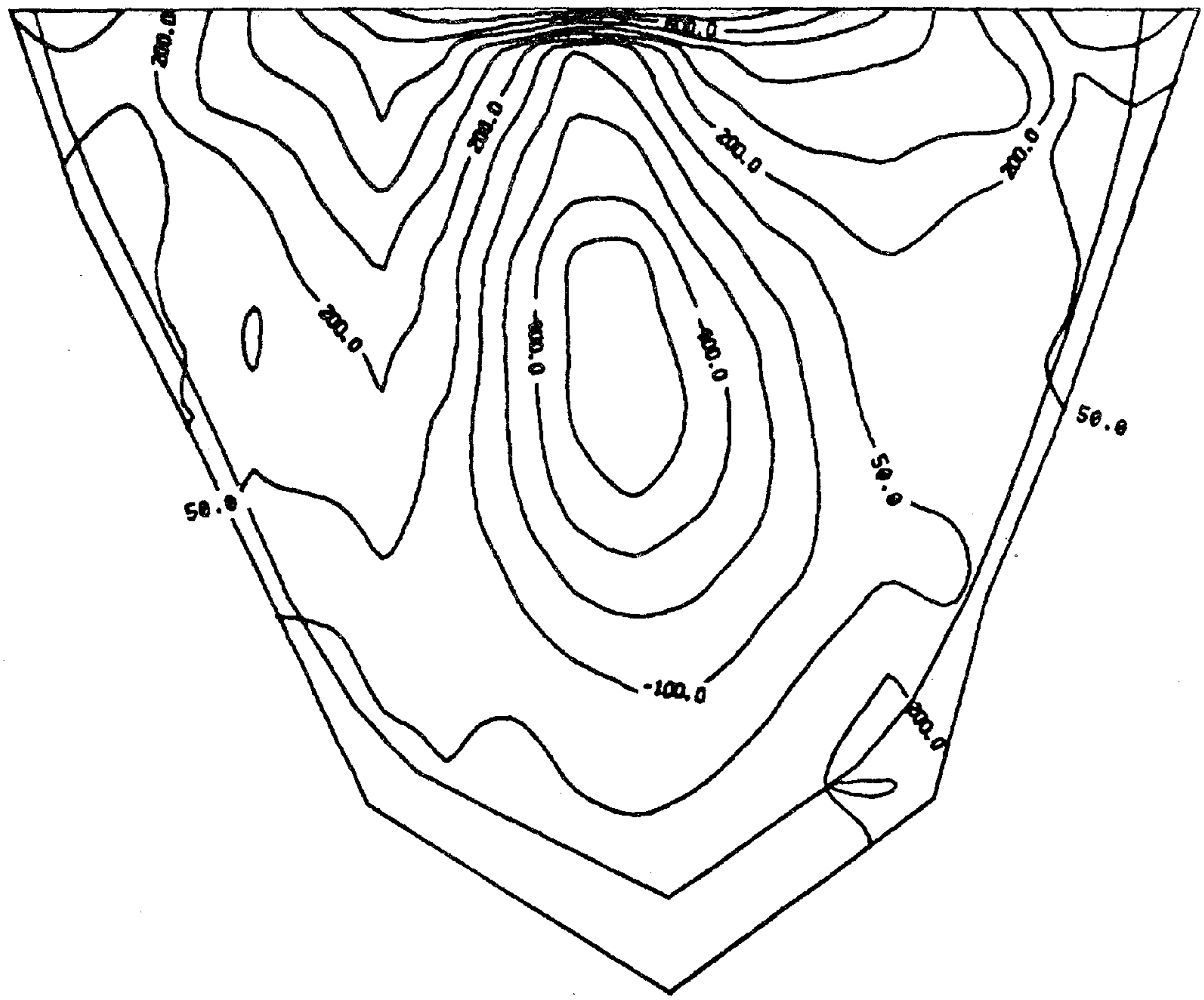

UPSTREAM FACE

MAXIMUM SIG-XX

UNIT : PSI

CONTOUR INTERVAL= 150.0

CROSS-CANYON EXCITATIONS

AND HYDROSTATIC + GRAVITY LOADS

(g)

FIG. I-23 (Cont.)

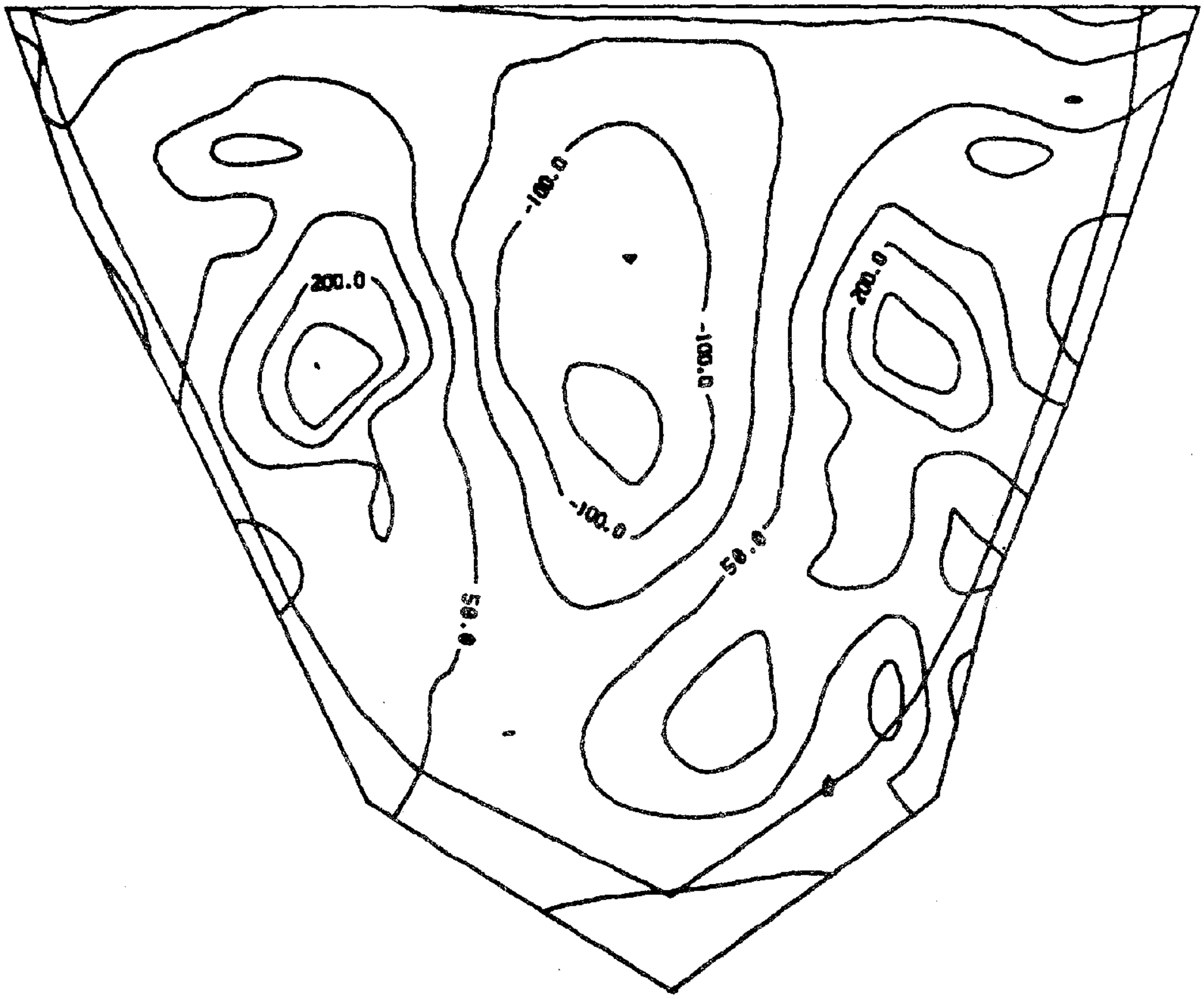

UPSTREAM FACE

MAXIMUM SIG-YY

UNIT : PSI

CONTOUR INTERVAL= 75.0

CROSS-CANYON EXCITATIONS

AND HYDROSTATIC + GRAVITY LOADS

(h)

FIG. I-23 (Cont.)

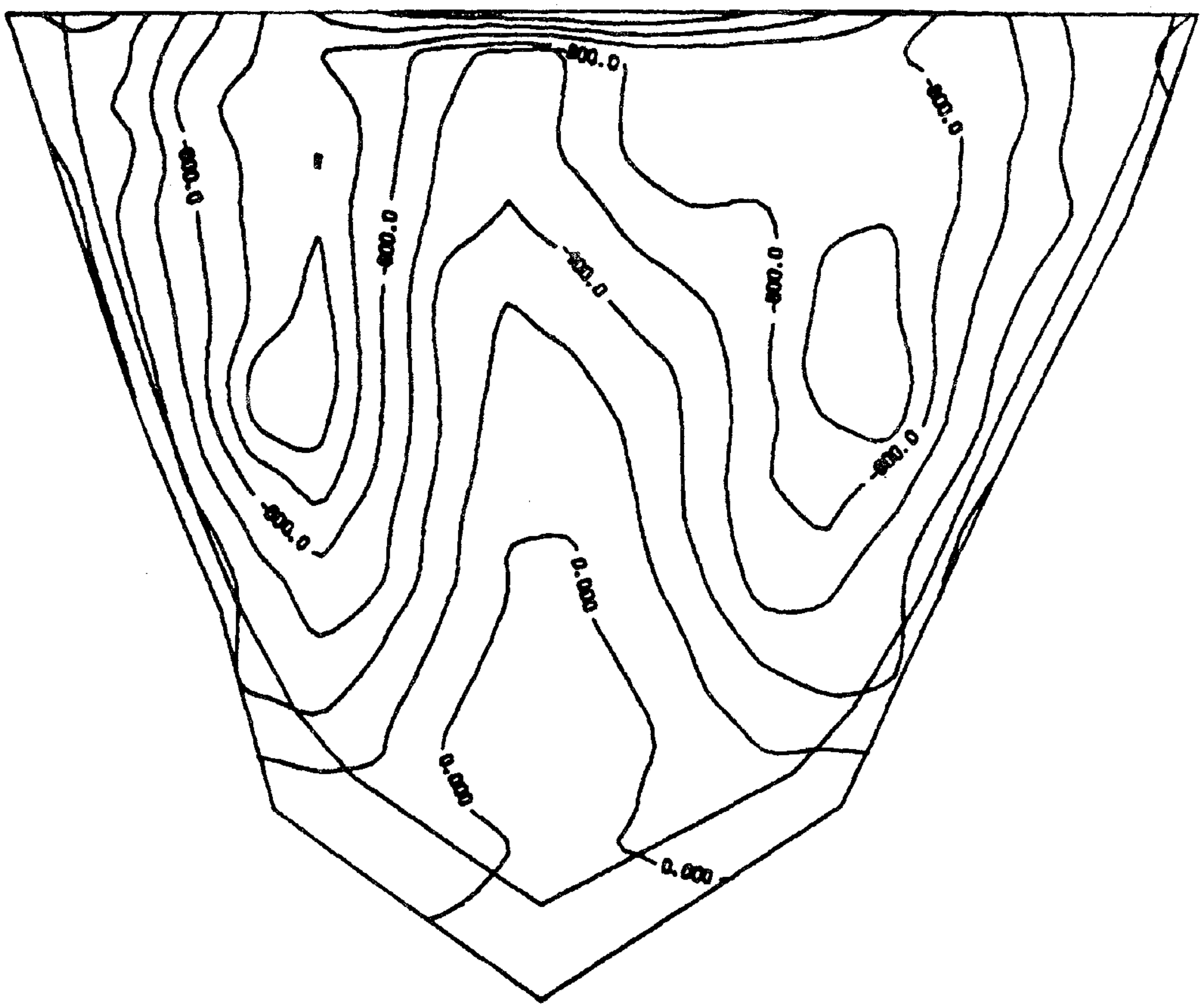

DOWNSTREAM FACE

MINIMUM SIG-XX

UNIT : PSI

CONTOUR INTERVAL= 200.0

UPSTREAM-DOWNSTREAM EXCITATIONS

AND HYDROSTATIC + GRAVITY LOADS

(a)

FIG. I-24 CANTILEVER STRESS AND ARCH STRESS ENVELOPES FOR DOWNSTREAM FACE OF TECHI DAM DUE TO STATIC LOADS AND DESIGN BASE EARTHQUAKE

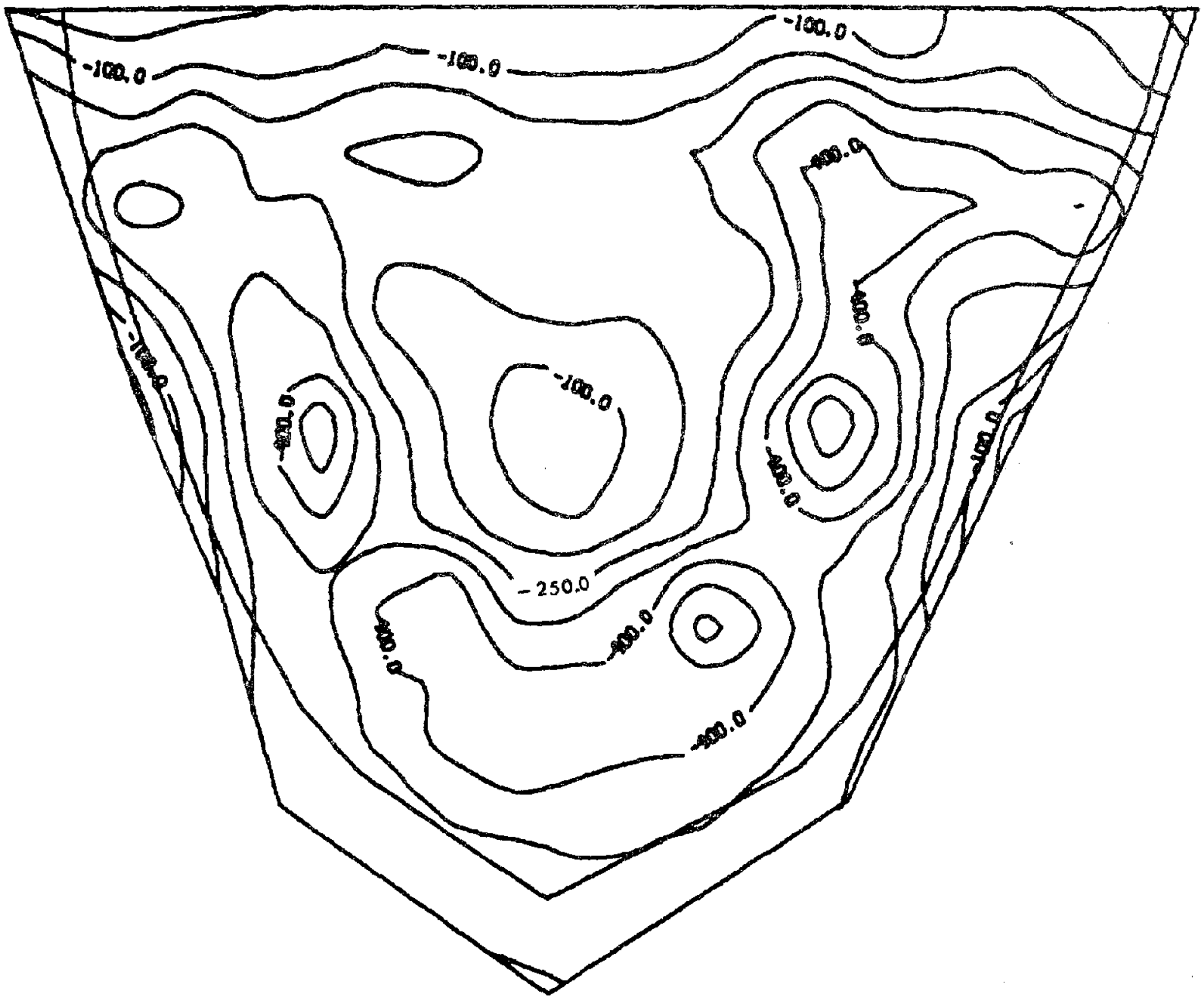

DOWNSTREAM FACE

MINIMUM SIG-YY

UNIT : PSI

CONTOUR INTERVAL= 75.0

UPSTREAM-DOWNSTREAM EXCITATIONS

AND HYDROSTATIC + GRAVITY LOADS

(b)

FIG. I-24 (Cont.)

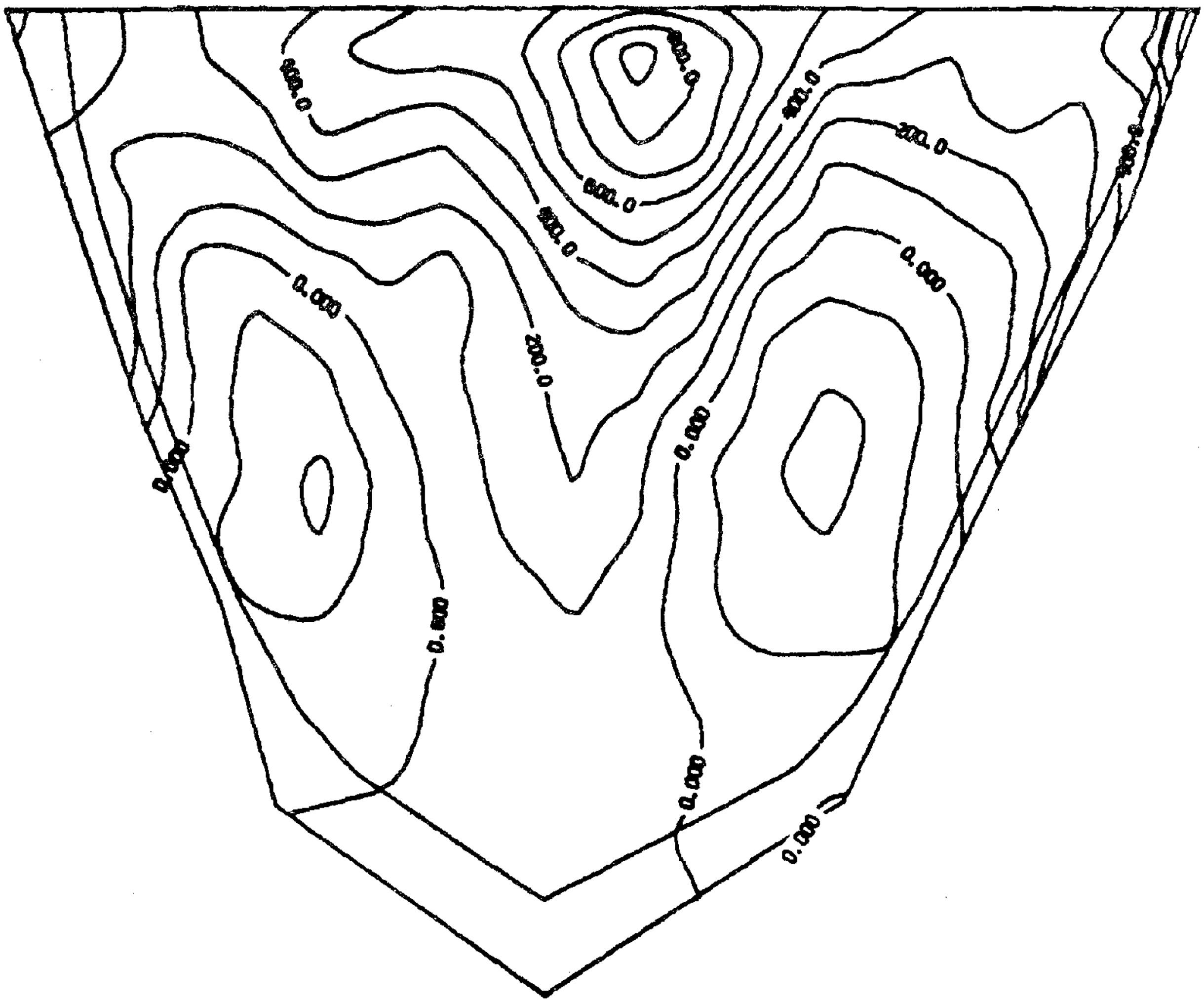

DOWNSTREAM FACE

MAXIMUM SIG-XX

UNIT : PSI

CONTOUR INTERVAL= 100.0

UPSTREAM-DOWNSTREAM EXCITATIONS
AND HYDROSTATIC + GRAVITY LOADS

(c)

FIG. I-24 (Cont.)

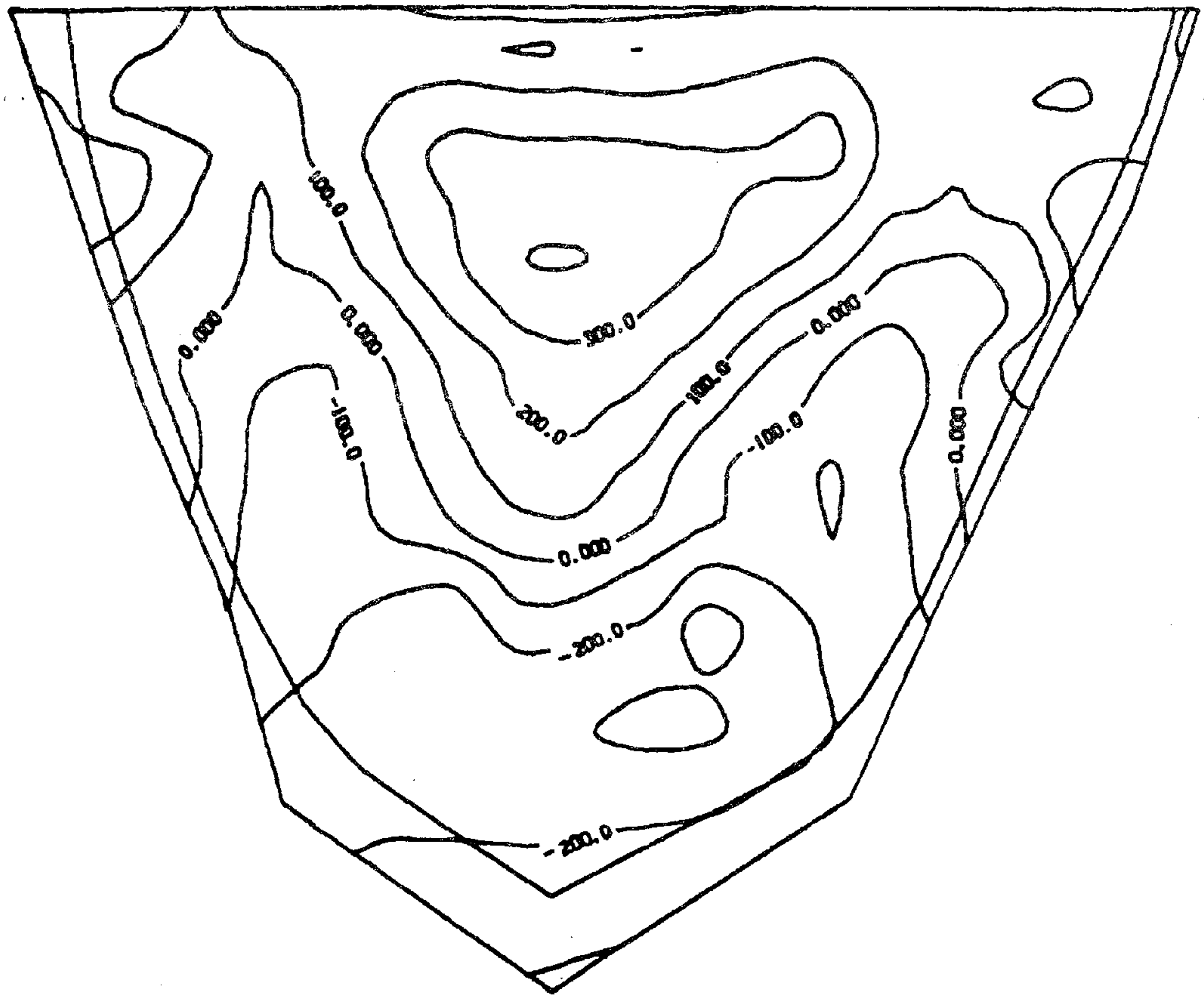

DOWNSTREAM FACE

MAXIMUM SIG-YY

UNIT : PSI

CONTOUR INTERVAL= 100.0

UPSTREAM-DOWNSTREAM EXCITATIONS

AND HYDROSTATIC + GRAVITY LOADS

(d)

FIG. I-24 (Cont.)

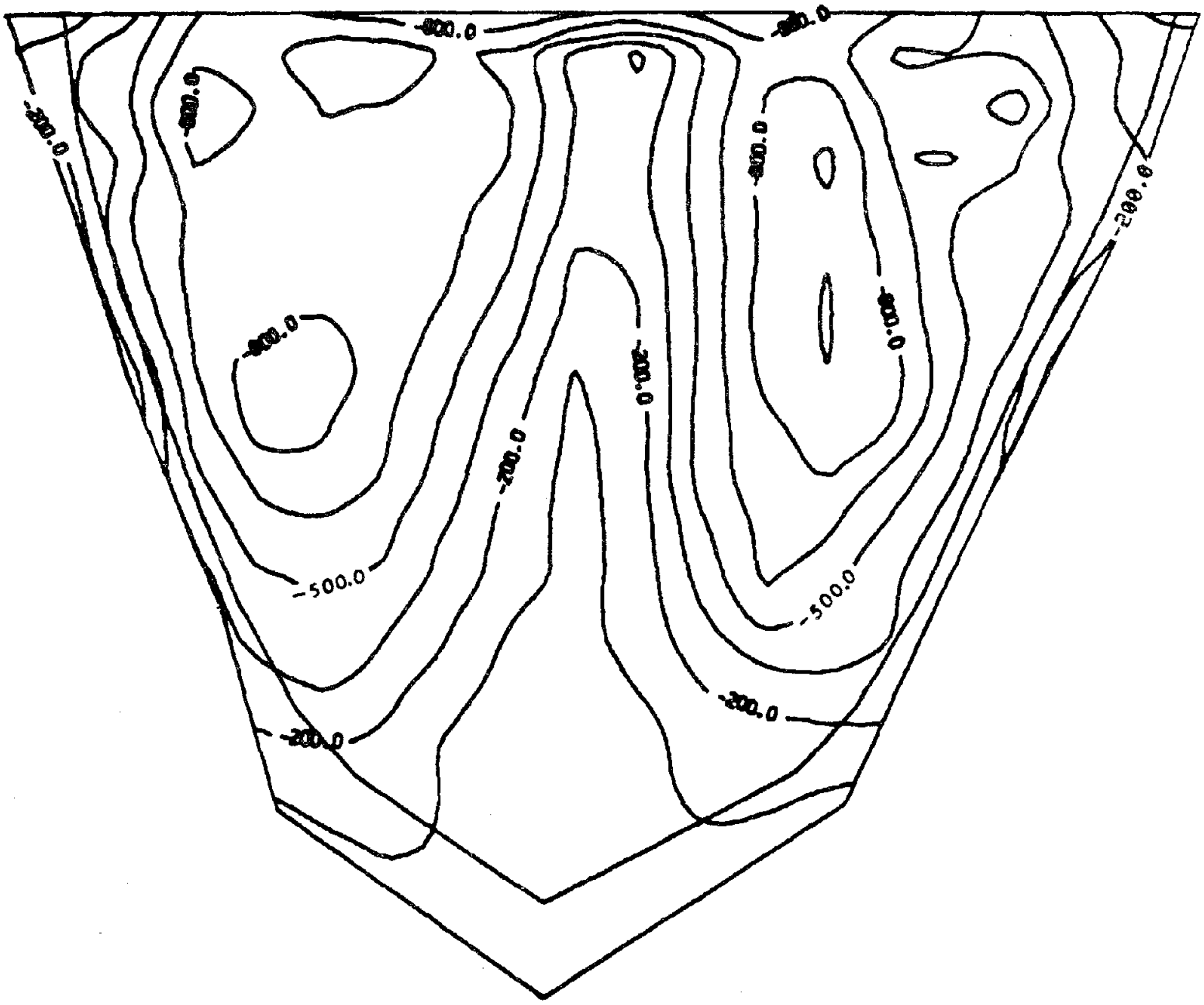

DOWNSTREAM FACE

MINIMUM SIG-XX

UNIT : PSI

CONTOUR INTERVAL= 150.0

CROSS-CANYON EXCITATIONS

AND HYDROSTATIC + GRAVITY LOADS

(e)

FIG. I-24 (Cont.)

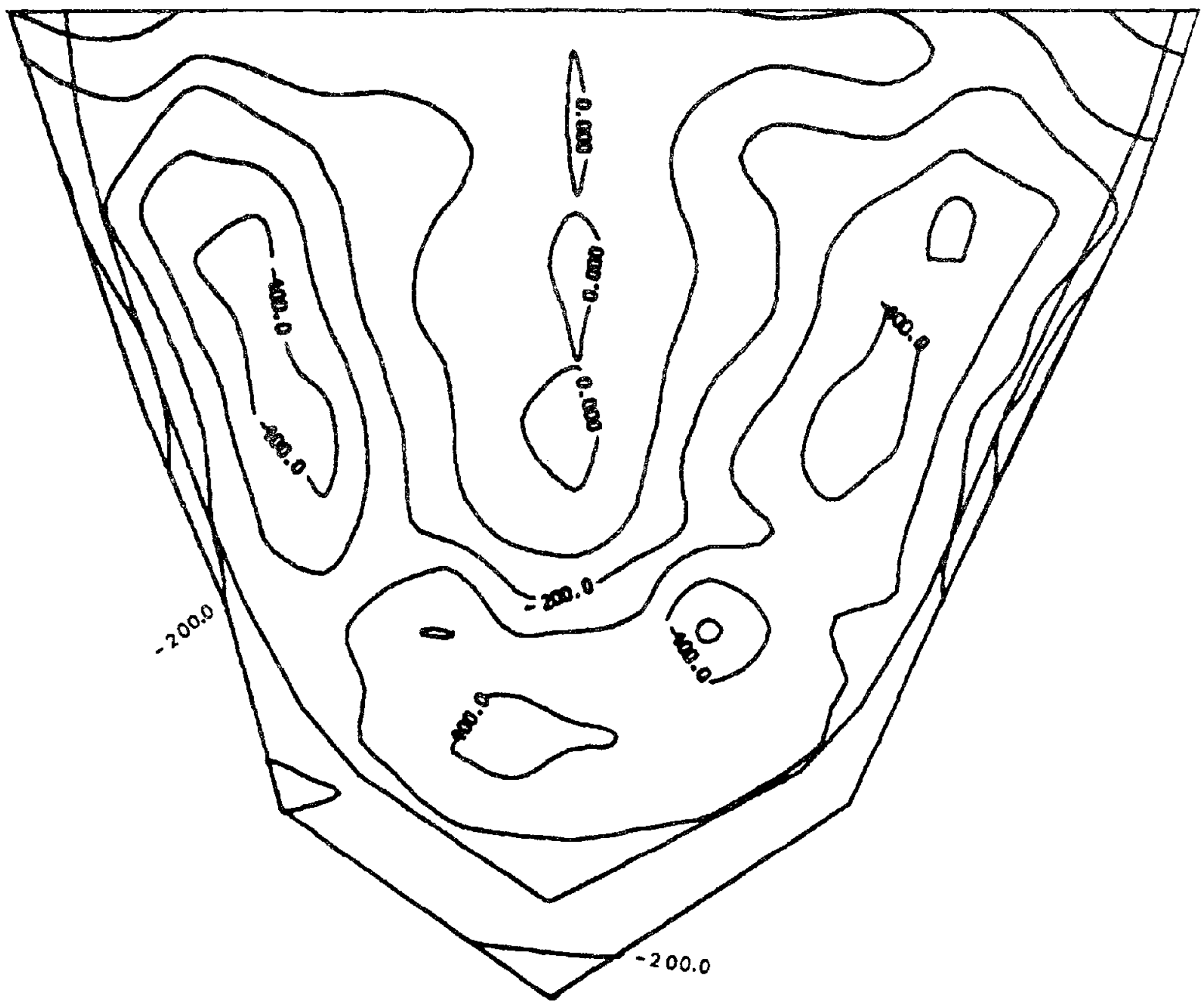

DOWNSTREAM FACE

MINIMUM SIG-YY

UNIT : PSI

CONTOUR INTERVAL= 100.0

CROSS-CANYON EXCITATIONS

AND HYDROSTATIC + GRAVITY LOADS

(f)

FIG. I-24 (Cont.)

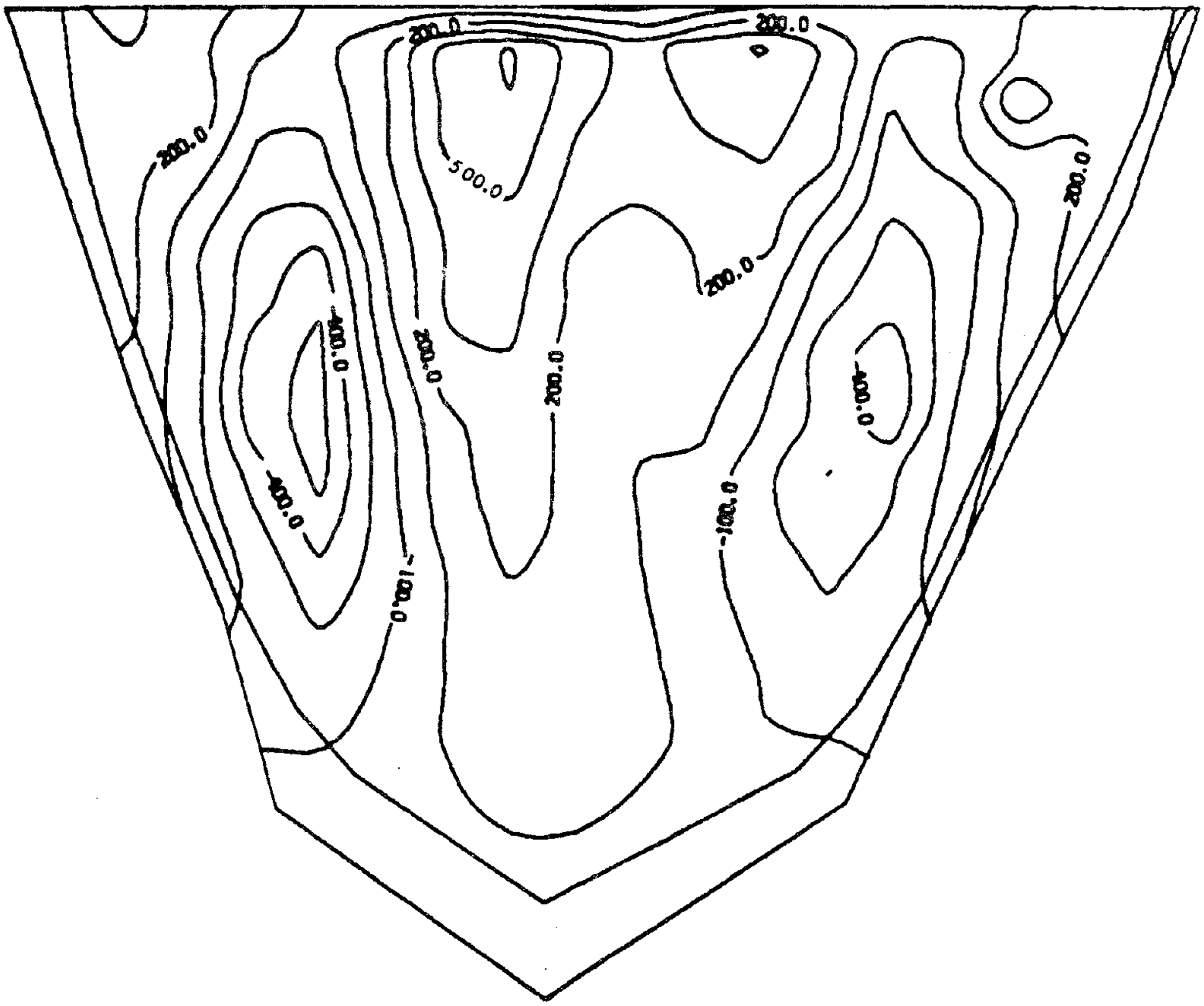

DOWNSTREAM FACE

MAXIMUM SIG-XX

UNIT : PSI

CONTOUR INTERVAL= 150.0

CROSS-CANYON EXCITATIONS

AND HYDROSTATIC + GRAVITY LOADS

(g)

FIG. I-24 (Cont.)

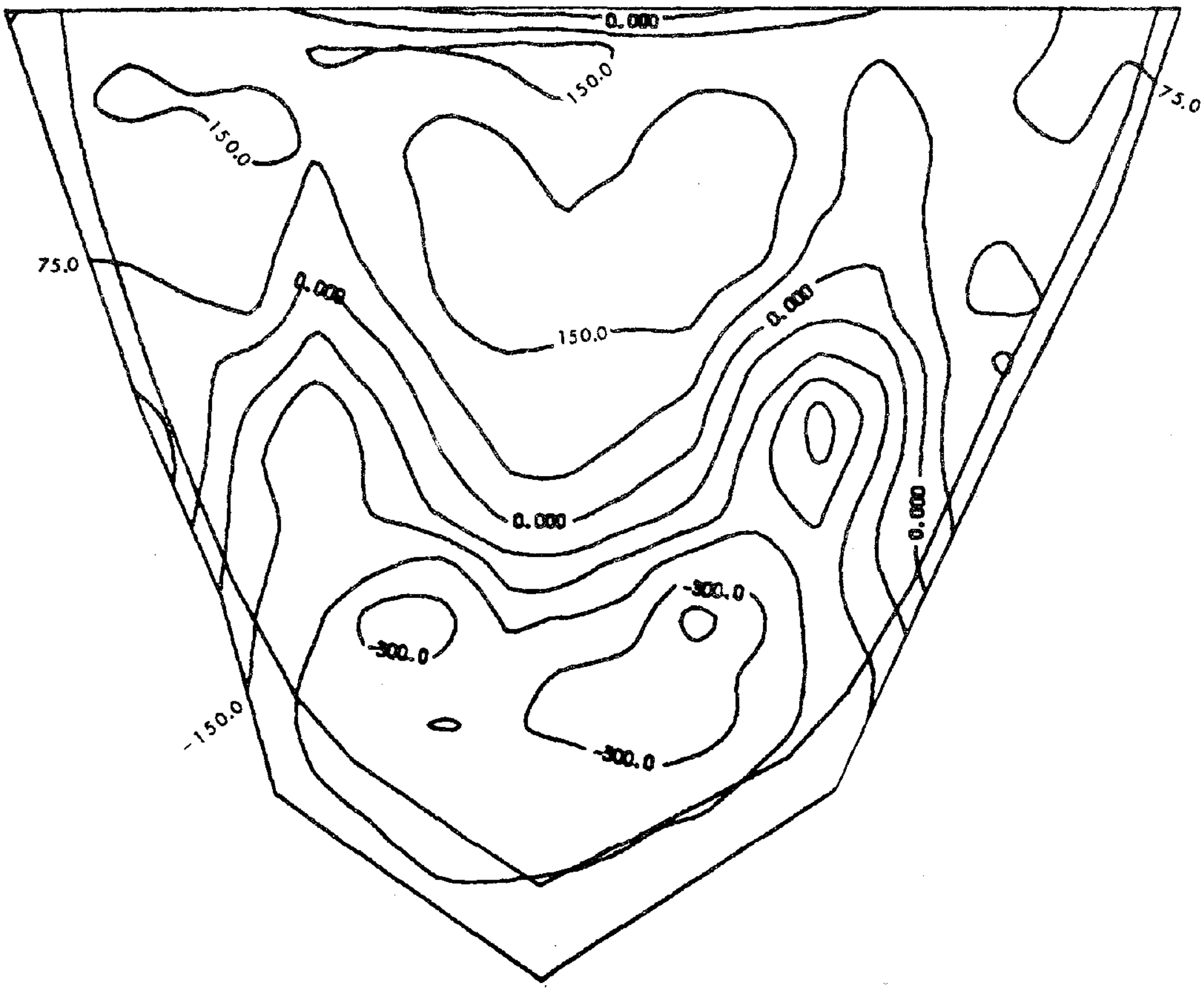

DOWNSTREAM FACE

MAXIMUM SIG-YY

UNIT : PSI

CONTOUR INTERVAL= 75.0

CROSS-CANYON EXCITATIONS

AND HYDROSTATIC + GRAVITY LOADS

(h)

FIG. I-24 (Cont.)

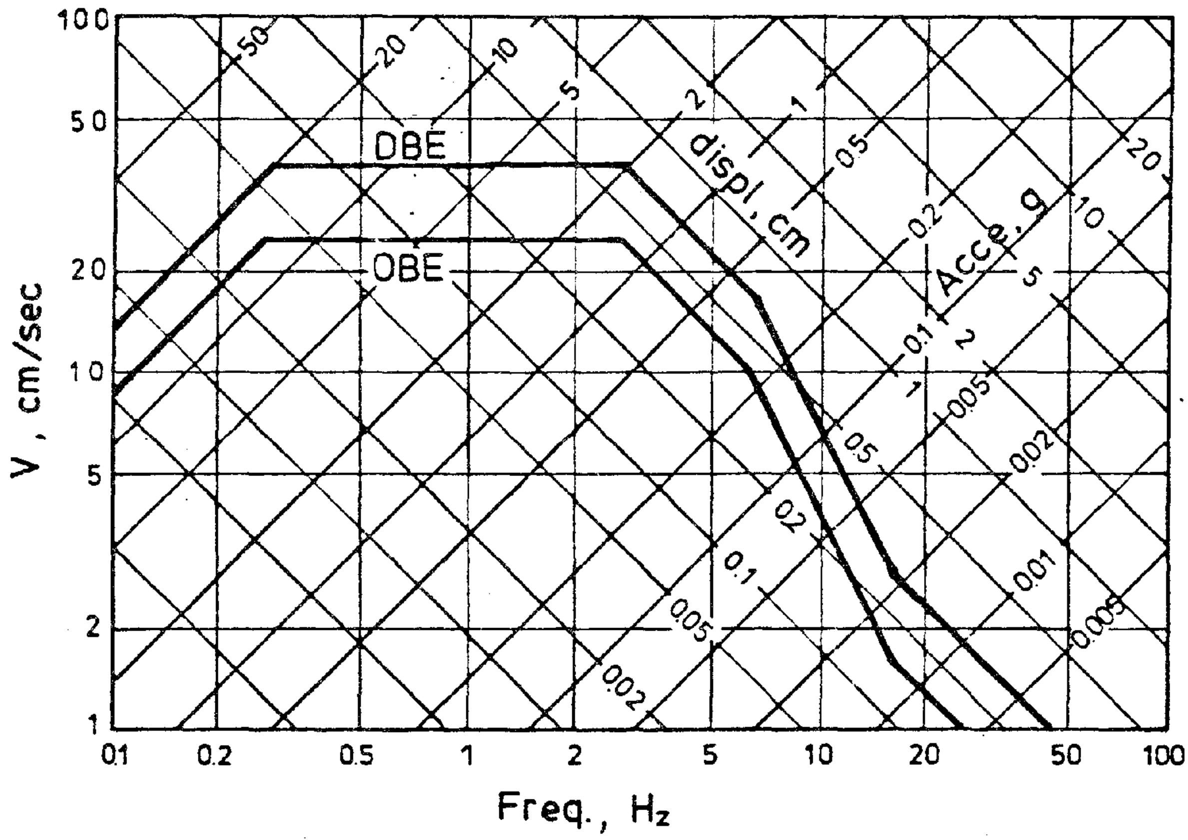

FIG. I-25 (a) 5% damping elastic response spectra for Operation Base Earthquake and Design Base Earthquake, based on Newmark's basic spectra with amplification factors for acceleration and velocity taken to be 2.6 and 1.9 , respectively.

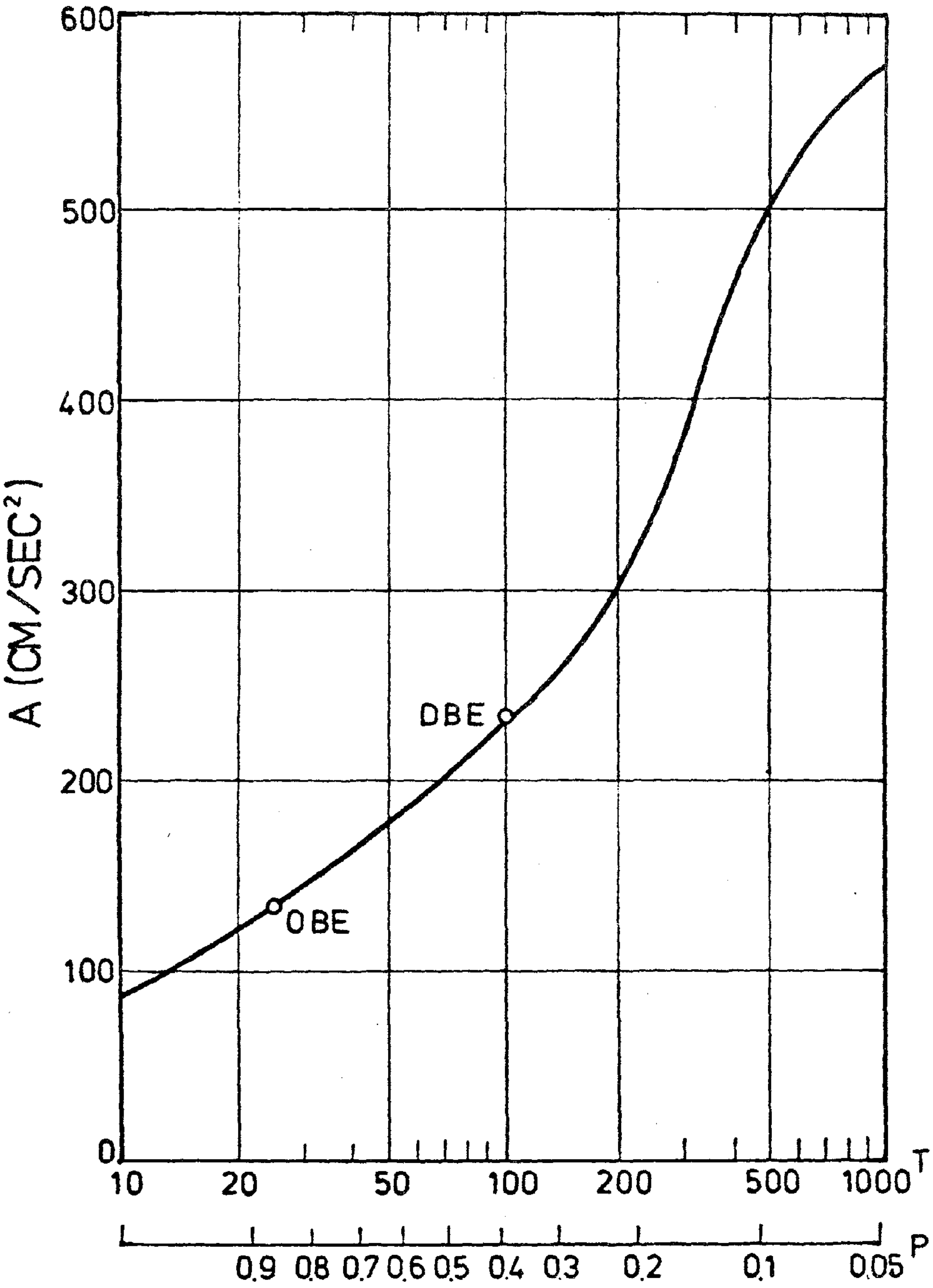

FIG. I-25(b) Relation between ground acceleration and probability of exceedance in fifty years, P, and return period T.

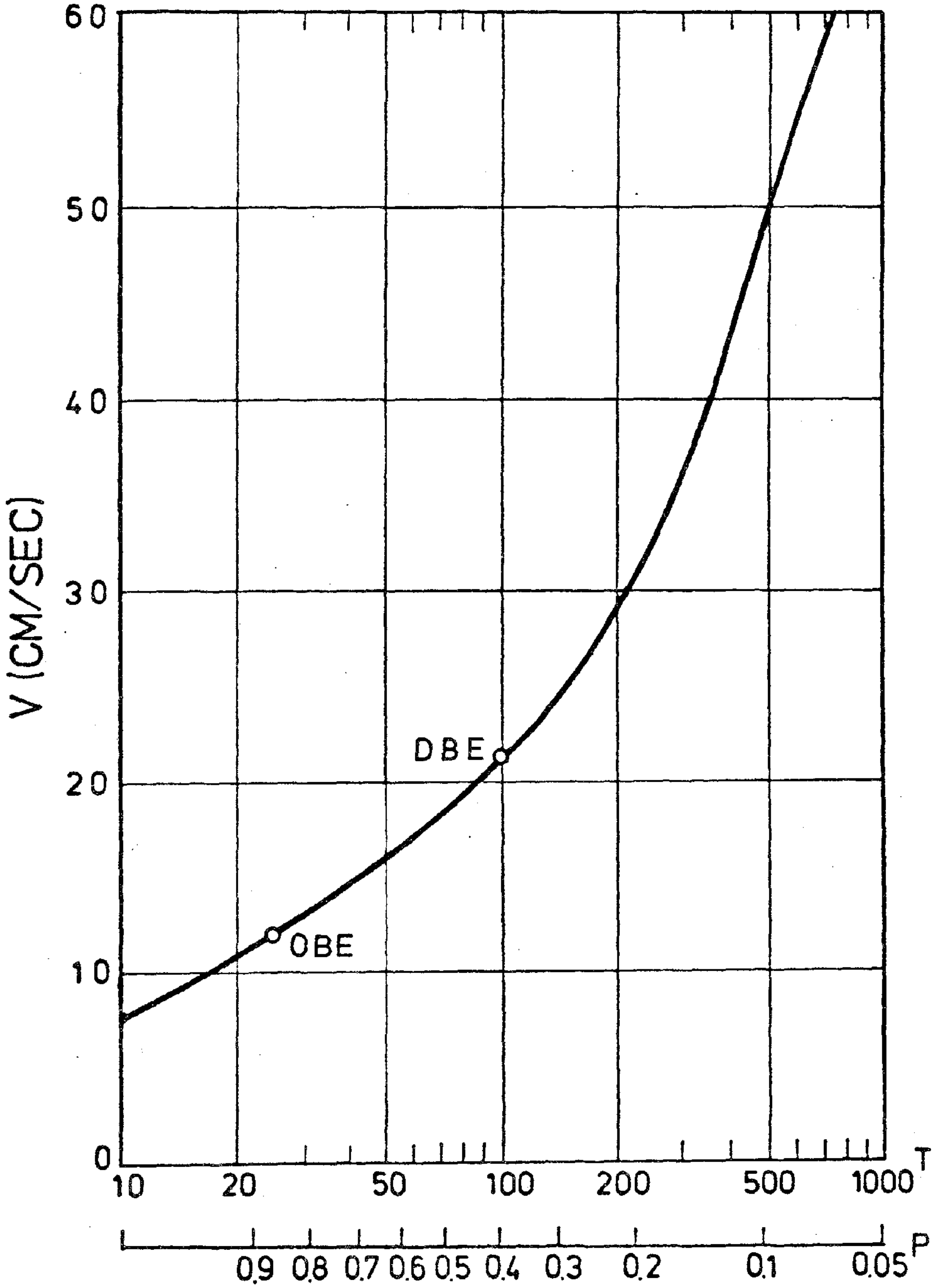

FIG. I-25(c) Relation between ground velocity and probability of exceedance in fifty years, P, and return period T. (Techi dam site)

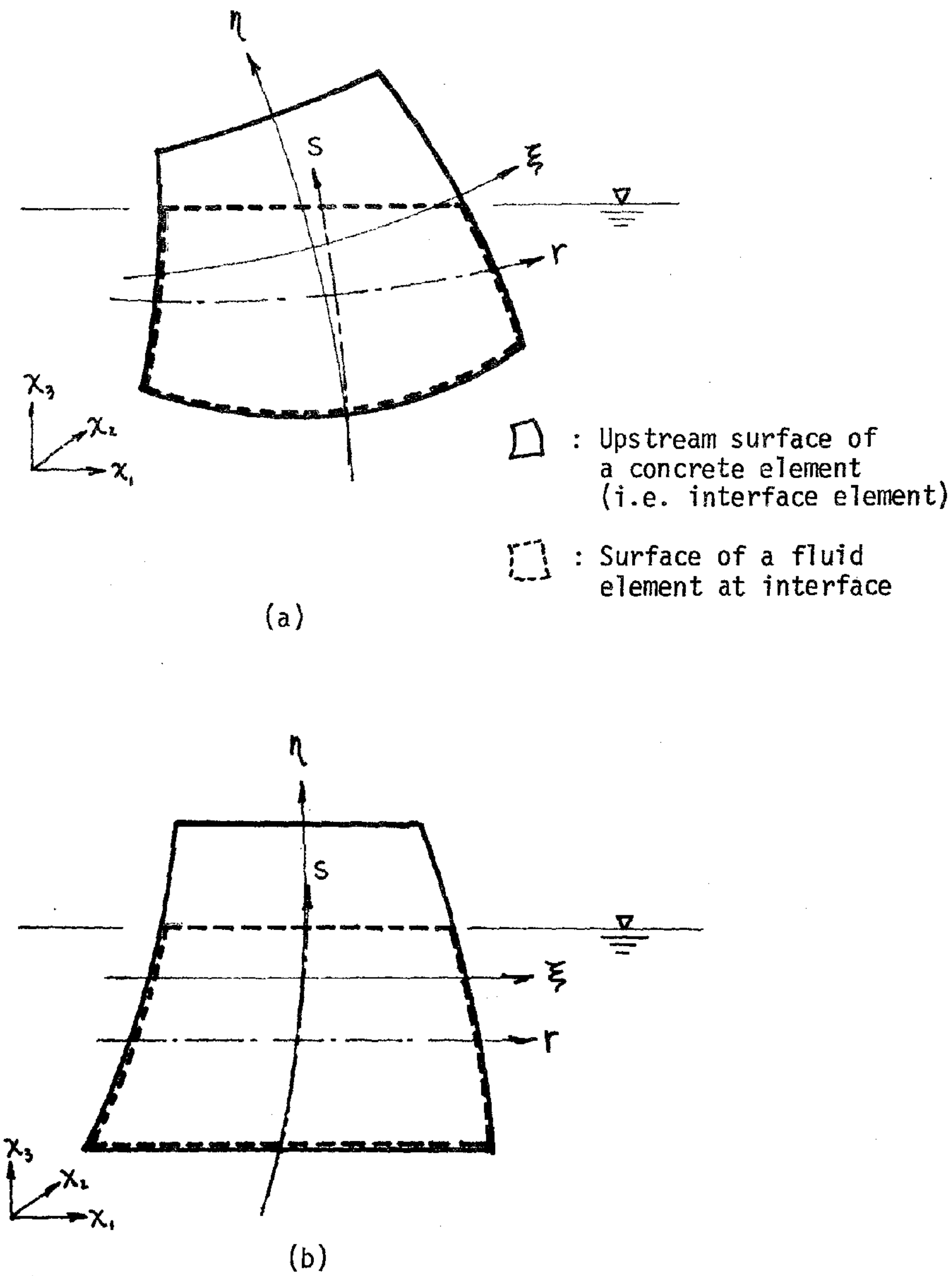

FIG. I-26 VARIABLE WATER LEVEL

REFERENCES

(1) Westergaard, H. M., "Water Pressure on Dams During Earthquakes", Transactions, ASCE, Vol. 98, 1933.

(2) Brahtz, H. A. and Heilbron, C. H., Discussion on "Water Pressure on Dams During Earthquakes" by Westergaard, H. M., Transactions, ASCE, Vol. 98, 1933.

(3) Zangar, C. N., "Hydrodynamic Pressures on Dams Due to Horizontal Earthquake Effects", Engineering Monograph No. 11, U.S. Bureau of Reclamation, May 1952.

(4) Chopra, A. K., "Hydrodynamic Pressures on Dams During Earthquakes", Journal of the Engineering Mechanics Division, ASCE, Vol. 93, No. EM6, Dec. 1967.

(5) Chopra, A. K., "Earthquake Behavior of Reservoir-Dam System", Journal of the Engineering Mechanics Division, ASCE, Vol. 94, No. EM6, Dec. 1968.

(6) Chakrabarti, P. and Chopra, A. K., "Hydrodynamic Effects in Earthquake Response of Gravity Dams", Journal of the Structural Division, ASCE, Vol. 100, No. ST6, June 1974.

(7) Chopra, A. K., "Earthquake Resistant Design of Concrete Gravity Dams", Journal of the Structural Division, ASCE, Vol. 104, No. ST6, June 1978.

(8) Priscu, R., Popovici, A., Ilie, L. and Stematiu, D., "New Aspects in the Earthquake Analysis of Arch Dams", Criteria and Assumptions for Numerical Analysis of Dams, Ed. by D. N. Naylor, etc., Proceedings of an International Symposium, Swansea, United Kingdom, Sept. 1975, pp. 709-725.

(9) Clough, R. W., Lecture Notes, February 1977.

(10) Clough, R. W. and Chopra, A. K., "Earthquake Response Analysis of Concrete Dams", Structural and Geotechnical Mechanics, Ed. by W. J. Hall, Prentice-Hall, 1977.

(11) Clough, R. W., Lecture Notes, April 1979.

(12) Zienkiewicz, O. C. and Newton, R. E., "Coupled Vibrations of a Structure Submerged in a Compressible Fluid", International Symposium on Finite Element Techniques, Stuttgart, May 1969.

(13) Zienkiewicz, O. C. and Nath, B., "Earthquake Response on Arch Dams - An Electric Analogue Solution", Proceedings, Institute of Civil Engineers, Vol. 25, 1963, pp.165-175.

(14) Nath, B., "Hydrodynamic Pressures on High Dams due to Vertical Earthquake Motions", Proceedings, Institute of Civil Engineers, March 1969.

(15) Liaw, C. Y. and Chopra, A. K., "Dynamics of Towers Surrounded by Water", International Journal of Earthquake Engineering and Structural Dynamics, Vol. 3, 1974, pp. 33-49.

(16) Saini, S. S., Bettess, P. and Zienkiewicz, O. C., "Coupled Hydrodynamic Response of Concrete Gravity Dams Using Finite and Infinite Elements", International Journal of Earthquake Engineering and Structural Dynamics, Vol. 6, 1978, pp. 363-374.

(17) Nath, B. and Jamshidi, J., "The w-Plane Finite Element Method for the Solution of the Steady-State Scalar Wave Equation in Two Dimensions", International Journal of Earthquake Engineering and Structural Dynamics, Vol. 8, 1980, pp. 181-191.

(18) Porter, C. S. and Chopra, A. K., "Dynamic Response of Simple Arch Dams Including Hydrodynamic Interaction", Earthquake Engineering Research Center, Report No. UCB/EERC-80/17, University of California, Berkeley, July 1980.

(19) Hall, J. F. and Chopra, A. K., "Dynamic Response of Embankment, Concrete-Gravity and Arch Dams Including Hydrodynamic Interaction", Earthquake Engineering Research Center, Report No. UCB/EERC-80/39, University of California, Berkeley, October 1980.

(20) Wilson, E. L. and Dovey, H. H., "Solution or Reduction of Equilibrium Equation for Large Complex Structural Systems", Advances in Engineering Software, Vol. 1, No. 1, 1978.

(21) Bathe, K. J. and Wilson, E. L., "Numerical Methods in Finite Element Analysis," Prentice Hall, 1976.

(22) Zienkiewicz, O. C., "The Finite Element Method", McGraw-Hill, 3rd Ed., 1978.

(23) Clough, R. W., Raphael, J. M. and Mojtahedi, S., "ADAP-A Computer Program for Static and Dynamic Analysis of Arch Dams", Earthquake Engineering Research Center, Report No. UCB/EERC-73/14, University of California, Berkeley, June 1973.

(24) Chopra, A. K., Chakrabarti, P. and Gupta, S., "Earthquake Response of Concrete Gravity Dams Including Hydrodynamic and Foundation Interaction Effects", Earthquake Engineering Research Center, Report No. UCB/EERC-80/01, University of California, Berkeley, Jan. 1980.

(25) Perumalswami, P. R., and Kar, L., "Earthquake Behavior of Arch Dam-Reservoir Systems", Proceedings, Fifth World Conference on Earthquake Engineering, Rome, June 1973.

(26) Muller, W. C., "Simplified Analysis of Linear Fluid-Structure Interaction", International Journal for Numerical Method in Engineerng, Vol. 17, pp. 113-121, 1981.

(27) Kuo, J. S.-H., "A Study on Hydrodynamic Effects on Arch Dams, Considering Incompressible Fluid: Added-Mass", 299 Report, SESM, Department of Civil Engineering, University of California, Berkeley, Feb. 1980.

(28) Kuo, J. S.-H. and Clough, R. W., "RSVOIR-A General Purpose Incompressible Fluid Added-Mass Preprocessor for Arch Dams of General Geometry", EERC Report to appear, University of California, Berkeley.

(29) Kreyszig, E., "Advanced Engineering Mathematics", John Wiley and Sons, Ltd., 3rd Ed., 1972, Sections 8.5 to 8.7.

(30) Clough, R. W. and Penzien, J., "Dynamics of Structures", McGraw-Hill, Inc., 1975.

(31) Liaw, C. Y. and Chopra, A. K., "Dynamics of Towers Surrounded by Water," International Journal of Earthquake Engineering and Structural Dynamics, Vol. 3, 1974, pp. 33-49.

(32) Liaw, C. Y. and Chopra, A. K., "Earthquake Response of Axisymmetric Tower Structures Surrounded by Water", Earthquake Engineering Research Center, Report No. EERC/UCB 73-25, University of California, Berkeley, 1973.

(33) Chakrabarti, P. and Chopra, A. K., "Earthquake Response of Gravity Dams Including Reservoir Interaction Effects", Earthquake Engineering Research Center, Report No. EERC/UCB 72-6, University of California, Berkeley, 1972.

(34) Mau, S. T., "A Preliminary Study on the Dynamic Characteristics of Techi Dam", Research Center for Earthquake Engineering, National Taiwan University, June 1980.

EARTHQUAKE ENGINEERING RESEARCH CENTER REPORTS

NOTE: Numbers in parentheses are Accession Numbers assigned by the National Technical Information Service; these are followed by a price code. Copies of the reports may be ordered from the National Technical Information Service, 5285 Port Royal Road, Springfield, Virginia, 22161. Accession Numbers should be quoted on orders for reports (PB --- ---) and remittance must accompany each order. Reports without this information were not available at time of printing. The complete list of EERC reports (from EERC 67-1) is available upon request from the Earthquake Engineering Research Center, University of California, Berkeley, 47th Street and Hoffman Boulevard, Richmond, California 94804.

UCB/EERC-77/01 "PLUSH - A Computer Program for Probabilistic Finite Element Analysis of Seismic Soil-Structure Interaction," by M.P. Romo Organista, J. Lysmer and H.B. Seed - 1977 (PB81 177 651)A05

UCB/EERC-77/02 "Soil-Structure Interaction Effects at the Humboldt Bay Power Plant in the Ferndale Earthquake of June 7, 1975," by J.E. Valera, H.B. Seed, C.F. Tsai and J. Lysmer - 1977 (PB 265 795)A04

UCB/EERC-77/03 "Influence of Sample Disturbance on Sand Response to Cyclic Loading," by K. Mori, H.B. Seed and C.K. Chan - 1977 (PB 267 352)A04

UCB/EERC-77/04 "Seismological Studies of Strong Motion Records," by J. Shoja-Taheri - 1977 (PB 269 655)A10

UCB/EERC-77/05 Unassigned

UCB/EERC-77/06 "Developing Methodologies for Evaluating the Earthquake Safety of Existing Buildings," by No. 1 - B. Bresler; No. 2 - B. Bresler, T. Okada and D. Zisling; No. 3 - T. Okada and B. Bresler; No. 4 - V.V. Bertero and B. Bresler - 1977 (PB 267 354)A08

UCB/EERC-77/07 "A Literature Survey - Transverse Strength of Masonry Walls," by Y. Omote, R.L. Mayes, S.W. Chen and R.W. Clough - 1977 (PB 277 933)A07

UCB/EERC-77/08 "DRAIN-TABS: A Computer Program for Inelastic Earthquake Response of Three Dimensional Buildings," by R. Guendelman-Israel and G.H. Powell - 1977 (PB 270 693)A07

UCB/EERC-77/09 "SUBWALL: A Special Purpose Finite Element Computer Program for Practical Elastic Analysis and Design of Structural Walls with Substructure Option," by D.Q. Le, H. Peterson and E.P. Popov - 1977 (PB 270 567)A05

UCB/EERC-77/10 "Experimental Evaluation of Seismic Design Methods for Broad Cylindrical Tanks," by D.P. Clough (PB 272 280)A13

UCB/EERC-77/11 "Earthquake Engineering Research at Berkeley - 1976," - 1977 (PB 273 507)A09

UCB/EERC-77/12 "Automated Design of Earthquake Resistant Multistory Steel Building Frames," by N.D. Walker, Jr. - 1977 (PB 276 526)A09

UCB/EERC-77/13 "Concrete Confined by Rectangular Hoops Subjected to Axial Loads," by J. Vallenas, V.V. Bertero and E.P. Popov - 1977 (PB 275 165)A06

UCB/EERC-77/14 "Seismic Strain Induced in the Ground During Earthquakes," by Y. Sugimura - 1977 (PB 284 201)A04

UCB/EERC-77/15 Unassigned

UCB/EERC-77/16 "Computer Aided Optimum Design of Ductile Reinforced Concrete Moment Resisting Frames," by S.W. Zagajeski and V.V. Bertero - 1977 (PB 280 137)A07

UCB/EERC-77/17 "Earthquake Simulation Testing of a Stepping Frame with Energy-Absorbing Devices," by J.M. Kelly and D.F. Tsztoo - 1977 (PB 273 506)A04

UCB/EERC-77/18 "Inelastic Behavior of Eccentrically Braced Steel Frames under Cyclic Loadings," by C.W. Roeder and E.P. Popov - 1977 (PB 275 526)A15

UCB/EERC-77/19 "A Simplified Procedure for Estimating Earthquake-Induced Deformations in Dams and Embankments," by F.I. Makdisi and H.B. Seed - 1977 (PB 276 820)A04

UCB/EERC-77/20 "The Performance of Earth Dams during Earthquakes," by H.B. Seed, F.I. Makdisi and P. de Alba - 1977 (PB 276 821)A04

UCB/EERC-77/21 "Dynamic Plastic Analysis Using Stress Resultant Finite Element Formulation," by P. Lukkunapvasit and J.M. Kelly - 1977 (PB 275 453)A04

UCB/EERC-77/22 "Preliminary Experimental Study of Seismic Uplift of a Steel Frame," by R.W. Clough and A.A. Huckelbridge 1977 (PB 278 769)A08

UCB/EERC-77/23 "Earthquake Simulator Tests of a Nine-Story Steel Frame with Columns Allowed to Uplift," by A.A. Huckelbridge - 1977 (PB 277 944)A09

UCB/EERC-77/24 "Nonlinear Soil-Structure Interaction of Skew Highway Bridges," by M.-C. Chen and J. Penzien - 1977 (PB 276 176)A07

UCB/EERC-77/25 "Seismic Analysis of an Offshore Structure Supported on Pile Foundations," by D.D.-N. Liou and J. Penzien 1977 (PB 283 180)A06

UCB/EERC-77/26 "Dynamic Stiffness Matrices for Homogeneous Viscoelastic Half-Planes," by G. Dasgupta and A.K. Chopra - 1977 (PB 279 654)A06

UCB/EERC-77/27 "A Practical Soft Story Earthquake Isolation System," by J.M. Kelly, J.M. Eidinger and C.J. Derham - 1977 (PB 276 814)A07

UCB/EERC-77/28 "Seismic Safety of Existing Buildings and Incentives for Hazard Mitigation in San Francisco: An Exploratory Study," by A.J. Meltsner - 1977 (PB 281 970)A05

UCB/EERC-77/29 "Dynamic Analysis of Electrohydraulic Shaking Tables," by D. Rea, S. Abedi-Hayati and Y. Takahashi 1977 (PB 282 569)A04

UCB/EERC-77/30 "An Approach for Improving Seismic - Resistant Behavior of Reinforced Concrete Interior Joints," by B. Galunic, V.V. Bertero and E.P. Popov - 1977 (PB 290 870)A06

UCB/EERC-78/01 "The Development of Energy-Absorbing Devices for Aseismic Base Isolation Systems," by J.M. Kelly and D.F. Tsztoo - 1978 (PB 284 978)A04

UCB/EERC-78/02 "Effect of Tensile Prestrain on the Cyclic Response of Structural Steel Connections, by J.G. Bouwkamp and A. Mukhopadhyay - 1978

UCB/EERC-78/03 "Experimental Results of an Earthquake Isolation System using Natural Rubber Bearings," by J.M. Eidinger and J.M. Kelly - 1978 (PB 281 686)A04

UCB/EERC-78/04 "Seismic Behavior of Tall Liquid Storage Tanks," by A. Niwa - 1978 (PB 284 017)A14

UCB/EERC-78/05 "Hysteretic Behavior of Reinforced Concrete Columns Subjected to High Axial and Cyclic Shear Forces," by S.W. Zagajeski, V.V. Bertero and J.G. Bouwkamp - 1978 (PB 283 858)A13

UCB/EERC-78/06 "Three Dimensional Inelastic Frame Elements for the ANSR-I Program," by A. Riahi, D.G. Row and G.H. Powell - 1978 (PB 295 755)A04

UCB/EERC-78/07 "Studies of Structural Response to Earthquake Ground Motion," by O.A. Lopez and A.K. Chopra - 1978 (PB 282 790)A05

UCB/EERC-78/08 "A Laboratory Study of the Fluid-Structure Interaction of Submerged Tanks and Caissons in Earthquakes," by R.C. Byrd - 1978 (PB 284 957)A08

UCB/EERC-78/09 Unassigned

UCB/EERC-78/10 "Seismic Performance of Nonstructural and Secondary Structural Elements," by I. Sakamoto - 1978 (PB81 154 593)A05

UCB/EERC-78/11 "Mathematical Modelling of Hysteresis Loops for Reinforced Concrete Columns," by S. Nakata, T. Sproul and J. Penzien - 1978 (PB 298 274)A05

UCB/EERC-78/12 "Damageability in Existing Buildings," by T. Blejwas and B. Bresler - 1978 (PB 80 166 978)A05

UCB/EERC-78/13 "Dynamic Behavior of a Pedestal Base Multistory Building," by R.M. Stephen, E.L. Wilson, J.G. Bouwkamp and M. Button - 1978 (PB 286 650)A08

UCB/EERC-78/14 "Seismic Response of Bridges - Case Studies," by R.A. Imbsen, V. Nutt and J. Penzien - 1978 (PB 286 503)A10

UCB/EERC-78/15 "A Substructure Technique for Nonlinear Static and Dynamic Analysis," by D.G. Row and G.H. Powell - 1978 (PB 288 077)A10

UCB/EERC-78/16 "Seismic Risk Studies for San Francisco and for the Greater San Francisco Bay Area," by C.S. Oliveira - 1978 (PB 81 120 115)A07

UCB/EERC-78/17 "Strength of Timber Roof Connections Subjected to Cyclic Loads," by P. Gülkan, R.L. Mayes and R.W. Clough - 1978 (HUD-000 1491)A07

UCB/EERC-78/18 "Response of K-Braced Steel Frame Models to Lateral Loads," by J.G. Bouwkamp, R.M. Stephen and E.P. Popov - 1978

UCB/EERC-78/19 "Rational Design Methods for Light Equipment in Structures Subjected to Ground Motion," by J.L. Sackman and J.M. Kelly - 1978 (PB 292 357)A04

UCB/EERC-78/20 "Testing of a Wind Restraint for Aseismic Base Isolation," by J.M. Kelly and D.E. Chitty - 1978 (PB 292 833)A03

UCB/EERC-78/21 "APOLLO - A Computer Program for the Analysis of Pore Pressure Generation and Dissipation in Horizontal Sand Layers During Cyclic or Earthquake Loading," by P.P. Martin and H.B. Seed - 1978 (PB 292 835)A04

UCB/EERC-78/22 "Optimal Design of an Earthquake Isolation System," by M.A. Bhatti, K.S. Pister and E. Polak - 1978 (PB 294 735)A06

UCB/EERC-78/23 "MASH - A Computer Program for the Non-Linear Analysis of Vertically Propagating Shear Waves in Horizontally Layered Deposits," by P.P. Martin and H.B. Seed - 1978 (PB 293 101)A05

UCB/EERC-78/24 "Investigation of the Elastic Characteristics of a Three Story Steel Frame Using System Identification," by I. Kaya and H.D. McNiven - 1978 (PB 296 225)A06

UCB/EERC-78/25 "Investigation of the Nonlinear Characteristics of a Three-Story Steel Frame Using System Identification," by I. Kaya and H.D. McNiven - 1978 (PB 301 363)A05

UCB/EERC-78/26 "Studies of Strong Ground Motion in Taiwan," by Y.M. Hsiung, B.A. Bolt and J. Penzien - 1978 (PB 298 436)A06

UCB/EERC-78/27 "Cyclic Loading Tests of Masonry Single Piers: Volume 1 - Height to Width Ratio of 2," by P.A. Hidalgo, R.L. Mayes, H.D. McNiven and R.W. Clough - 1978 (PB 296 211)A07

UCB/EERC-78/28 "Cyclic Loading Tests of Masonry Single Piers: Volume 2 - Height to Width Ratio of 1," by S.-W.J. Chen, P.A. Hidalgo, R.L. Mayes, R.W. Clough and H.D. McNiven - 1978 (PB 296 212)A09

UCB/EERC-78/29 "Analytical Procedures in Soil Dynamics," by J. Lysmer - 1978 (PB 298 445)A06

UCB/EERC-79/01 "Hysteretic Behavior of Lightweight Reinforced Concrete Beam-Column Subassemblages," by B. Forzani, E.P. Popov and V.V. Bertero - April 1979(PB 298 267)A06

UCB/EERC-79/02 "The Development of a Mathematical Model to Predict the Flexural Response of Reinforced Concrete Beams to Cyclic Loads, Using System Identification," by J. Stanton & H. McNiven - Jan. 1979(PB 295 875)A10

UCB/EERC-79/03 "Linear and Nonlinear Earthquake Response of Simple Torsionally Coupled Systems," by C.L. Kan and A.K. Chopra - Feb. 1979(PB 298 262)A06

UCB/EERC-79/04 "A Mathematical Model of Masonry for Predicting its Linear Seismic Response Characteristics," by Y. Mengi and H.D. McNiven - Feb. 1979(PB 298 266)A06

UCB/EERC-79/05 "Mechanical Behavior of Lightweight Concrete Confined by Different Types of Lateral Reinforcement," by M.A. Manrique, V.V. Bertero and E.P. Popov - May 1979(PB 301 114)A06

UCB/EERC-79/06 "Static Tilt Tests of a Tall Cylindrical Liquid Storage Tank," by R.W. Clough and A. Niwa - Feb. 1979 (PB 301 167)A06

UCB/EERC-79/07 "The Design of Steel Energy Absorbing Restrainers and Their Incorporation into Nuclear Power Plants for Enhanced Safety: Volume 1 - Summary Report," by P.N. Spencer, V.F. Zackay, and E.R. Parker - Feb. 1979(UCB/EERC-79/07)A09

UCB/EERC-79/08 "The Design of Steel Energy Absorbing Restrainers and Their Incorporation into Nuclear Power Plants for Enhanced Safety: Volume 2 - The Development of Analyses for Reactor System Piping,""Simple Systems" by M.C. Lee, J. Penzien, A.K. Chopra and K, Suzuki "Complex Systems" by G.H. Powell, E.L. Wilson, R.W. Clough and D.G. Row - Feb. 1979(UCB/EERC-79/08)A10

UCB/EERC-79/09 "The Design of Steel Energy Absorbing Restrainers and Their Incorporation into Nuclear Power Plants for Enhanced Safety: Volume 3 - Evaluation of Commercial Steels," by W.S. Owen, R.M.N. Pelloux, R.O. Ritchie, M. Faral, T. Ohhashi, J. Toplosky, S.J. Hartman, V.F. Zackay and E.R. Parker - Feb. 1979(UCB/EERC-79/09)A04

UCB/EERC-79/10 "The Design of Steel Energy Absorbing Restrainers and Their Incorporation into Nuclear Power Plants for Enhanced Safety: Volume 4 - A Review of Energy-Absorbing Devices," by J.M. Kelly and M.S. Skinner - Feb. 1979(UCB/EERC-79/10)A04

UCB/EERC-79/11 "Conservatism In Summation Rules for Closely Spaced Modes," by J.M. Kelly and J.L. Sackman - May 1979(PB 301 328)A03

UCB/EERC-79/12 "Cyclic Loading Tests of Masonry Single Piers; Volume 3 - Height to Width Ratio of 0.5," by P.A. Hidalgo, R.L. Mayes, H.D. McNiven and R.W. Clough - May 1979(PB 301 321)A08

UCB/EERC-79/13 "Cyclic Behavior of Dense Course-Grained Materials in Relation to the Seismic Stability of Dams," by N.G. Banerjee, H.B. Seed and C.K. Chan - June 1979(PB 301 373)A13

UCB/EERC-79/14 "Seismic Behavior of Reinforced Concrete Interior Beam-Column Subassemblages," by S. Viwathanatepa, E.P. Popov and V.V. Bertero - June 1979(PB 301 326)A10

UCB/EERC-79/15 "Optimal Design of Localized Nonlinear Systems with Dual Performance Criteria Under Earthquake Excitations," by M.A. Bhatti - July 1979(PB 80 167 109)A06

UCB/EERC-79/16 "OPTDYN - A General Purpose Optimization Program for Problems with or without Dynamic Constraints," by M.A. Bhatti, E. Polak and K.S. Pister - July 1979(PB 80 167 091)A05

UCB/EERC-79/17 "ANSR-II, Analysis of Nonlinear Structural Response, Users Manual," by D.P. Mondkar and G.H. Powell July 1979(PB 80 113 301)A05

UCB/EERC-79/18 "Soil Structure Interaction in Different Seismic Environments," A. Gomez-Masso, J. Lysmer, J.-C. Chen and H.B. Seed - August 1979(PB 80 101 520)A04

UCB/EERC-79/19 "ARMA Models for Earthquake Ground Motions," by M.K. Chang, J.W. Kwiatkowski, R.F. Nau, R.M. Oliver and K.S. Pister - July 1979(PB 301 166)A05

UCB/EERC-79/20 "Hysteretic Behavior of Reinforced Concrete Structural Walls," by J.M. Vallenas, V.V. Bertero and E.P. Popov - August 1979(PB 80 165 905)A12

UCB/EERC-79/21 "Studies on High-Frequency Vibrations of Buildings - 1: The Column Effect," by J. Lubliner - August 1979 (PB 80 158 553)A03

UCB/EERC-79/22 "Effects of Generalized Loadings on Bond Reinforcing Bars Embedded in Confined Concrete Blocks," by S. Viwathanatepa, E.P. Popov and V.V. Bertero - August 1979(PB 81 124 018)A14

UCB/EERC-79/23 "Shaking Table Study of Single-Story Masonry Houses, Volume 1: Test Structures 1 and 2," by P. Gülkan, R.L. Mayes and R.W. Clough - Sept. 1979 (HUD-000 1763)A12

UCB/EERC-79/24 "Shaking Table Study of Single-Story Masonry Houses, Volume 2: Test Structures 3 and 4," by P. Gülkan, R.L. Mayes and R.W. Clough - Sept. 1979 (HUD-000 1836)A12

UCB/EERC-79/25 "Shaking Table Study of Single-Story Masonry Houses, Volume 3: Summary, Conclusions and Recommendations," by R.W. Clough, R.L. Mayes and P. Gülkan - Sept. 1979 (HUD-000 1837)A06

UCB/EERC-79/26 "Recommendations for a U.S.-Japan Cooperative Research Program Utilizing Large-Scale Testing Facilities," by U.S.-Japan Planning Group - Sept. 1979(PB 301 407)A06

UCB/EERC-79/27 "Earthquake-Induced Liquefaction Near Lake Amatitlan, Guatemala," by H.B. Seed, I. Arango, C.K. Chan, A. Gomez-Masso and R. Grant de Ascoli - Sept. 1979(NUREG-CR1341)A03

UCB/EERC-79/28 "Infill Panels: Their Influence on Seismic Response of Buildings," by J.W. Axley and V.V. Bertero Sept. 1979(PB 80 163 371)A10

UCB/EERC-79/29 "3D Truss Bar Element (Type 1) for the ANSR-II Program," by D.P. Mondkar and G.H. Powell - Nov. 1979 (PB 80 169 709)A02

UCB/EERC-79/30 "2D Beam-Column Element (Type 5 - Parallel Element Theory) for the ANSR-II Program," by D.G. Row, G.H. Powell and D.P. Mondkar - Dec. 1979(PB 80 167 224)A03

UCB/EERC-79/31 "3D Beam-Column Element (Type 2 - Parallel Element Theory) for the ANSR-II Program," by A. Riahi, G.H. Powell and D.P. Mondkar - Dec. 1979(PB 80 167 216)A03

UCB/EERC-79/32 "On Response of Structures to Stationary Excitation," by A. Der Kiureghian - Dec. 1979(PB 80 166 929)A03

UCB/EERC-79/33 "Undisturbed Sampling and Cyclic Load Testing of Sands," by S. Singh, H.B. Seed and C.K. Chan Dec. 1979(ADA 087 298)A07

UCB/EERC-79/34 "Interaction Effects of Simultaneous Torsional and Compressional Cyclic Loading of Sand," by P.M. Griffin and W.N. Houston - Dec. 1979(ADA 092 352)A15

UCB/EERC-80/01 "Earthquake Response of Concrete Gravity Dams Including Hydrodynamic and Foundation Interaction Effects," by A.K. Chopra, P. Chakrabarti and S. Gupta - Jan. 1980(AD-A087297)A10

UCB/EERC-80/02 "Rocking Response of Rigid Blocks to Earthquakes," by C.S. Yim, A.K. Chopra and J. Penzien - Jan. 1980 (PB80 166 002)A04

UCB/EERC-80/03 "Optimum Inelastic Design of Seismic-Resistant Reinforced Concrete Frame Structures," by S.W. Zagajeski and V.V. Bertero - Jan. 1980(PB80 164 635)A06

UCB/EERC-80/04 "Effects of Amount and Arrangement of Wall-Panel Reinforcement on Hysteretic Behavior of Reinforced Concrete Walls," by R. Iliya and V.V. Bertero - Feb. 1980(PB81 122 525)A09

UCB/EERC-80/05 "Shaking Table Research on Concrete Dam Models," by A. Niwa and R.W. Clough - Sept. 1980(PB81 122 368)A06

UCB/EERC-80/06 "The Design of Steel Energy-Absorbing Restrainers and their Incorporation into Nuclear Power Plants for Enhanced Safety (Vol 1A): Piping with Energy Absorbing Restrainers: Parameter Study on Small Systems," by G.H. Powell, C. Oughourlian and J. Simons - June 1980

UCB/EERC-80/07 "Inelastic Torsional Response of Structures Subjected to Earthquake Ground Motions," by Y. Yamazaki April 1980(PB81 122 327)A08

UCB/EERC-80/08 "Study of X-Braced Steel Frame Structures Under Earthquake Simulation," by Y. Ghanaat - April 1980 (PB81 122 335)A11

UCB/EERC-80/09 "Hybrid Modelling of Soil-Structure Interaction," by S. Gupta, T.W. Lin, J. Penzien and C.S. Yeh May 1980(PB81 122 319)A07

UCB/EERC-80/10 "General Applicability of a Nonlinear Model of a One Story Steel Frame," by B.I. Sveinsson and H.D. McNiven - May 1980(PB81 124 877)A06

UCB/EERC-80/11 "A Green-Function Method for Wave Interaction with a Submerged Body," by W. Kioka - April 1980 (PB81 122 269)A07

UCB/EERC-80/12 "Hydrodynamic Pressure and Added Mass for Axisymmetric Bodies," by F. Nilrat - May 1980(PB81 122 343)A08

UCB/EERC-80/13 "Treatment of Non-Linear Drag Forces Acting on Offshore Platforms," by B.V. Dao and J. Penzien May 1980(PB81 153 413)A07

UCB/EERC-80/14 "2D Plane/Axisymmetric Solid Element (Type 3 - Elastic or Elastic-Perfectly Plastic) for the ANSR-II Program," by D.P. Mondkar and G.H. Powell - July 1980(PB81 122 350)A03

UCB/EERC-80/15 "A Response Spectrum Method for Random Vibrations," by A. Der Kiureghian - June 1980(PB81 122 301)A03

UCB/EERC-80/16 "Cyclic Inelastic Buckling of Tubular Steel Braces," by V.A. Zayas, E.P. Popov and S.A. Mahin June 1980(PB81 124 885)A10

UCB/EERC-80/17 "Dynamic Response of Simple Arch Dams Including Hydrodynamic Interaction," by C.S. Porter and A.K. Chopra - July 1980(PB81 124 000)A13

UCB/EERC-80/18 "Experimental Testing of a Friction Damped Aseismic Base Isolation System with Fail-Safe Characteristics," by J.M. Kelly, K.E. Beucke and M.S. Skinner - July 1980(PB81 148 595)A04

UCB/EERC-80/19 "The Design of Steel Energy-Absorbing Restrainers and their Incorporation into Nuclear Power Plants for Enhanced Safety (Vol 1B): Stochastic Seismic Analyses of Nuclear Power Plant Structures and Piping Systems Subjected to Multiple Support Excitations," by M.C. Lee and J. Penzien - June 1980

UCB/EERC-80/20 "The Design of Steel Energy-Absorbing Restrainers and their Incorporation into Nuclear Power Plants for Enhanced Safety (Vol 1C): Numerical Method for Dynamic Substructure Analysis," by J.M. Dickens and E.L. Wilson - June 1980

UCB/EERC-80/21 "The Design of Steel Energy-Absorbing Restrainers and their Incorporation into Nuclear Power Plants for Enhanced Safety (Vol 2): Development and Testing of Restraints for Nuclear Piping Systems," by J.M. Kelly and M.S. Skinner - June 1980

UCB/EERC-80/22 "3D Solid Element (Type 4-Elastic or Elastic-Perfectly-Plastic) for the ANSR-II Program," by D.P. Mondkar and G.H. Powell - July 1980(PB81 123 242)A03

UCB/EERC-80/23 "Gap-Friction Element (Type 5) for the ANSR-II Program," by D.P. Mondkar and G.H. Powell - July 1980 (PB81 122 285)A03

UCB/EERC-80/24 "U-Bar Restraint Element (Type 11) for the ANSR-II Program," by C. Oughourlian and G.H. Powell July 1980(PB81 122 293)A03

UCB/EERC-80/25 "Testing of a Natural Rubber Base Isolation System by an Explosively Simulated Earthquake," by J.M. Kelly - August 1980(PB81 201 360)A04

UCB/EERC-80/26 "Input Identification from Structural Vibrational Response," by Y. Hu - August 1980(PB81 152 308)A05

UCB/EERC-80/27 "Cyclic Inelastic Behavior of Steel Offshore Structures," by V.A. Zayas, S.A. Mahin and E.P. Popov August 1980(PB81 196 180)A15

UCB/EERC-80/28 "Shaking Table Testing of a Reinforced Concrete Frame with Biaxial Response," by M.G. Oliva October 1980(PB81 154 304)A10

UCB/EERC-80/29 "Dynamic Properties of a Twelve-Story Prefabricated Panel Building," by J.G. Bouwkamp, J.P. Kollegger and R.M. Stephen - October 1980(PB82 117 128)A06

UCB/EERC-80/30 "Dynamic Properties of an Eight-Story Prefabricated Panel Building," by J.G. Bouwkamp, J.P. Kollegger and R.M. Stephen - October 1980(PB81 200 313)A05

UCB/EERC-80/31 "Predictive Dynamic Response of Panel Type Structures Under Earthquakes," by J.P. Kollegger and J.G. Bouwkamp - October 1980(PB81 152 316)A04

UCB/EERC-80/32 "The Design of Steel Energy-Absorbing Restrainers and their Incorporation into Nuclear Power Plants for Enhanced Safety (Vol 3): Testing of Commercial Steels in Low-Cycle Torsional Fatigue," by P. Spencer, E.R. Parker, E. Jongewaard and M. Drory

UCB/EERC-80/33 "The Design of Steel Energy-Absorbing Restrainers and their Incorporation into Nuclear Power Plants for Enhanced Safety (Vol 4): Shaking Table Tests of Piping Systems with Energy-Absorbing Restrainers," by S.F. Stiemer and W.G. Godden - Sept. 1980

UCB/EERC-80/34 "The Design of Steel Energy-Absorbing Restrainers and their Incorporation into Nuclear Power Plants for Enhanced Safety (Vol 5): Summary Report," by P. Spencer

UCB/EERC-80/35 "Experimental Testing of an Energy-Absorbing Base Isolation System," by J.M. Kelly, M.S. Skinner and K.E. Beucke - October 1980(PB81 154 072)A04

UCB/EERC-80/36 "Simulating and Analyzing Artificial Non-Stationary Earthquake Ground Motions," by R.F. Nau, R.M. Oliver and K.S. Pister - October 1980(PB81 153 397)A04

UCB/EERC-80/37 "Earthquake Engineering at Berkeley - 1980," - Sept. 1980(PB81 205 874)A09

UCB/EERC-80/38 "Inelastic Seismic Analysis of Large Panel Buildings," by V. Schricker and G.H. Powell - Sept. 1980 (PB81 154 338)A13

UCB/EERC-80/39 "Dynamic Response of Embankment, Concrete-Gravity and Arch Dams Including Hydrodynamic Interaction," by J.F. Hall and A.K. Chopra - October 1980(PB81 152 324)A11

UCB/EERC-80/40 "Inelastic Buckling of Steel Struts Under Cyclic Load Reversal," by R.G. Black, W.A. Wenger and E.P. Popov - October 1980(PB81 154 312)A08

UCB/EERC-80/41 "Influence of Site Characteristics on Building Damage During the October 3, 1974 Lima Earthquake," by P. Repetto, I. Arango and H.B. Seed - Sept. 1980(PB81 161 739)A05

UCB/EERC-80/42 "Evaluation of a Shaking Table Test Program on Response Behavior of a Two Story Reinforced Concrete Frame," by J.M. Blondet, R.W. Clough and S.A. Mahin

UCB/EERC-80/43 "Modelling of Soil-Structure Interaction by Finite and Infinite Elements," by F. Medina - December 1980(PB81 229 270)A04

UCB/EERC-81/01 "Control of Seismic Response of Piping Systems and Other Structures by Base Isolation," edited by J.M. Kelly - January 1981 (PB81 200 735)A05

UCB/EERC-81/02 "OPTNSR - An Interactive Software System for Optimal Design of Statically and Dynamically Loaded Structures with Nonlinear Response," by M.A. Bhatti, V. Ciampi and K.S. Pister - January 1981 (PB81 218 851)A09

UCB/EERC-81/03 "Analysis of Local Variations in Free Field Seismic Ground Motions," by J.-C. Chen, J. Lysmer and H.B. Seed - January 1981 (AD-A099508)A13

UCB/EERC-81/04 "Inelastic Structural Modeling of Braced Offshore Platforms for Seismic Loading," by V.A. Zayas, P.-S.B. Shing, S.A. Mahin and E.P. Popov - January 1981(PB82 138 777)A07

UCB/EERC-81/05 "Dynamic Response of Light Equipment in Structures," by A. Der Kiureghian, J.L. Sackman and B. Nour-Omid - April 1981 (PB81 218 497)A04

UCB/EERC-81/06 "Preliminary Experimental Investigation of a Broad Base Liquid Storage Tank," by J.G. Bouwkamp, J.P. Kollegger and R.M. Stephen - May 1981(PB82 140 385)A03

UCB/EERC-81/07 "The Seismic Resistant Design of Reinforced Concrete Coupled Structural Walls," by A.E. Aktan and V.V. Bertero - June 1981(PB82 113 358)A11

UCB/EERC-81/08 "The Undrained Shearing Resistance of Cohesive Soils at Large Deformations," by M.R. Pyles and H.B. Seed - August 1981

UCB/EERC-81/09 "Experimental Behavior of a Spatial Piping System with Steel Energy Absorbers Subjected to a Simulated Differential Seismic Input," by S.F. Stiemer, W.G. Godden and J.M. Kelly - July 1981

UCB/EERC-81/10 "Evaluation of Seismic Design Provisions for Masonry in the United States," by B.I. Sveinsson, R.L. Mayes and H.D. McNiven - August 1981

UCB/EERC-81/11 "Two-Dimensional Hybrid Modelling of Soil-Structure Interaction," by T.-J. Tzong, S. Gupta and J. Penzien - August 1981(PB82 142 118)A04

UCB/EERC-81/12 "Studies on Effects of Infills in Seismic Resistant R/C Construction," by S. Brokken and V.V. Bertero - September 1981

UCB/EERC-81/13 "Linear Models to Predict the Nonlinear Seismic Behavior of a One-Story Steel Frame," by H. Valdimarsson, A.H. Shah and H.D. McNiven - September 1981(PB82 138 793)A07

UCB/EERC-81/14 "TLUSH: A Computer Program for the Three-Dimensional Dynamic Analysis of Earth Dams," by T. Kagawa, L.H. Mejia, H.B. Seed and J. Lysmer - September 1981(PB82 139 940)A06

UCB/EERC-81/15 "Three Dimensional Dynamic Response Analysis of Earth Dams," by L.H. Mejia and H.B. Seed - September 1981 (PB82 137 274)A12

UCB/EERC-81/16 "Experimental Study of Lead and Elastomeric Dampers for Base Isolation Systems," by J.M. Kelly and S.B. Hodder - October 1981

UCB/EERC-81/17 "The Influence of Base Isolation on the Seismic Response of Light Secondary Equipment," by J.M. Kelly - April 1981

UCB/EERC-81/18 "Studies on Evaluation of Shaking Table Response Analysis Procedures," by J. Marcial Blondet - November 1981

UCB/EERC-81/19 "DELIGHT.STRUCT: A Computer-Aided Design Environment for Structural Engineering," by R.J. Balling, K.S. Pister and E. Polak - December 1981

UCB/EERC-81/20 "Optimal Design of Seismic-Resistant Planar Steel Frames," by R.J. Balling, V. Ciampi, K.S. Pister and E. Polak - December 1981

UCB/EERC-82/01 "Dynamic Behavior of Ground for Seismic Analysis of Lifeline Systems," by T. Sato and A. Der Kiureghian - January 1982 (PB82 218 926) A05

UCB/EERC-82/02 "Shaking Table Tests of a Tubular Steel Frame Model," by Y. Ghanaat and R. W. Clough - January 1982 (PB82 220 161) A07

UCB/EERC-82/03 "Experimental Behavior of a Spatial Piping System with Shock Arrestors and Energy Absorbers under Seismic Excitation," by S. Schneider, H.-M. Lee and G. W. Godden - May 1982

UCB/EERC-82/04 "New Approaches for the Dynamic Analysis of Large Structural Systems," by E. L. Wilson - June 1982

UCB/EERC-82/05 "Model Study of Effects on the Vibration Properties of Steel Offshore Platforms," by F. Shahrivar and J. G. Bouwkamp - June 1982

UCB/EERC-82/06 "States of the Art and Practice in the Optimum Seismic Design and Analytical Response Prediction of R/C Frame-Wall Structures," by A. E. Aktan and V. V. Bertero - July 1982.

UCB/EERC-82/07 "Further Study of the Earthquake Response of a Broad Cylindrical Liquid-Storage Tank Model," by G. C. Manos and R. W. Clough - July 1982

UCB/EERC-82/08 "An Evaluation of the Design and Analytical Seismic Response of a Seven Story Reinforced Concrete Frame - Wall Structure," by A. C. Finley and V. V. Bertero - July 1982

UCB/EERC-82/09 "Fluid-structure Interactions: Added Mass Computations for Incompressible Fluid," by J. S.-H. Kuo - August 1982